GENETIC DELETION AND INHIBITION OF SELENOPROTEIN K REDUCES MELANOMA GROWTH AND METASTASIS BY ALTERING INTRACELLULAR CALCIUM

A DISSERTATION SUBMITTED TO THE GRADUATE DIVISION OF THE UNIVERISTY OF HAWAI'I AT MĀNOA IN PARTIAL FULFILLMENT OF THE REQUIREMENTS FOR THE DEGREE OF

DOCTOR OF PHILOSOPHY

IN

CELL AND MOLECULAR BIOLOGY

MAY 2019

By

Michael P. Marciel

Thesis Committee:

Peter H. Hoffmann, Chairman
Robert A. Nichols
Matthew W. Pitts
Michelle L. Matter
Saguna Verma

Keywords: selenoprotein K, melanoma, DHHC6

Abstract

Melanoma is the deadliest form of skin cancer, resulting in over 9,000 deaths annually in the United States alone. Along with limiting ultraviolet exposure, it is vital that new therapies are generated that target melanoma progression. A recent interest in targeting store operated calcium entry (SOCE) as a treatment for different cancers types has recently emerged. SOCE is the main mechanism by which non-excitable cells import calcium (Ca^{2+}) from the extracellular space and this process is critical for normal growth, proliferation, and migration in a variety of cell types. Several studies have demonstrated that knockdown or complete genetic deletion of SELENOK reduced SOCE in immune cells and retarded their ability to differentiate, proliferate, and migrate. However, the effect of inhibiting SELENOK in cancer has not yet been investigated. We hypothesized that deletion of SELENOK in melanoma cells may decrease their ability to proliferate and metastasize by a reducing SOCE. This hypothesis was tested using three approaches (*i*) SELENOK null mice were crossed with a murine model of melanoma, and melanoma progression in the absence of SELENOK was observed, (*ii*) SELENOK null melanoma cells were generated using a CRISPR-Cas9 approach in a human melanoma cell line, and tested for their ability to proliferate and migrate *in vitro*, and, (*iii*) an inhibitor based on the structure of SELENOK was generated and tested for its ability to inhibit the SELENOK mediated palmitoylation in a cell free environment. The data presented herein show that SELENOK deletion inhibited calcium flux and calcium dependent signaling *in vitro* which reduced that capacity of melanoma cells to migrate and proliferate.

Furthermore, SELENOK deletion decreased primary growth and metastasis of tumor cells in a spontaneous mouse model of melanoma. Last, the inhibitor based on SELENOK was shown to be able to disrupt SELENOK mediated palmitoylation and thus may serve as a basis for future inhibitors. This dissertation will attempt to outline the data representing the first investigation into the role of SELENOK in metastatic melanoma.

Table of Contents

List of Figures

Abbreviations

AIDS: acquired immunodeficiency syndrome

AML: acute myeloid leukemia

ASAP2: Arf-GAP with Src homology 3 domian, ankyrin repeat, and plekstrin homology domain-containing protein 2

BD: binding domain

BTSC: brain tumor stem cell

$Ca2^{+}$: calcium

Calx: Na^{+}/Ca^{2+} exchange protein

CD: cluster of differentiation

CDK: Ca^{2+}/ CaM-dependent protein kinase II, cyclic-dependent kinase

CDKN2A: cyclin-dependent kinase inhibitor 2A

COX-2: cyclooxygenase-2

CRD: cysteine rich domain

CREB: cAMP responsive binding element

CsA: cyclosporin A

CSC: cancer stem cell

CTL: cytotoxic T lymphocyte

CVB3: coxsackievirus

Cys: cysteine

DAG: diacylglycerol

ECM: extracellular matrix

EMT: epithelial to mesenchymal transition

ER: endoplasmic reticulum

ERAD: ER-associated degradation

Erf2- ethylene-responsive factor-2

Erf4- ethylene-responsive factor-4

GPCR: G-coupled protein receptor, receptor tyrosine kinases

Gpx1: glutathione peroxidase 1

Gpx4: glutathione peroxidase 4

GRB2: growth factor receptor bound protein 2

Grm1: glutamate receptor 1

HCV: hepatitis C virus

HIV-1: human immunodeficiency virus-1

hTERT: human telomerase reverse transcriptase

IDP: intrinsically disordered protein

IHC: immunohistochemistry

IL-2: interleukin-2

IP3: inositol trisphosphate

IP3R: inositol trisphosphate receptor

KO: knockout

LPS: lipopolysaccharide

MAP: mitogen activated protein

MC1R: melanocortin receptor 1

MCP-1: monocyte chemoattractant protein-1

mTor: mammalian target of rapamycin

NER: nucleotide excision repair

NFAT: nuclear factor of activated T cells

NLS: nuclear localization sequence

NPC: nutritional prevention of cancer

OA: okadaic acid

PAT: protein acyltransferase

PIP2: phosphatidylinositol 4,5 bisphosphate

PKA: protein kinase A

PKB: protein kinase B

PKC: protein kinase C

PLC: phospholipase C

Prom1: prominin 1

PTEN: phosphatase and tensin homolog

ROS: reactive oxygen species

RTK: receptor tyrosine kinase

sdAb: single domain antibody

Se: selenium

Sec: selenocysteine

SELENOK: selenoprotein K

SELENOS: selenoprotein S

SH3: Src Homology 3

SH3BD: Src Homology 3 binding domain

SNP: single nucleotide polymorphism

SOCE: store-operated calcium entry

Sos: son of sevenless

STIM1: stromal interaction molecule 1

STIM2: stromal interaction molecule 2

TCR: T cell receptor

TCR: T cell receptors

TFRC: transferrin receptor protein 1

Tg: transgenic

TLR: toll like receptor

TNFα: tumor necrosis factor alpha

Trp2: tyrosine-related protein 2

uv: ultraviolet light

VCP/p97: valosin-containing protein

w.t.: wild type

WNV: West Nile virus

XP: Xeroderma Pigmentosum

α-MSH: α-melanocyte-stimulating hormone

Chapter 1. Natural history of selenium and selenoprotein K

Introduction

Selenium (Se) is an essential trace mineral fundamental to human health and biology [1]. The biological effects of Se are exerted through its incorporation into the 21st amino acid selenocysteine (Sec), the defining component of selenoproteins [2] . There are 25 selenoprotein family members in humans that perform a wide variety of functions including the regulation of redox tone, control of reactive oxygen species, regulating thyroid hormone metabolism, facilitating sperm maturation, and promoting optimal immunity [3]. Many of the selenoproteins family members exhibit a common thioredoxin-like fold within their catalytic domains with a conserved Cys-X-X-Sec (CXXU) or Cys-X-X-Ser (CXXS) motfi [4, 5]. Additionally, many of these selenoproteins perform well defined catalytic activities (e.g. glutathione peroxidases, iodothyronine deiodinase, thioredoxin reductases, methionine sulfoxide reductases), while other selenoproteins do not contain the thioredoxin-like fold and whose functions are relatively unknown (e.g. selenoproteins M, T, O, V) [6] . Selenoprotein K (SELENOK) does not contain a CXXU motif nor does it appear to catalyze redox reactions. SELENOK is proposed to be an intrinsically disordered protein [7] which suggests its function is dependent on a partner protein with which it complexes. Intrinsically disordered proteins serving as docking platforms for signaling molecules or binding partners has been previously established for other nonenzymatic proteins [8]. Indeed, a great deal of what has been discovered about SELENOK function has been gained by examining its binding partners [9-11]. This chapter provides a summary of what is known about SELENOK and its implications in terms of calcium (Ca^{2+}) flux and human health.

Background

Dietary Selenium and human health

A short summary of dietary selenium and its impact on human health is useful here. Se enters the food web via vegetation which acquire it from the soil, and thus Se deficiency has been identified in parts of the world with low soil Se content. An example of this is certain regions with recent volcanic deposits such as in the Pacific Northwest [12] and large swaths of land in the Se-poor belt in Central China [13]. Human Se deficiency is associated with Keshan Disease, a cardiomyopathy and Keshin-Beck Disease, which causes severe arthritis [14]. Selenium exerts its biological effects via its incorporation into selenocysteine (Sec), which is a component of all selenoproteins, some of which perform vital enzymatic functions [1]. Se is found in high abundance in the liver spleen, and lymph tissue. Furthermore, Se levels affects cell mediated immunity, humoral immunity, and cytotoxicity [15]. In general, Se deficiency in animals leads to a less responsive immune system which Se supplementation can reverse [15]. For example, Se supplementation in Se-deficient individuals can enhance proliferation of T cells (clonal expansion), enhanced response to antigen challenge, and increased ability of T cells to differentiate into cytotoxic T cells and kill tumor cells [16]. The mechanism by which Se enhances T cell activity may be due in part by the ability of Se to upregulate receptors that regulate their growth such as interleukin-2 (IL-2) receptor [17]. Se affects other components of the immune system in various ways that will be described below.

Viral Infection

As mentioned previously, Keshan Disease is a prevalent cardiomyopathy that mostly affects individuals in Se-poor areas in China. Keshan Disease may be due in part to coxsackievirus (CVB3) in which the harmless virus can become virulent under Se-deficient conditions during infection [18]. Se supplementation can not only enhance antiviral immunity against CVB3 but also prevents oxidative damage to the viral genome that can increase the virulence of CVB3 [18]. This was demonstrated by an experiment where CVB3 was isolated from Se-deficient mice and

passaged into Se-adequate mice. If increased virulence is due to viral replication under Se-deficient conditions, then the Se-adequate mice would not be protected from the passed virus and will develop myocarditis. Indeed, the mice inoculated with CVB3 from Se-deficient mice developed myocarditis, which was not observed in mice inoculated with CVB3 isolated from Se-adequate mice [18]. Sequencing of the viral genome of CVB3 isolated from Se-deficient mice showed six point mutations that may contribute to their increased virulence, but the mechanism by which these mutations lead to increased virulence is unclear [18]. Similarly, studies utilizing mouse models of infection with influenza A demonstrate that this virus undergoes increased mutational changes in genomic RNA under Se-deficient conditions [19].

Se is critically involved in the etiology of human immunodeficiency virus-1 (HIV-1) infected individuals and acts as an inhibitor of HIV replication [20]. Specifically, Se supplementation increases glutathione peroxidase activity and thus decreases aberrant NF-kappa B activation by H_2O_2 in HIV-1 infected cells [20]. HIV-1 progression, including the onset of acquired immunodeficiency syndrome (AIDS), is caused by a progressive decrease in CD4+ T cells, which is paralleled by a decrease in Se plasma levels [21-24]. Furthermore, low Se serum concentration ([Se]) in HIV-1 infected patients is associated with increased disease progression and greater HIV-1 related mortality rates [25, 26].

Cancer

Epidemiological studies, performed since the 1970s, examining the relationship between Se intake and cancer mortality have demonstrated a protective role for Se in cancer progression [27-29]. The Nutritional Prevention of Cancer (NPC) Trial observed 1321 subjects with a history of skin cancer that were supplemented with either 200 µg Se/day (Se-yeast) or placebo. Subjects receiving Se supplementation demonstrated 50% less total cancer related mortality, 37% less total cancer morbidity, 46% fewer cancers of the lung, 58% fewer cancers of the colon, and 63% percent less cases of prostate cancer [30]. The NPC Trial was undertaken in a region where selenium uptake by the general population already exceeded the levels required to optimize selenoprotein enzyme function [31]. This implies, without excluding selenoenzyme activity, that

the anticancer effects observed with above normal levels of selenium intake may be due to production of antitumorigenic metabolites or enhanced immune response [32]. On the other hand, studies have shown the inefficacy of selenium supplementation in inhibiting the progression of cancer [33, 34]. Indeed, a study of syngeneic mesothelioma by Rose et al., which utilized immune competent mice, demonstrated accelerated tumor progression in mice fed a higher selenium diet due to the increased reducing capacity of the tumor cells themselves [35]. The often confounding results listed above underscores the importance of the ability to discern the effects of the bioavailability of Se on the cancer cells themselves, versus the antitumorigenic effects that Se may be exerting via the immune system and the prevention of genetic alterations in healthy cells.

Selenoptrotein K structure

SELENOK is a small (94 amino acids), integral, single-pass transmembrane protein localized to the endoplasmic reticulum (ER) with a canonical ER retention motif specific for ER transmembrane proteins (KKXX) located on the cytosolic side: KKRR. The Sec residue is located near the C-terminus at residue 92 (Figure 1.1A). The currently known topological data classifies SELENOK as a type III transmembrane protein whereby the N-terminus is luminal. An online protein folding modeler was used to generate the predicted tertiary structure of SELENOK, which is in agreement with the current topological data (Figure 1.1B) [36]. The cytosolic portion of SELENOK contains an abundance of proline and glycine residues and, for the most part, has been predicted to be intrinsically disordered (lacking a clear fixed or ordered three-dimensional structure). However, some features have been elucidated from experimentation; a calpain cleavage site (aa 81-82), a Src Homology 3 (SH3) binding domain (SH3BD) with the canonical consensus motif (R/K-X-X-P-X-X-P), along with possible glycosylation and phosphorylation sites. There is evidence that SELENOK can form an intermolecular diselenide bond and therefore, at minimum, may exist as a homodimer [69]. However, this has only been observed in SELENOK containing micelles and SELENOK conformation has not been confirmed in the cell.

Tissue Distribution

SELENOK mRNA and protein are widely expressed throughout mouse tissues, although particularly high levels have been observed in lymphoid tissue and the testes [37]. Initial studies using Northern blot analysis revealed relatively high SELENOK mRNA expression in the heart [38], but this has not been supported by additional studies. SELENOK protein expression was shown to be positively correlated with increasing Se intake in mice (from 0.25 to 1.0 ppm) by western blot detection of all tissues examined except for the heart [39]. Dietary [Se] regulates the expression of selenoproteins at the mRNA and protein levels. Under low Se conditions, the translation of selenoproteins stall at the Sec-encoding UGA codon and both the mRNA and the truncated protein are degraded through nonsense-mediated decay and destruction via C-end degrons, respectively [40, 41] .

Dietary [Se] affects expression levels of different selenoproteins to varying degrees [42] and one can rank order the least to most Se sensitive selenoproteins in a "hierarchy of selenoproteins" [42, 43]. This hierarchy is tissue and cell line specific, often making it difficult to discern to discern its nature experimentally. However, differences between selenoproteins in sensitivity to limiting [Se] was first demonstrated by experiments comparing the activities of glutathione peroxidases 1 and 4 (GPX1 and GPX4) in rat liver, kidney, and heart [44]. Under Se deficiency, GPX1 activity was sharply reduced while GPX4 activity was maintained. Furthermore, different tissues demonstrated various levels of activity between the two GPXs, confirming the tissue dependent aspect selenoprotein Se sensitivity. Finally, in addition to tissue specific Se sensitivity, sex also influences the selenoprotein hierarchy [45].

SELENOK may be involved in regulating ER stress

The ER is essential for proper cellular activities such as protein maturation, lipid synthesis, detoxification, and transport of secreted and membrane proteins. Importantly, tightly controlled protein folding takes place in the ER and misfolded proteins undergo ER-associated degradation (ERAD) [46]. An imbalance between the demand of ER function and ER capacity can cause ER

stress that can eventually lead to apoptosis [46]. Therefore, ER homeostasis must be tightly regulated and may involve one or more of the ER-resident selenoproteins; type 2 iodothyronine deiodinase and selenoproteins F, K, M, N, S, and T [47]. The gene encoding SELENOK contains a functional ER stress response element and SELENOK has been shown to play an important role in protecting HepG2 cells from ER stress-induced apoptosis [5]. Furthermore, SELENOK has been shown to participate in ERAD specifically by binding to an ERAD complex with other proteins such as Derlin-1 [11]. Along with another selenprotein, selenoprotein S (SELENOS), SELENOK participates in ERAD by recruiting cytosolic valosin-containing protein (VCP/p97) to promote translocation of misfolded proteins from the ER lumen [9]. It remains unclear how the Sec residue may or may participate in retrograde translocation of misfolded proteins and, in SELENOK knockout (KO) mice, there are no apparent signs of ER stress [37, 48]. The latter finding suggests some redundancy or compensation, perhaps involving SELENOS, may occur in the absence of SELENOK expression to mitigate ER stress.

SELENOK is involved in immunity and Calcium Flux rom the ER

A major finding from experiments performed in immune cells from SELENOK KO mice suggested a role for SELENOK in immunity and receptor-mediated Ca^{2+} flux. SELENOK KO mice are fertile and healthy with no obvious phenotype [37]. Similarly, development of the immune system (total cell and proportion of sub-types) was not affected in SELENOK-deficient mice compared to wild type (w.t) controls. However, certain immune dysfunctions were observed when mice were challenged with immunogenic agents. Treatment of mice with poly (i:c) resulted in lower levels of monocyte chemoattractant protein-1 (MCP-1) and KC chemokine production and lower levels of neutrophil infiltration compared to w.t. control groups [36]. SELENOK KO macrophages secreted lower levels of interleukin-6 (IL-6) and tumor necrosis factor alpha (TNFα) in response to lipopolysaccharide (LPS) challenge and SELENOK KO macrophages exhibit decreased oxidative burst after phagocytosis via the Fcγ receptor [36]. SELENOK KO mice infected with West Nile virus (WNV) demonstrate a decreased ability to clear the virus, were more susceptible to the resulting neuropathology caused by prolonged viral burden, and had higher mortality rates compared to w.t controls. Furthermore, T cells,

macrophages, and neutrophils from SELENOK KO mice demonstrated reduced migration after treatment with chemotactic compounds compared to w.t. controls [36]. Finally, receptor mediated calcium flux was impaired in SELENOK-deficient T cells, macrophages, and neutrophils after stimulation with chemokines and other reagents that trigger G-coupled protein receptor signaling in these immune cells [36].

The calcium mediated immune deficiencies observed in the SELENOK KO mice may be due to deficient store-operated calcium entry (SOCE) in immune cells. SOCE is a specifically defined set of events by which non-excitable cells import extracellular calcium into the cytosol, induce Ca^{2+} dependent signal transduction, and replenish their calcium stores [49, 50]. SOCE is initiated when various receptor plasma membrane receptors (G-coupled protein receptors, tyrosine kinases, Fcγ receptors, T cell receptors) are engaged by their respective ligands, leading to phospholipase C (PLC) activation which cleaves phosphatidylinositol 4,5 bisphosphate (PIP_2) into Inositol 1,4,5-trisphosphate (IP3) and diacylglycerol (DAG). IP3 then binds to the inositol trisphosphate receptor (IP3R) and leads to Ca^{2+} efflux from the ER into the cytosol, down its electrochemical gradient. This loss of Ca^{2+} is sensed by stromal interaction molecule 1 (STIM1) which oligomerizes and translocates to ER PM junctions termed puncta and interacts with Orai Ca^{2+} calcium channels and allows Ca^{2+} to enter the cytosol from the extracellular space [51]. Evidence that SELENOK promotes SOCE was obtained in subsequent investigations, revealing that SELENOK acts as a co-factor, along with the acyl transferase DHHC6, to catalyze the palmitoylation of the IP3R, allowing for its proper expression in the ER membrane [52]. The details of these findings are described in more detail below.

The role of SELENOK in promoting protein palmitoylation

Investigation into the role that SELENOK plays in immune system activation during atherosclerosis revealed that SELENOK was required for lipid raft localization of the oxidized low density lipoprotein receptor, CD36, on macrophages [53]. SELENOK-deficient macrophages were found to have decreased CD36 palmitoylation, which is crucial for stabilizing CD36 and its clustered expression in the plasma membrane [54]. S-palmitoylation of cysteine

residues is a post translational modification that promotes the anchorage of integral and peripheral proteins in the membrane, and also modulates hydrophobic protein-protein interactions [55]. Subsequent studies found that palmitoylation of other proteins required SELENOK including Arf-GAP with Src homology 3 domain, ankyrin repeat, and plekstrin homology domain-containing protein 2 (ASAP2) and the IP3R (Figure 1.2) [10, 56]. There are very likely other proteins that require SELENOK for protein palmitoylation. As alluded to above, S-palmitoylation is the addition of the 16-carbon fatty acid, palmitate, to cysteine residues on target substrate proteins via a thioester bond [57]. Since SELENOK itself is not an enzyme it must bind to a partner enzyme to promote palmitoylation. A major clue to help identity the enzymatic binding partner of SELENOK was the fact that SELENOK is the only selenoprotein with an SH3 binding domain and one member of the enzyme family involved in palmitoylation reactions contained an SH3 domain. Indeed, SELENOK interacts with the protein acyl-transferase (PAT), DHHC6 (letters represent the amino acids aspartic acid, histidine, histidine, and cysteine in the catalytic domain), in the ER membrane through SH3/SH3BD interactions and this is how SELENOK participates in palmitoylation reactions [10].

The specific mechanism by which SELENOK exerts its effects on DHHC6 to increase its catalytic efficiency required new tools to be built so that the enzymatic reaction of acyl transfer could be examined in more detail. The palmitoylation reactions catalyzed by DHHC enzymes have been shown to proceed via a two-step mechanism [58] (see Chapter 3 for more details on DHHC family). In the first, so-called autopalmitoylation step, a Cys residue within the DHHC catalytic domain reacts with palmitoyl-CoA to form a palmitoyl-PAT intermediate. In the second step, the palmitoyl group is transferred from the PAT to a Cys residue on the target protein. The first step is rapid, whereas the second is much slower. Thus, after the first step, the unstable thioester bond between Cys on the PAT and the palmitic acid may hydrolyze before transfer of the palmitic acid to a target protein, termed the “futile cycle” [59]. The Hoffmann laboratory was able to synthesize soluble versions of DHHC6 and have shown that it can bind recombinant SELENOK in a complex that exhibited acyl transferase activity. The data from these experiments showed that SELENOK increases the catalytic efficiency of palmitoylation by stabilizing the acyl-DHHC6 intermediate and protecting it from hydrolysis, thereby preventing

the futile cycle [60]. This binding of a PAT enzyme with a cofactor to promote intermediate stabilization was previously found in another protein pair in yeast. In particular, the yeast ethylene-responsive factor-2 (Erf2) is an ortholog for mammalian DHHC9 and binds to yeast ethylene-responsive factor-4 (Erf4) in a manner that stabilizes the acyl-Erf2 intermediate and increases its catalytic efficiency [61]. Erf4 is not a selenoprotein (yeast do not express selenoproteins), so the manner in which these two cofactors increase catalytic efficiency must necessarily be different. As discussed below in more detail, the Sec residue in SELENOK plays a critical role in promoting palmitoylation.

The Sec residue in SELENOK is responsible for its bioactivity

To understand the importance of the Sec residue in SELENOK it is necessary to differentiate its chemical properties from the amino acid most similar to Sec, cysteine (Cys). Sec and Cys are structurally identically except for a selenium atom in Sec in place of the sulfur atom in Cys. The pK_a of the thiol in free Cys in 8.5 whereas the pK_a of the selenol in free Sec is 5.7 [62]. Thus, Sec is more likely to be anionic under physiological conditions and exhibits superior nucleophilic reactivity compared to Cys [63]. Sec containing proteins are less likely to be irreversibly oxidized compared to cysteine containing proteins due to the propensity of selenic acid to be readily reduced compared to sulfinic acid [63]. Irreversibly oxidation of Cys can cause enzymatic inactivation and therefore, Sec containing enzymes may be more resistant to oxidative inactivation because of their ability to cycle through oxidation states much faster compared to Cys containing enzymes [63, 64]. The enhanced nucleophilic reactivity and the resistance to enzymatic inactivation by oxygen may explain why Sec containing oxioreductases, such as thioredoxin reductase, methionine sulfoxide, and glutathione peroxidase are 100- to 1,000-fold more active compared to their Cys mutated counterparts [65-68]. The observations listed above may help to explain the experimental evidence that show the requirement of the Sec residue for the bioactivity of SELENOK.

The Sec residue in SELENOK is located near the C-terminus (amino acid 92), which is a feature found in approximately one-third of selenoproteins [69]. While the Sec residue in SELENOK has

been shown to exhibit some antioxidant activity *in vitro* [38, 70] a role for regulating redox reactions in *in vivo* has yet to be established. Indeed, SELENOK does not contain defined redox motifs such as those observed in glutathione peroxidases or thioredoxin reductases and ER stress not observed in SELENOK-deficient mice [37]. As described above, SELENOK KO mice were observed to have impaired SOCE in T cells, neutrophils, and macrophages when stimulated with chemokines and other reagents that trigger receptor mediated signaling in these immune cells [37]. Importantly, when these immune cells were stimulated with thapsigargin, a drug that induces SOCE in a manner that bypasses the IP3R, the w.t. and KO cells did not differ. This implicated the IP3R as a molecule somehow involved in SELENOK-dependent SOCE.

The exact mechanism by which SELENOK regulated SOCE was not initially clear, but the requirement of the Sec residue in this process became evident when it was observed that a calpain protease (calpain-2), that cleaved the C-terminal end of SELENOK (residues 81-94, including Sec_{92}) from the remaining protein, abolished the SOCE promoting activity of SELENOK [71]. Interestingly, resting macrophages actively cleave SELENOK via calpain-2 to maintain low levels of calcium flux. However, when macrophages are activated, the endogenous inhibitor of calpains, calpastatin, is upregulated, which allows full-length SELENOK to be expressed. Expression of full length SELENOK can then lead enhanced IP3R mediated calcium flux and turn on cellular programs related to active macrophage function. In this sense, dietary Se along with the calpain-2/calpastatin system are both regulators of SELENOK function. In fact, the endogenous inhibitor of calpain-2, calpastatin, protects SELENOK from cleavage and thereby serves as a positive regulator of SELENOK function [71, 72]. Dietary Se levels regulate the levels of Sec incorporation into SELENOK while calpain-2 regulates cleavage of the functional domain. To date, no other selenoproteins have been described as being proteolytically modulated by calpain enzymes, although investigations into this issue have not been extensive.

The definitive experiments showing the requirement of the Sec residue at position 92 of SELENOK for its function were recently published [60]. Recombinant versions of SELENOK containing either Sec_{92}, Cys_{92}, or Ala_{92} complexed to a soluble version of DHHC6 were used in PAT reactions to test the bioactivity of each. The results showed that only Sec_{92} improved the

catalytic efficiency of DHHC6, while Cys_{92} or Ala_{92} were equally insufficient to allow SELENOK to increase the catalytic efficiency of DHHC6. As mentioned above, selenoester bonds have been shown to have high reactivity in acyl transfer reactions [73]. This is consistent with the Sec residue in SELENOK being particularly suited to combine with DHHC6 for catalyzing protein palmitoylation as an important post-translational modification, and the fact that our studies showed that Sec cannot be replaced with Cys for protecting the thioester bond in the acyl-DHHC6 intermediate from hydrolysis. The role SELENOK plays in palmitoylation reactions and how it is regulated are illustrated in Figure 1.3.

SELENOK in cancer

There is a paucity of information on the exact role that SELENOK plays in carcinogenesis or tumor progression. However, the effects of SELENOK loss-of-function or gain-of-function in different tumor lines have been studied. For example, knockdown of SELENOK in human choriocarcinoma cells enhanced the proliferative, migratory, and invasive capacity of these cells, while over-expressing SELENOK had the opposite effect [74]. Similarly, overexpression of SELENOK in human gastric cancer BGC-823 cells reduced cell adhesion and migration [75]. Micro RNAs may also regulate SELENOK levels in certain cancers [76] and this may be cancer type specific or even vary between the cancer cell population within tumors. Given that SELENOK forms complexes with other proteins in order to exert it biological functions, manipulating the levels of SELENOK may alter the stoichiometry of the members within these complexes. Therefore, it may be that alterations in SELENOK expression that alter the optimum level within the complexes can disrupt functions required by different cancer cells at various stages, or different immortalized cell lines at different stages.

In a study assessing if the risk of prostate cancer is affected by polymorphisms in the gene encoding SELENOK, it was found that if Se status was taken into account, that a single nucleotide polymorphism (SNP) of *SELENOK*, located in the promoter region of the gene, is associated with advanced stage or high-grade disease risk [77]. Whether this SNP of SELENOK confers SELENOK-deficiency or SELENOK over-expression is unknown and is difficult to infer

based on the complex relationship between SELENOK and cancer, therefore more physiological models of SELENOK and cancer are needed.

The subsequent chapters present the results of our attempt to elucidate the role of SELENOK in a model of cancer with the following specific objectives: (i) determine the *in vivo* effects of SELENOK deficiency on primary melanoma tumor progression and metastasis, (ii) determine the mechanisms by which SELENOK affects melanoma cell proliferation, migration, and colony formation *in vitro*, and (iii) test a novel inhibitor against SELENOK for treating melanoma.

Figures

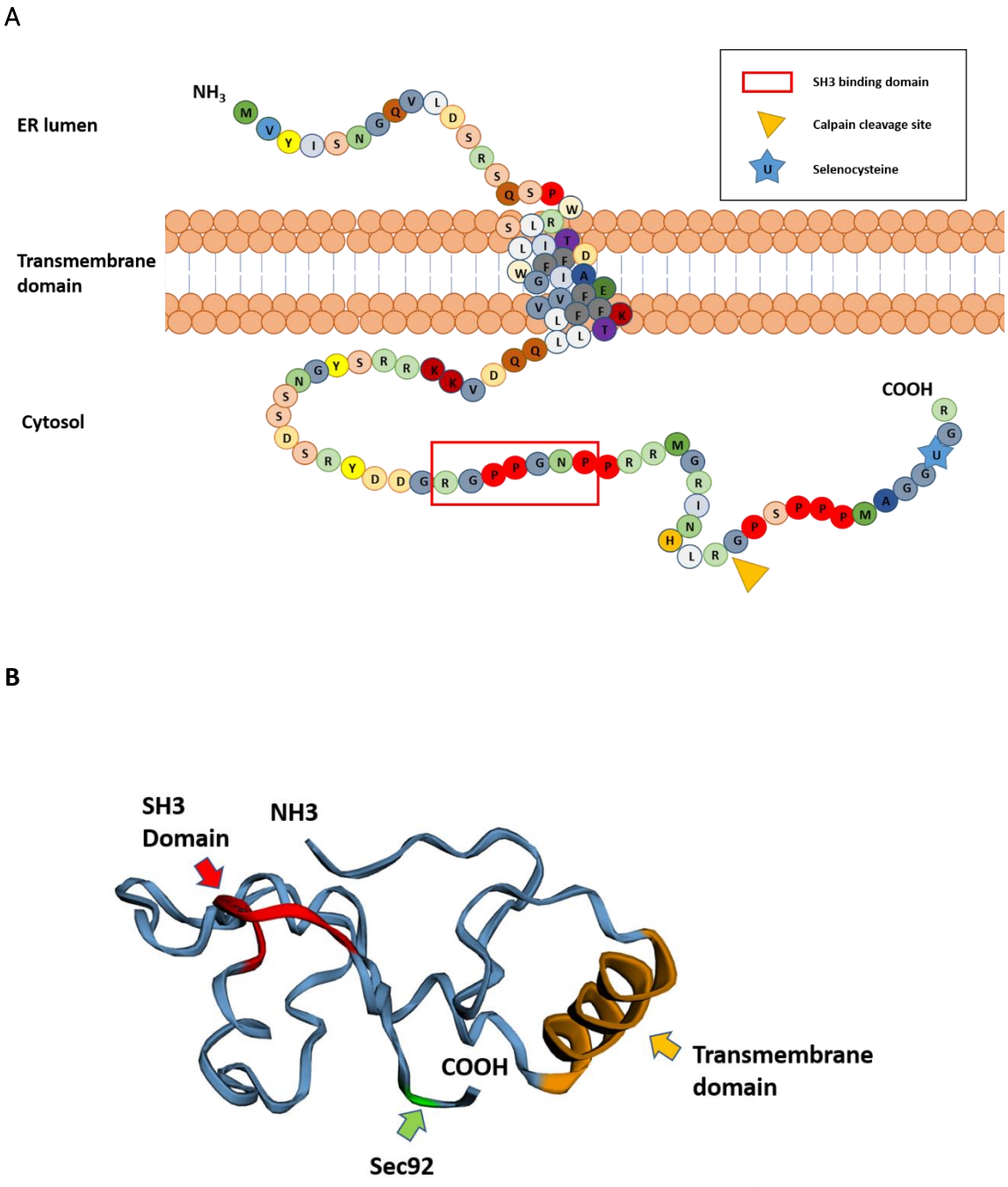

Figure 1.1 Predicted structure of SELENOK. (**A**) Schematic showing primary amino acid sequence and the predicted structure of SELENOK. SELENOK contains a single transmembrane

domain, a calpain cleavage site between residues 81 and 82, a proline rich SH3 binding domain (SH3BD), and a single Sec residue at amino acid position 92. (**B**) Predicted protein folding model was for SELENOK was generated using Phyre2 online protein fold recognition server and EzMol was used to generate protein display and image production. Red area represents the SH3 binding domain, orange area represents the transmembrane domain, and the green area represents the Sec residue.

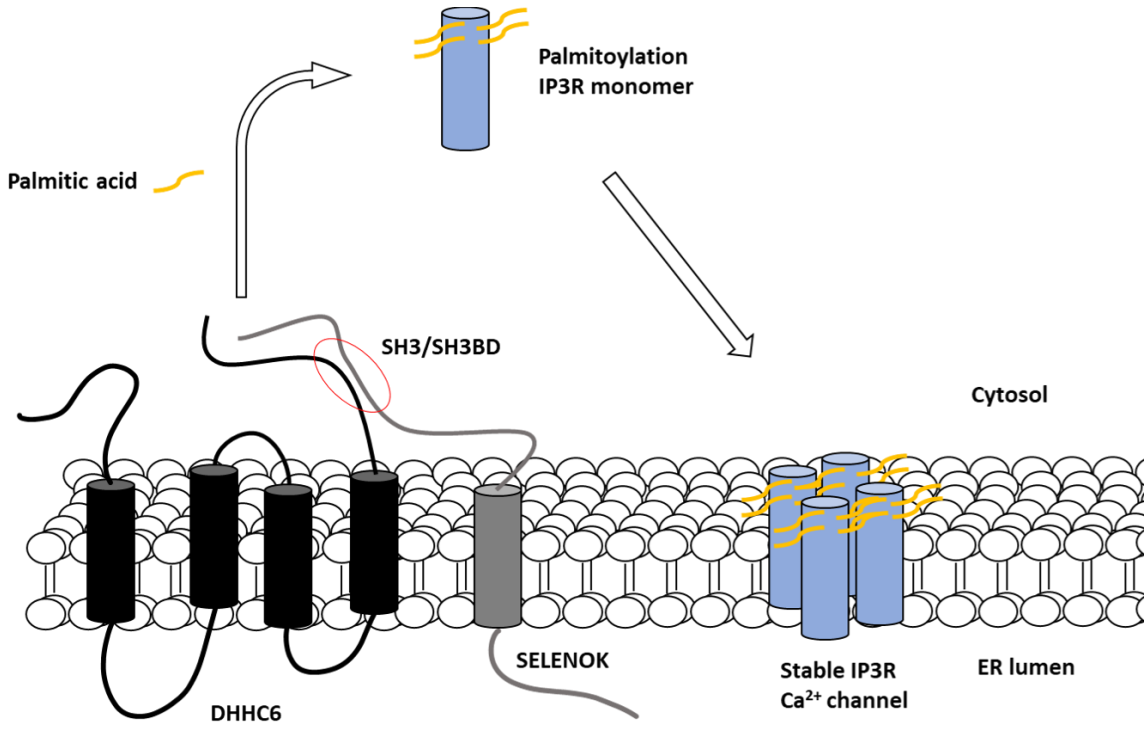

Figure 1.2 SELENOK/DHHC6 is necessary for palmitoylation and expression of the IP3R. Model demonstrating SELENOK and DHHC6 interacting via SH3/SH3BD (SH3 binding domain) motifs and subsequent transfer of palmitate to the IP3R, resulting in the stable expression of the IP3R in the membrane of the ER.

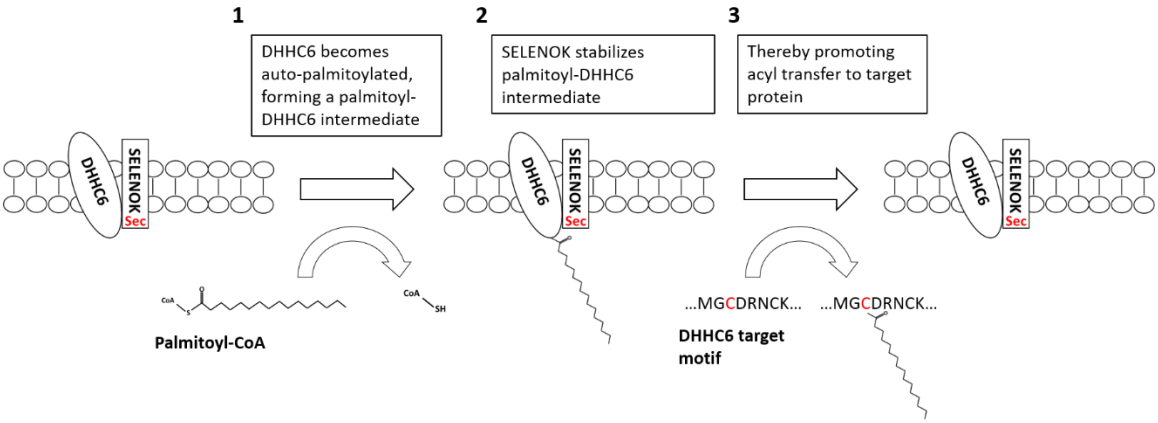

Figure 1.3 SELENOK stabilizes the DHHC6 palmitoylated intermediate and enhances palmitoylation of DHHC6 target. DHHC6 palmitoylates its targets protein in a two step-process: 1) DHHC6 is auto-palmitoylated in the presence of palmitoyl-CoA, and 2) the palmitate group is transferred to a DHHC6 target. MGCDRNCK represents the palmitoylation consequence sequence on the N terminus of CD36. SELENOK may prevent hydrolysis (futile cycle) of palmitoylated DHHC6.

Chapter 2. Selenoprotein K deficiency inhibits melanoma by decreasing cytosolic calcium levels required for tumor growth and metastasis

Introduction

Ca^{2+} is a ubiquitous signaling cation and a widely used secondary messenger that is critical to a variety of cellular processes. The primary store of intracellular Ca^{2+} is the ER, and cytosolic Ca^{2+} concentration is maintained at nanomolar levels by plasma membrane Ca^{2+} ATPases and SR/ER Ca^{2+} ATPases that pump Ca^{2+} into the extracellular space and the ER lumen respectively [78]. Activation of various surface receptors activates phospholipase C that subsequently hydrolyzes phosphatidylinositol 4,5-bisphosphate into diacylglycerol and inositol 1,4,5-trisphosphate (IP3). IP3 is an agonist of ER-membrane IP3 receptors (IP3Rs) and ligand engagement results in Ca^{2+} release from the ER lumen, which is sensed by the EF-hand motif of stromal interaction molecules (STIM1 and STIM2) within the ER [79]. This induces STIM1 to oligomerize and translocate to ER-plasma membrane junctions where it interacts with Orai Ca^{2+} calcium channels and allows Ca^{2+} to enter the cytosol from the extracellular space [51]. This process is termed store operated Ca^{2+} entry (SOCE) [80] and is the primary mechanism by which non-excitable cells utilize for activating Ca^{2+} dependent signaling cascades that are required for cellular functions such as proliferation and migration [49].

When healthy, normal cells transform into malignant tumor cells Ca^{2+} homeostasis and signaling may be altered in a process referred to as Ca^{2+} remodeling [81]. SOCE and the downstream Ca^{2+} dependent signaling cascades, are exploited by cancer cells to increase their capacity to proliferate, migrate, and survive. Because SOCE is important for both primary tumor growth and metastasis to other sites, molecules regulating SOCE are logical targets for developing anti-cancer therapeutics [82, 83]. However, little is known regarding the targetable mechanisms that drive SOCE in malignant melanoma. Therefore, there is a need to elucidate the extent to which SOCE drives malignant melanoma and to elucidate new SOCE associated targets.

SELENOK is a member of the selenoprotein family, of which there are 25 members in humans, that each contain the 21st amino acid, selenocysteine. SELENOK is an ER transmembrane protein that regulates IP3R driven Ca^{2+} flux [37]. Expression levels of SELENOK are regulated by dietary selenium [37, 84] and its function is regulated in in some cell types by calpain cleavage [71]. The mechanism by which SELENOK regulates Ca^{2+} flux is its role as a cofactor that binds to the acyl transferase, DHHC6, to catalyze the palmitoylation of the IP3R [52]. In the absence of SELENOK/DHHC6 catalyzed addition of palmitate to the tetrameric IP3R, Ca^{2+} release from the ER is impaired [10]. The following chapter provides evidence that SELENOK is indeed necessary for effective Ca^{2+} flux in human melanoma cells and SELENOK deficiency reduces their growth and stemness properties, leading to reduced proliferation and migration *in vitro* and *in vivo*.

Background

Melanoma

Melanoma is a malignancy that arises in the melanocytes present in the basal layer of the epidermis. Although Melanoma comprises of only 4 percent of all skin cancers, it is responsible for 80 percent of deaths in all dermatological cancer [85]. The 10-year survival rate for patients with late stage metastatic melanoma has been estimated to be as low as 7 percent [85]. The Clark Model of Melanoma was established in the 1970s and describes the stepwise transition of melanocytes to malignant melanoma with the following six steps of tumor progression: 1) acquired melanocytic nevus (mole); 2) a melanocytic nevus with proliferation into the basal layer of the epidermis; 3) a melanocytic nevus with aberrant differentiation and abnormal appearance of cell nuclei; 4) radial growth of primary melanoma; 5) vertical growth of primary melanoma; and 6) metastatic melanoma. A genetic basis of melanoma progression has been established based on the Clark model [85, 86]. The acquisition of melanocytic nevi frequently express activating BRAF mutations [85] followed by a temporary cessation in proliferative activity.

The next step in the evolution of melanoma, involving the proliferation of transformed cells into the basal layer of the epidermis, may involve the inactivation of CDKN2A. This is supported by the observation that 25-40 percent of patients with familial melanoma (and develop dysplastic nevi) have germline mutations in cyclin-dependent kinase inhibitor 2A (CDKN2A) [87]. The radial expansion of melanoma, whereby the neoplastic melanocytes invade into the epidermis, is associated with the activation of human telomerase reverse transcriptase (hTERT) [88]. Finally, vertical growth of primary melanoma and the ability of transformed melanocytes to metastasize and colonize distant tissues involve various mutations that increase survival, inhibit apoptosis, and promote epithelial to mesenchymal transition (EMT). Specifically, loss of phosphatase and tensin homolog (PTEN) inhibits apoptosis via AKT activation, constitutive activation of Ras or over-expression of protein kinases, and loss of E-cadherin and $\alpha V\beta 3$ integrin [89].

Risk factors and molecular mechanisms of ultraviolet damage response

The risk factors for the development of melanoma include a family history of melanoma, multiple benign or abnormal nevi, immunosuppression, sun sensitivity, and exposure to ultraviolet (*uv*) radiation [90]. Each risk factor has a variety of environmental and genetic detriments that are not mutually exclusive. For example, sensitivity to *uv* light is associated with polymorphisms that affect the risk of developing melanoma, particularly polymorphisms within the alleles encoding the melanocortin receptor 1 (MC1R) and genes involved in nucleotide excision repair (NER) [91]. The importance of NER is clear in the case of patients with Xeroderma Pigmentosum (XP), a rare disorder exemplified by *uv* hypersensitivity syndrome caused by the homozygous deletion in any one of the eight necessary effector proteins that execute NER. XP patients exhibit extreme *uv* sensitivity and develop premalignant lesion and skin cancer at a high frequency. While people with XP clearly demonstrate the importance of NER in skin cancer prevention, NER polymorphism and skin cancer incidence may contribute to skin cancer development, including melanoma, in the general population [91]. *uv* radiation causes genomic damage, such as thymine dimers and the formation of DNA damaging reactive oxygen species (ROS) [92]. Molecularly, *uv* exposure induces the generation of α-melanocyte-stimulating hormone (α-MSH) MC1R. MC1R engagement by α-MSH leads to the activation of adenylyl cyclase which converts ATP to cAMP [93, 94]. cAMP accumulation activates protein kinase A (PKA), leading to a variety of downstream events including upregulation of genes associated with the production of melanin via the cAMP responsive binding element (CREB) [95] and upregulation of genes involved in NER [96, 97]. Therefore, individuals with sub-optimal MC1R signaling have a higher risk of developing melanoma, not only because their skin is under-melanized, but also because they have impaired DNA damage repair mechanisms.

Ca^{2+} signaling in cancer

Tightly controlled and regulated calcium signaling is necessary for normal cellular functioning such as proliferation, gene transcription and survival. This regulation involves specialized Ca^{2+}

pumps, channels, exchangers, calcium binding proteins that maintain calcium homeostasis in the cell [49, 98]. Cells at rest typically maintain an intracellular Ca^{2+} concentration ($[Ca^{2+}]$) of approximately 100 nM and a $[Ca^{2+}]$ of 100-800 μM in the ER [99]. The extremely low $[Ca^{2+}]$ in the cytosol is necessary for Ca^{2+} to act as a ubiquitous secondary messenger, allowing the cell to "decode" the spatially and/or temporally variable changes in cytosolic free Ca^{2+} and transduce the appropriate signals downstream [98]. When normal cells transform into malignant tumor cells, calcium homeostasis and calcium signaling may be altered. Perhaps most simply, protein expression of specific Ca^{2+} channels and pumps can be altered in various cancer types. For example, expression studies have identified numerous Ca^{2+} channels and pumps as potential therapeutic targets for brain [100] breast [101], prostate [102], and ovarian cancers [103], implying their aberrant expression in these cancers. It should be noted that post-translational modifications of the components of calcium signaling may also contribute to Ca^{2+} remodeling in cancer, such as altered Ca^{2+} pump or channel localization [104]. For example, while not occurring in a cancer cell type, phosphorylation of STIM1 inhibits SOCE in endothelial cells and may be involved in regulating endothelial permeability responses [105].

Because SOCE is the major mechanism by which non-excitable cells import calcium from the extracellular space and refill their calcium store, many of the calcium signaling tools mentioned above are directly involved in SOCE. Recently, an interest in targeting SOCE components as a treatment for various cancers has emerged. For example, Yang et al. demonstrated that pharmacological blockade or silencing of STIM1 or Orai1 reduced migration and metastasis of breast cancer cells [106]. SOCE is also involved in melanoma cell proliferation and migration [107], and cell migration, proliferation, and angiogenesis in cervical cancer [108]. This chapter will focus on the effects of SELENOK on one of the main components of SOCE, namely the IP3R. Therefore, the IP3R and select downstream signaling pathways induced by IP3R mediated Ca^{2+} flux will be discussed in detail. However, because of the ubiquitous nature of Ca^{2+} signaling, many Ca^{2+} dependent signaling pathways may be affected by reduced Ca^{2+} flux, but are not mentioned here.

Inositol trisphosphate receptor and its regulation

IP3Rs are a family of intracellular ligand-gated Ca^{2+} release channels localized primarily in the ER in almost all cell types [109]. IP3R modulates cytoplasmic free [Ca^{2+}], and thereby is involved in the regulation of processes as diverse as learning and memory, synaptic transmission, membrane trafficking, motility, cell proliferation, and apoptosis [110]. Modulation of cytosolic [Ca^{2+}] via IP3R involves the activation of PLC by a diverse set of cell surface receptors including G-coupled protein receptor (GPCRs), receptor tyrosine kinases (RTKs), toll like receptors (TLRs), and T cell receptors (TCRs). PLC converts the membrane bound lipid PIP_2 into IP3 and DAG [110]. IP3 diffuses in the cytoplasm and binds to the IP3R at the cytoplasmic surface of the ER. The ER is the major calcium storage organelle in most cells and therefore opening of IP3R results in calcium movement down its electrochemical gradient from the ER into the cytoplasm. Ca^{2+} release from the IP3R is tightly spatially and temporally regulated by a variety of factors such as the availability of Ca^{2+}, binding proteins, and the properties of the various isoforms of the (IP3R). This regulation restricts the range of action of Ca^{2+} to approximately 5 μm [111] and enables IP3R mediated Ca^{2+} signaling to be remarkably specific as well as diverse.

The IP3R family (IP3R1, IP3R2, and IPR3) is encoded by three separate genes in vertebrate cells [112, 113] where the primary amino acid sequences of the three isoforms share 60-80% sequence identity [114]. In mammals, the IP3R is expressed in all cell types [115, 116], and except for the central nervous system, each cell type expresses more than one isotype [117]. IP3R1 expression is prominent in the brain and cerebellum and IP3R2 expression is prominent in epithelia cells in the kidney and heart [118]. IPR3 is highly expressed in the testis and in fibroblast cells [118, 119]. Cell type dependent, differential expression of IP3R isoforms that differ in cellular localization and ligand sensitivity implies that each isoform confers specificity for unique cellular processes. For example, each isoform may have different sensitivity to ubiquitin-related downregulation after activation via IP3 [120] and numerous studies have demonstrated that the IP3 binding affinity differs among the three channel isoforms [121]. However, the hierarchy of IP3 binding affinity for the three channel isoforms varies from study to study [122-124].

The IP3R is a tetramer with each subunit having a molecular mass of ~300 kDa [125]. The structure of each IP3R molecule consists of a large NH_2 terminus (comprises 85% of the protein's mass) localized to the cytoplasm, a hydrophobic, six membrane-spanning regions in the ER membrane that forms the ion-conducting pore, and a short cytoplasmic COOH terminus [110]. The NH_2 terminus contains the IP3 binding domain at residues 226-578 and a regulatory domain at residues 586-2276 [110]. Genetic deletions within the regulatory domain result in a disruption of channel function [126]. The two major regulators of IP3R function are IP3 and Ca^{2+}, both of which can act as co-agonists [127, 128]. IP3 regulation of IP3R can be viewed as modulation of IP3R potentiation to [Ca^{2+}]. More specifically, IP3-induced Ca^{2+} flux is regulated in a biphasic manner, resulting in potentiation of the IP3R at low [Ca^{2+}] and inhibition at high [Ca^{2+}] for all three isoforms of IP3R [129]. A model has been proposed whereby IP3 binding prevents binding of Ca^{2+} to the regulatory domain and reciprocally, Ca^{2+} binding of the regulatory domain prevents IP3 binding [130]. Additionally, IP3Rs are regulated by phosphorylation by numerous protein kinases including PKA, protein kinase B (PKB/Akt), protein kinase C (PKC), Ca^{2+}/ CaM-dependent protein kinase II, cyclic-dependent kinases (CDKs), Rho kinases, mammalian target of rapamycin (mTor), cGMP-dependent protein kinases, and a variety of protein tyrosine kinases [131]. PKB/Akt is a proto-oncogene associated in cellular survival and growth [132]. Each of the three isoforms of IP3R have the conserved phosphorylation motif RXRXX(S/T) at their C-terminus and phosphorylation at this site promotes survival [133, 134]. Furthermore, the antiapoptotic protein Blc-2 has been shown to physically interacts with IP3R1 isoform, increasing IP3R1 phosphorylation and calcium flux through the IP3R1, thus promoting survival [135]. Pertinent to the data presented in this chapter, the IP3R is palmitoylated on three cysteine residues (C56, C849, and C2214), and one or more of these post-translational modifications is necessary for its proper expression in the ER membrane [52].

Mitogen activated protein pathway

The Ras/Raf/MEK (mitogen-activated protein kinase/ERK kinase)/ERK (extracellular-signal-regulated kinase) pathway is a conserved signaling pathway that governs proliferation, differentiation and survival in all eukaryotes [136]. The signaling cascade is activated by a wide variety of receptors (RTKs, integrins, and ion channels) and their various ligands (growth factors, differentiation factors, and tumor-promoting molecules). In general, a set of adaptor proteins such as growth-factor-receptor-bound protein 2 (GRB2) link guanine nucleotide exchange factors like son of sevenless (SOS) to the receptors, thereby transducing the signal to small GTP-binding proteins (Ras, Rap1). These small GTP-binding proteins activate the main component of the cascade composed of a MAPKKK (Raf), a MAPKK (MEK1/2), and MAPK (ERK). A phosphorylated/activated ERK dimer can then translocate to the nucleus where and phosphorylate a variety of transcription factors regulating gene expression [137].

Dysregulation of the small GTPase Ras or its downstream effectors such as ERK have been shown to be critical in the tumorigenesis of many cancer types [138]. In melanoma, activating Ras mutations are associated with only 15 percent of cases [85] and are limited to N-Ras [139]. While activating Ras mutations are rare in Melanoma, BRAF somatic mutations are associated with 50 percent of melanomas which results in constitutive activation of ERK [85]. Mutations in N-Ras stabilize the GTP bound form of the protein and thus maintains N-Ras in an activated state [140]. Mutations in BRAF occur within the kinase domain and approximately 80 percent of them due to a single substitution (V599E) [141]. BRAF mutations occur at similar levels in benign nevi and in metastatic melanoma [142]. Because most benign nevi can stay dormant for decades, the similarity in observed frequency of BRAF mutations suggest that nevi must acquire additional mutations to become malignant, such as loss of tumor suppressors as described in the Clarke Model [85].

Calcineurin-Calmodulin-NFAT axis

Nuclear factor of activated T cells (NFAT) proteins are expressed in most immune cells and promote the transcription of genes vital to the proper functioning of the immune system [143] and the proliferation and survival of many other cell types [144]. NFAT activity is regulated by the calcium/calmodulin dependent phosphatase calcineurin [144]. Specifically, calcium influx from SOCE (described in chapter 1) activates the calcium sensor calmodulin which binds to the regulatory domain of calcineurin, causes a conformational change that removes the autoinhibitory domain from the active site, which results in the activation of the phosphatase [145]. Activated calcineurin then dephosphorylates multiple serine residues near the N-terminus of NFAT proteins, revealing a previously masked nuclear localization sequence (NLS) and results in the translocation of NFAT from the cytoplasm to the nucleus [146]. Because NFATs bind their DNA target sequences with relatively weak affinities, they rely on a variety of cooperative transcription factors to enhance binding to promoter regions [147, 148]. Thus, NFAT complexes can integrate Ca^{2+}/calcineurin activity, along with additional signals, to result in a diverse set of cellular programs, including differentiation, growth, and survival [149].

Dysregulation of calcineurin/NFAT signaling has been observed in a variety of solid tumors and lymphomas [150] and NFAT may be a downstream mediator of oncogenic BRAF in metastatic melanoma [151]. NFAT proteins may play an important role in the dysregulation of cell cycle control via aberrant Ca^{2+} signaling. For example, overexpression of a constitutively active mutant of NFAT1 has been shown to be sufficient to induce a transformed phenotype in preadipocyte 3T3-L1 fibroblasts and is associated with aberrant expression of cell-cycle related genes such as pRB, c-myc, cyclin D1, and cyclin D2 [152]. Furthermore, ectopic expression of highly activated NFATc1 has been observed in pancreatic cancer cells *in vitro* that promoted c-myc generation and thus increased G1/S phase transition in Panc-1 and ASPC-1 cell lines [153]. Additionally, NFAT signaling has been implicated in the development of tumors of epithelial origin such as colon carcinoma. In the human colon carcinoma cell lines Caco-2, HCT116, and HT29, activation of NFAT1 and NFAT2 was shown to induce the transcriptional upregulation of the gene encoding cyclooxygenase-2 (COX-2), which can lead to increased cell survival,

angiogenesis, and proliferation [154]. Finally, research in our laboratory has demonstrated that inhibiting SOCE in a human melanoma cell line, decreases calcineurin activity and results in less NFAT translocation to the nucleus that may impair cellular programs that contribute to tumorigenesis (data in results).

Cancer stem cells

Cancer stem cells (CSCs) are a small subset of a tumor population with the indefinite potential for self-renewal that drive tumorigenesis [155]. A tumor can be conceptualized as an abnormal organ that originated from a tumorigenic cancer cell that that acquired the ability to indefinitely proliferate. Viewed from this perspective, fundamental properties of cell biology can be applied to the tumor, such as normal stem cell biology. Indeed, although most tumors have a clonal origin [156, 157] they contain a heterogeneous combination of cells; this suggests that, akin to normal stem cells, tumors contain a specialized cell type that give rise to heterogenous cell progeny and can indefinably replicate. Evidence for this theory was first documented when mouse myeloma cells, obtained from myelomatous ascites, were tested in an *in vitro* colony-forming assay and only 1 in 100 – 10,000 cells were able to form colonies [158]. Furthermore, only 1-4% of leukemia cells were able to form spleen colonies when transplanted [159] and a small subset of human adult acute myeloid leukemia (AML) cells (0.2%), which could be identified as $CD34^{+}CD38^{-}$, could transfer AML to NOD/SCID mice while other subsets could not [160]. Correctly identifying the sub-population of cancer cells that contribute to tumorigenesis can lead to more directed therapeutics for treating cancer.

One of the most consistently observed markers of CSCs is prominin 1 (Prom1 or CD133) [161-164]. Prom1 is a member of the pentaspan transmembrane glycoprotein family [165] and was originally discovered as a marker specific for hematopoietic stem cells [166]. Prom1 function is mostly unknown, however it is selectively associated with plasma membrane protrusions via cholesterol binding [167] and may play a role in the maintenance of retinal photoreceptors [168]. Prom1 was associated with and used to isolate brain tumor stem cells (BTSCs) from human samples. The BTSCs demonstrated a marked capacity for proliferation, self-renewal, and

differentiation [164]. Similarly, Prom1 was shown to be critical for growth and metastasis of human metastatic melanoma cells and shRNA knockdown of Prom1 resulted in reduced spheroid formation and migratory capacity [169]. Furthermore, microarray analysis of Prom1 knockdown FEMX-1 melanoma cells showed upregulation of genes associated with Wnt inhibitors, suggesting that Prom1 interacts with the canonical Wnt pathway [169].

Melanoma tumor cells utilize SOCE for their growth and proliferation similar to what has been observed in immune cells. Because genetic deletion of SELENOK in immune cells inhibited SOCE it is logical that KO of SELENOK in melanoma tumor cells may reduce their ability to grow and proliferate via a similar mechanism. Furthermore, previous investigations undertaken by the Hoffmann laboratory demonstrated the necessity of the Sec residue in SELENOK for its biological function. Therefore, we utilized two tools to elucidate the role of SELENOK in metastatic melanoma: (i) complete KO of SELENOK in a mouse model of melanoma and (ii) a CRISPR-Cas9 generated, truncated version of SELENOK that does not contain the Sec residue in a melanoma cell line. The effects of SELENOK deletion/truncation on melanoma cells are presented below.

Results

Loss of functional SELENOK in melanoma cells leads to decreased proliferation

In some cases, but not all, molecular components of SOCE are overexpressed in melanoma tumor tissue compared to healthy tissue [170]. Therefore, SELENOK levels in early and late stage malignant melanoma tissues from a small group of patients (N = 10) were examined by histological analysis and rank ordered from 0 (negative) to 3 (strong signal in at least 25% of cells). No differences were found compared to normal control tissue (Figure S2.1). Next, western blot analysis was performed to test whether SELENOK protein expression is increased in metastatic melanoma cell lines compared to primary melanocytes. SELENOK protein expression in three NCI-60 validated human melanoma cell lines (SK-MEL-2, SK-MEL-28, and MALME-3m) and primary human melanocytes were evaluated and protein expression of SELENOK was not significantly increased in the melanoma cell lines compared to primary melanocytes (Figure 2.1A).

SELENOK is required for the post-translational palmitoylation of the IP3R and its stable expression in the ER membrane allows for proper SOCE in immune cells [10]. Previous studies have demonstrated that knockdown (KD) of molecules involved in SOCE (e.g., Orai1) resulted in decreased migration and proliferation of melanoma cells [107]. Therefore, it is conceivable that SELENOK-deficient melanoma cells may exhibit impaired SOCE dependent growth and migration. To test this hypothesis, a CRISPR/Cas9 approach was used to generate a functional knock-out of SELENOK in the SK-MEL28 cell line with the domain necessary for palmitoylation of IP3R removed but with the SH3BD left intact (Figure 2.1B). Preserving the SH3BD while truncating the palmitoylation functional domain in SELENOK allows SELENOK to interact with DHHC6 but prevents the enhanced palmitoylation efficiency that full-length SELENOK provides [52]. This CRISPR/Cas 9 truncated version of SELENOK is similar to the calpain cleaved version of SELENOK in resting macrophages [71] and putatively decreases palmitoylation of the IP3R by a similar mechanism. Two independent clones were identified and subsequently expanded to produce stable cell lines as determined by western blot analysis

(Figure 2.1C). One of these cell lines contained an edited allele encoding a truncated version of SELENOK and one unedited allele encoding the full-length version of SELENOK (clone 3) or both alleles of SELENOK truncated (clone 7). The western blot results were consistent with Sanger sequencing of the clones (Figure S2.2). First, a proliferation assay was performed that compared the rates of proliferation of unedited SK-MEL28 cells, clone 3, and clone 7 for four days. Clone 3 cells and unedited cells proliferated at comparable rates, whereas clone 7 proliferation rates were reduced up to approximately 3-fold (Figure 2.1D). This suggests that at least one allele of SELENOK is necessary for normal proliferation in SK-MEL28 cells. Next, an *in vitro* model for wound healing was performed to determine if SELENOK truncation would reduce the ability of the cells to grow and migrate into the scratched area. These results showed that clone 7 cells filled the scratched area to a significantly lower degree compared to unedited cells and clone 3 cells (30 % change in area compared to 75 % change in area respectively) (Figure 2.1E).

SELENOK-truncated melanoma cells exhibit lower cytosolic Ca^{2+} levels

The reduced migration and proliferation resulting from SELENOK truncation shown above may be due to reduced Ca^{2+} signaling caused by a decrease in IP3R expression, similar to what has been observed in SELENOK deficient immune cells [37]. To determine if SELENOK truncation affects intracellular [Ca^{2+}], ester caged IP3 was loaded into unedited or SELENOK-truncated clone 7 cells, and *uv* light was used to uncage the IP3 to induce Ca^{2+} movement from the ER into the cytosol via the IP3R. Compared to unedited controls, SELENOK-truncated clone 7 cells demonstrated at least a 3-fold reduction in intracellular [Ca^{2+}] in the cytosol in response to IP3 engagement of the IP3R (Figure 2.2A). In separate trials, both cell types were treated with thapsigargin, which bypasses the IP3R and results in rapid Ca^{2+} efflux from the ER. Intracellular [Ca^{2+}] was similar in response to thapsigargin treatment for both clone 7 cells and unedited cells (figure 2.2B), suggesting that reduced intracellular [Ca^{2+}] in clone 7 cells is specific to IP3R deficiency. Peak intracellular [Ca^{2+}] from repeat experiments are shown in Figure 2.2C-D. Control experiments were performed in order to test if the difference in intracellular [Ca^{2+}] observed would occur at varying levels of caged IP3 concentrations including *uv* pulse alone.

The results indicated that SELENOK-truncated clone 7 cells demonstrated at least 2-fold lower intracellular [Ca^{2+}] at all IP3 concentrations tested compared to unedited cells (Figure S2.3A-B). A small increase in intracellular [Ca^{2+}] was observed when the cells were exposed to *uv* pulse alone (no IP3 loaded), however, no difference between unedited and clone 7 cells was observed (Figure S2.3C).

Calcineurin activity and NFAT nuclear localization are reduced in SELENOK- truncated melanoma cells.

Modulation of Ca^{2+} levels in the cytoplasm can affect a wide variety of Ca^{2+} dependent cell signaling systems including calcineurin signaling [144]. Dysregulation of calcineurin activity has been observed in many cancers [149] and is a downstream mediator of the common BRAF mutation common in melanomas [150]. Therefore, the enzymatic activity of the phosphatase calcineurin was measured in unedited and clone 7 cells. Calcineurin activity in SELENOK-truncated clone 7 cells was lower compared to unedited cells (Figure 2.3A). The calcineurin inhibitor Cyclosporin A (CsA), lowered unedited cell calcineurin activity levels to 0.0035 nmol phosphate/min, equivalent to the rate exhibited in clone 7 cells, but did not affect calcineurin activity in clone 7 cells. Importantly, differences in phosphatase activity between unedited and clone 7 cells were not due to the activity of PP1 or PP2A phosphatases (Figure S2.4A) or differences in levels of calcineurin subunits A and B or calmodulin (Figure S2.5).

When calcineurin is activated it cleaves multiple phosphate groups from NFAT and induces its translocation to the nucleus [146]. Therefore, to test if SELENOK-truncation affects NFAT translocation to the nucleus, recombinant GFP-NFAT was transfected into unedited and clone 7 cells and translocation was visualized using confocal microscopy. Higher levels of NFAT in the cytosol of clone 7 cells compared to unedited cells was observed (Figure 2.3B), which is consistent with lower levels of endogenous calcineurin activity in SELENOK-truncated clone 7 cells. Taken together, these results suggest that reduced Ca^{2+} flux due to the absence of functional SELENOK in clone 7 cells, results in lower Ca^{2+}/calmodulin-dependent calcineurin

activity and thus decreased translocation of the transcription factor NFAT to the nucleus, which may result in impaired downstream programs such as growth, proliferation, and migration.

SELENOK deficiency alters transcriptional control of metabolism and migration and stemness

Because the calmodulin-calcineurin-NFAT signaling axis was altered in SELENOK-truncated clone 7 cells compared to unedited cells, SELENOK truncation may lead to altered gene transcription. Gene array experiments were conducted that led to the identification of 166 up-regulated and 113 downregulated transcripts by greater than 2-fold in clone 7 cells compared to unedited control under basal conditions. The full list of transcripts up- or down- regulated by greater than 2-fold is shown below (Figure S2.6) and a heat map was generated that includes genes related to cancer growth, metabolism, metastasis, and stemness (Figure 2.4A). Transcripts decreased by SELENOK-truncation included some involved in promoting growth and metabolism (e.g. XYLT1 and ACSM3), invasion and metastasis (e.g. MMP1 and TRPV4), and stemness (e.g. Prom1). Furthermore, SELENOK-truncation increased level of transcripts involved in promoting cell attachment (e.g. ITGA2 and ITGB5).

In order to confirm the gene array results, real-time PCR was performed. The real-time PCR results were consistent with the gene array analysis for the genes selected (Figure 2.4B). Next, protein levels for ITGA2, ITGB5, and Prom1 were evaluated by western blot and flow cytometry. Consistent with the changes in mRNA, protein levels were increased for ITGA2 and ITGB5, and decreased for Prom1 in SELENOK-truncated cells (Figure 2.5A-C). Signaling pathway analyses revealed how the factors listed above and other signaling nodes that are cancer related were affected by SELENOK truncation (Figure S2.7) Taken together these results suggest that SELENOK truncation in melanoma cells lead to reduced IP3R generated Ca^{2+} flux and altered cell programs that resulted in decreased growth and metabolism, an increase in cell attachment, and an attenuated stem-like phenotype under non-stimulated conditions.

SELENOK truncation increases adhesion and reduces migration in melanoma cells

The increased protein expression in the integrins ITGA2 and ITGB5 in SELENOK-truncated clone 7 cells, although modest, suggested that SELENOK deficiency may alter cell migration and attachment. To determine if SELENOK deficiency impairs migration rates of melanoma cells, an electrode/resistance assay was performed using unedited and SELENOK-truncated clone 7 cells. The rate of migration of both cell types was estimated by the resulting resistance, measured in μm/h, caused by cellular movement into the "wound". Unedited cell movement into the cleared area was approximated to be 300 μm/h while clone 7 cell movement was estimated to be approximately 150 μm/h. (Figure 2.6A). Extracellular matrix (ECM) proteins play an integral role in the initial steps of migration and invasion during metastasis [171], so adherence and transwell assays using collagen I or fibronectin matrices were performed. SELENOK-truncated clone 7 cells showed relative lower transwell migration and relative higher adherence in the presence of both collagen I and fibronectin compared to unedited cells (Figure 2.6B-C). These results suggest that deficiency in functional SELENOK in melanoma cells increases adhesion to ubiquitous components of the ECM while reducing their ability to migrate.

***In vivo* SELENOK-deficiency reduces melanoma progression and metastasis**

To determine the role of SELENOK in melanoma progression *in vivo,* we utilized a spontaneous melanoma transgenic (Tg) mouse model that overexpresses glutamate receptor 1 (Grm1) under the control of the melanocyte specific tyrosine-related protein 2 (Trp2) promoter [142, 172]. This mouse model is characterized by the development of melanoma on the ears, tails, perianal region, and metastases to the draining lymph nodes, liver and lung between 2-4 months of age with 100% penetrance. Using these mice, a breeding scheme was developed to delete the *SELENOK* gene on the Grm1-Tg background. This breeding scheme resulted in littermates having three different genotypes: Grm1/SELENOK$^{+/+}$, Grm1/SELENOK$^{+/-}$, and Grm1/SELENOK$^{-/-}$. The littermates grouped by different SELENOK expression levels (normal vs. deletion) were used to evaluate the progression of primary and secondary tumors under differing SELENOK expression conditions. Male and female cohorts from the littermate control

groups were analyzed separately for tumors on the tails and ears at 4 months of age. Gross anatomical evaluation of littermates demonstrated that Grm1-Tg mice with both alleles of SELENOK knocked out exhibited lower levels of primary tumors and less metastases to the draining lymph nodes (Figure 2.7). The Grm1-Tg mice with either one or two alleles of SELENOK developed intermediate to severe melanoma on the tails and ears and metastases to the draining lymph nodes, observable as pigmented cells in the inguinal and auxiliary lymph nodes. The results were similar for males and females, suggesting no sex differences in terms of SELENOK deficiency on melanoma in this model. The melanoma in the Grm1-Tg mouse model is not lethal [142], therefore, survival analyses was not performed. However, the mice in the littermates were followed up to 8 months of age and the Grm1/SELENOK$^{-/-}$ mice continued to exhibit a lesser burden of primary and secondary tumor formation compared to Grm1/SELENOK$^{+/+}$ and Grm1/SELENOK$^{+/-}$ littermates for both sexes (Video 1).

To confirm deletion of SELENOK in Grm1/SELENOK$^{-/-}$ mice and the consequent reduction of IP3R expression as observed SELENOK-truncated SK-MEL28 cells, western blot was performed. As expected, the littermates with complete deletion of SELENOK exhibited relatively lower levels of IP3R compared to Grm1/SELENOK$^{+/+}$ and Grm1/SELENOK$^{+/-}$ littermates in splenocytes (Figure 2.8A). To quantify tumor expression in the tails and ears of the littermates, a microscopy approach was used involving color threshold analyses of melanin levels in tail and ear tissue cross-sections. The three littermate genotypes, Grm1/SELENOK$^{+/+}$, Grm1/SELENOK$^{+/-}$, and Grm1/SELENOK$^{-/-}$ were analyzed for both male and female mice at 4 months of age (N = 7 per sex per genotype). In addition, two control groups not expected to develop tumors due to absence of the Grm1 transgene were also analyzed: C57BL/6J and SELENOK$^{-/-}$ mice (N = 7 per sex per genotype). Analyses of pigmented areas, likely due to melanin producing melanoma cells, demonstrated that Grm1/SELENOK$^{+/+}$ and Grm1/SELENOK$^{+/-}$ mice expressed pigmented tissue 60-70% relative to normal tissue. However, Grm1/SELENOK$^{-/-}$ mice expressed only 30% pigmented tissue compared to normal tissue, which is comparable to both control groups (Figure 2.8B-C). The results were similar for both male and female cohorts in both tissues examined. Next, cells were dissociated from the tails, using the same groups as above, and flow cytometry was employed to determine levels of

cells expressing the Prom1 cancer stem cell marker [173]. Results indicated that and Grm1/SELENOK$^{+/+}$ and Grm1/SELENOK$^{+/-}$ mice exhibited approximately 40% Prom1+ cells compared to approximately 25% Prom1+ cells in Grm1/SELENOK$^{-/-}$ mice and controls (Figure 2.8D), which is consistent with the cell line data above showing that SELENOK deficiency decreases cellular markers of stemness.

Finally, to evaluate metastasis in the different Grm1/SELENOK littermate expression controlled groups and the non-tumor forming control groups, the draining lymph nodes (inguinal and axillary) were evaluated utilizing two approaches. First, light microscopy was used to evaluate the amount of melanin producing, infiltrating cells in the lymph nodes for qualitative assessment (Figure 2.9A). Second, immunofluorescent detection of the melanocyte specific marker, Trp2, was quantified (Figure 2.9B-C). The latter was included because melanoma cells that have metastasized to secondary tissue in this model may lose the ability to express melanin [172]. Specificity of this immunofluorescent approach was confirmed (Figure S2.8). Both approaches showed reduced melanoma expression in the lymph nodes of the Grm1/SELENOK$^{-/-}$ mice compared to Grm1/SELENOK$^{+/+}$ and Grm1/SELENOK$^{+/-}$ mice, which had similar levels of melanoma in their lymph nodes. Overall, these data suggest that SELENOK expression is required for the progression of primary melanoma tumors as well as metastasis to the draining lymph nodes.

Discussion

Thus far, a role for SELENOK in cancer progression has not been described. The data presented here suggest that SELENOK acts to promote melanoma tumor progression and metastasis to distant sites. Mechanistically, the data suggest that SELENOK promotes the progression of metastatic melanoma by ensuring the palmitoylation and thus stable expression of the IP3R in the ER membrane, which is required for efficient Ca^{2+} flux. High intracellular [Ca^{2+}] is required for induction of downstream Ca^{2+} calcium dependent signaling pathways that turn on cellular programs related to growth, migration, and proliferation. Numerous studies have demonstrated a strong correlation between SELENOK and maintenance of IP3R-dependent Ca^{2+} flux in a variety of immune cells [37, 174]. The data presented here suggest a role in promoting IP3R-dependent Ca^{2+} flux-dependent functions such a growth, stemness, proliferation, and invasion in cancer cells both *in vitro* and *in vivo*.

The importance of SOCE in regulating melanoma and proliferation and cell migration was previously suggested by experiments including a knockdown of STIM1 or Orai1 in human melanoma cell lines and a pharmacological inhibitor of SOCE [107]. Similar results were found for knockdown of STIM1 and Orai1 in breast tumor cells [106] and in glioblastoma tumor cells [100]. The gene array data suggest that growing melanoma cells require SELENOK for initiating transcriptional programs related to their metabolism, stemness, and invasive properties. However, further experiments need to be performed in order to conclude that induction of these cellular programs rely solely on SOCE. Interestingly, Stim and Orai1 transcripts were not affected by SELENOK expression in melanoma cells. Several experiments were attempted to clarify if Ca^{2+}/calmodulin-dependent calcineurin activity directly modulated the transcripts levels observed by SELENOK deficiency. Using CsA or FK506 inhibitors on unedited and clone 7 cells followed by real-time PCR measuring levels of the mRNA transcripts in question, we were not able to generate consistent results. This may have been due to technical issues or the non-synchronized nature of the growing cells that led to the inconclusive results. Therefore, the results support a role for SELENOK in regulation of transcriptional programs supporting melanoma growth and stemness, but no direct evidence suggesting that those transcriptional

changes are due to effects of SELENOK on cytosolic Ca^{2+} levels that then subsequently induce the changes in gene expression. It is worth noting that a lower activity of calcineurin caused by SELENOK deficiency leading to lower NFAT nuclear localization could reduce levels of some of the transcripts observed, but it is less intuitive how that may lead to higher transcript levels observed for other genes. Increases in mRNA for select genes could be due to secondary effects arising from lower NFAT translocation such as compensation from other transcription factors, but more experiments are required to confirm this.

Metastasis is a stepwise process that involves loss of adhesion from the primary tumor, migration through the ECM and extravasation through the basement membrane, and adhesion and survival at a distal site. All the steps listed for metastasis rely on tightly regulated Ca^{2+} flux [175], and the results provided above suggest that loss of SELENOK in SK-MEL28 cells leads to increased adhesion and decreased migration/metastasis. One intact allele of SELENOK was sufficient for *in vitro* melanoma cell function and *in vivo* tumor progression. This suggests that high level of SELENOK protein is not necessarily required for malignant melanoma progression, which is consistent with the human tissue and NCI-60 melanoma cell lines data showing that SELENOK protein levels are not increased in melanoma compared to normal cells or tissues. Furthermore, the CRISPR/Cas9 version of SK-MEL28 with one truncated allele of SELENOK, and cells derived from the Grm1-Tg/SELENOK$^{+/-}$ mice indicate that SELENOK expression levels are normally well above what is necessary and sufficient. That is, SELENOK is not limiting and as such, further increases in SELENOK expression would bot be expected to have additional effects.

Changes in the expression of STIM1 and Orai1 have been found in a many cancer types, including melanoma [176], and thus have been implicated cancer progression. However, some reports have shown no differences in STIM1 or Orai1 levels in non-malignant vs. malignant cells [177]. Indeed, there remains heterogeneity in the levels of these and other SOCE components (e.g. IP3Rs) in melanoma [170]. Since SELENOK is a cofactor that binds to the DHHC6 enzyme to catalyze the palmitoylation of the IP3R required for its stability in the ER membrane, it could be that only small amounts of SELENOK are required, and an increase in SELENOK may not

lead to more IP3R expression in the ER membrane. However, genetic engineering of the SELENOK gene *in vitro* and *in vivo* that led to significantly lower levels of full-length protein plainly reduced SOCE in melanoma cells. This suggests that a threshold of SELENOK protein levels exists that is necessary for efficient Ca^{2+} flux in melanoma cells, resembling what has been observed in immune cells, but that threshold is well below normal expression levels.

Targeting components of SOCE or Ca^{2+} signaling as a therapy for cancer is an emerging area of interest in cancer research [82]. Orai and STIM proteins appear to be attractive molecular targets for cancer therapeutics [178]. However, Ca^{2+} flux is ubiquitous and plays a critical role in normal cells for proliferation, survival, metabolism, differentiation, etc., [179]. Furthermore, specific calcium pathways have also been identified as integral in the establishment and maintenance of multidrug resistance and the tumor microenvironment [180]. Homozygous mutations or disruption of both alleles of STIM1 or Orai1 results in perinatal lethality and STIM-2 knockout mice only survive ~5 wks of age [181-184]. The observation that SELENOK knockout mice show very little phenotypic defects and their fertility is not affected, suggests that therapeutic targeting of SELENOK may produce far fewer side effects. While CsA has been shown to be an effective treatment for melanoma *in vitro* [185], its use may negatively affect healthy cells that rely on NFAT for their normal growth and proliferation. The possibility of reduced side effects, along with the impressive reduction of melanoma with SELENOK deficiency in a mouse model of melanoma presented herein, support further investigation of SELENOK as a treatment of melanoma or other metastatic cancers that hijack SOCE. Genetic ablation of the gene encoding SELENOK eliminates its protein expression throughout development, which is not equivalent to using inhibitor drugs to inhibit its function. Therefore, future studies involving inducible knockdown of SELENOK, that would better reflect therapeutic intervention are planned. Finally, previous work in the Hoffmann laboratory identified the functional domain of SELENOK for its cofactor activity for DHHC6, which consists of amino acids 82-94 [10, 71], which helped guide the development of peptide inhibitors described in chapter 3. Overall, the *in vitro* and *in vivo* data regarding SELENOK deficiency and melanoma support further investigation into this protein as a potential therapeutic target for metastatic melanoma and possibly other cancers.

Materials and Methods

Mice

Generation of SELENOK$^{-/-}$ have been previously described [37] and C5BL/6J obtained from Jackson Laboratories were used as controls. Grm1-transgenic (Tg) mice [142, 172] were obtained from Dr. Suzie Chen at Rutgers University and used to establish a transgenic colony. The SELENOK$^{-/-}$ mice were crossed with the Grm1-Tg mice and the F1 generations crossed with each other to generate littermates with the following phenotypes: Grm1-Tg/SELENOK$^{+/+}$, Grm1-Tg/ SELENOK$^{+/-}$, and Grm1/ SELENOK$^{-/-}$. All animal protocols were approved by the University of Hawaii Institutional Animal Care and Use Committee.

Cells, antibodies, and reagents

Lysates from primary melanocytes were purchased from ScienCell Research Laboratories (Carlsbad, CA) and NCI-60 validated human melanoma cell lines obtained from the University of Hawaii Cancer Center included SK-MEL2, SK-MEL28, and MALME-3M. These cell lines were cultured in RPMI media with 10% fetal bovine serum and 1% Antibiotic-Antimycotic (all from GIBCO/ThermoFisher). Primary antibodies for western blots included rabbit monoclonal anti-SELENOK (Epigemonics, Inc., custom antibody), anti-IP3R1 (Santa Cruz Biotechnology) (fology, sc-271197), anti-GAPDH (Santa Cruz Biotechnology, sc-47724), anti-Prom1 (Cell Signaling, 58605). Antibodies from Abcam included anti-Trp2 (ab74073), anti-calcineurin A and B (ab137335, ab154650 respectively), and anti-calmodulin (ab 105498). Western blot secondary antibodies were purchased from Li-Cor Technologies and immunofluorescence secondary Alexafluor595 antibody from ThermoFisher.

Proliferation assays

For measurements of proliferation, cells were grown to 90% confluency in flasks and then trypsinized, resuspended and plated at 1000 cells per well in 4 separate black 96-well plates. On days 1, 2, 3, and 4 one plate was removed from incubation and centrifuged at 400 RCF for 4 min to pellet cells. Subsequently, media was removed, and plates were wrapped in parafilm and stored at -80°C. On day 5, pellets were thawed and lysed, and cells were quantified using a CyQUANT® Kit (ThermoFisher, Inc.). A fluorescence plate reader (Molecular Devices, Inc.) was used to quantify fluorescence of samples and cell count was inferred from a previously recorded standard curve using SK-MEL28 cells.

Scratch assays were performed by first growing cells to 90% confluency in a six-well plate. A "wound" is created in the center of each well by dragging a p-200 pipette tip through the cells at day 0 and pictures were taken using an Olympus 1X71 inverted microscope and Picture Frame software. After 18 h a secondary set of pictures were taken, and ImageJ was used to measure the area of the "wound" on day 0 and day 1. Results represent the change in area of the "wound" from day 0 to day 1.

Migration assays

Cellular migration rates were measured using transwell assays as previously described (Sulzmaier 2016). The lower sides of transwell filters (8 µm pore size; Greiner Bio-One) were coated with 15 µg/ml human plasma fibronectin (Life Technologies) or collagen I overnight at 4°C. Cells (1×10^6) were plated on the top-side of the filters in serum free media, with the bottom chambers containing incomplete media supplemented with 10 ng/ml EGF. Cells were incubated for 20 hours at 37 °C; 5% CO_2. The number of cells that migrated through the membrane was measured through Calcein-AM dye (Sigma-Aldrich) uptake and fluorescence at 495 nm excitation/515 nm emission.

The wound healing assay was performed on an 1600R ECIS instrument (Applied Biophysisc, Inc.) as described previously [186]. Cells were grown to 80% confluency and trypsinized (0.05%

trypsin/EDTA), washed and seeded in fresh media onto ECIS 8W10E+ PET slides at a concentration of 2.5×10^5 cells/mL. The rate of migration was measured as a function of time needed to climb back up to base resistance levels. Migration rate = electrode radius (μm)/ ∂time (h); ∂time = t2–t1 where t2 = time point in hours when resistance reading reaches base reading, t1 = time point in hours when cells were wounded.

Adhesion assays

The cell attachment assay has been previously described [187]. Briefly, microtiter plates coated overnight at 4°C with human plasma fibronectin (Millipore) or collagen I (Upstate NY) at 10 μg/ml were blocked with 3% BSA for 1 h at 37°C, wells were rinsed once with PBS (pH 7.4) and cells were added (1×10^5 cells/ml) in serum free media. Cells were incubated for 60 min at 37°C; 5% CO_2. After 60 min plates were washed 1X with PBS, fixed with 3% paraformaldehyde, stained with 0.5% crystal violet, 20% MEOH, washed under running distilled water, solubilized in 0.5% Triton X-100 in distilled water overnight R.T. and read on an ELISA plate reader at 595 nm.

Flow cytometry

Flow cytometry was performed using 5×10^5 cells by incubating with phycoerythrin (PE)-conjugated isotype control IgG or PE-conjugated IgG specific for Prom1 or ITGA2 or ITGB5 (all from BioLegend) and used 5 μL antibody per test as recommended by the vendor. Dead cells were excluded from analyses using violet blue exclusion dye (BioLegend). Samples were analyzed using the Attune NxT flow cytometer (ThermoFisher) and FlowJo software. Epidermal cells were disassociated from mouse tails by first separating the epidermis from the dermis using an Epidermis Dissociation Kit (Miltenyi) and generating a single cell suspension using GentleMacs. Cells were incubated with Fc-block followed by APC-anti-Prom1 (both Biolegend per vendor's instructions). Cells were then fixed using 2% paraformaldehyde and analyzed on a Fortessa flow cytometer (BD Biosciences).

Western blot

Cells were lysed in buffer containing 150 mM NaCl, 50 mM Tris, 1% Triton X-100, 1% sodium deoxycholate, and protease inhibitor cocktail (Roche Applied Science, Indianapolis, IN, USA) at 4°C for 1 h. Insoluble material was removed by centrifugation at 20,000 RCF for 10 min, and total protein in the supernatant was determined using a Bradford assay reagent (Bio-Rad, Hercules, CA, USA). After adjusting to equal protein concentration, cell lysates were boiled in SDS sample buffer and then separated by SDS-PAGE, followed by transfer of the proteins onto nitrocellulose membranes. Blots were incubated with the one or more of the primary antibodies listed in cells, antibodies, and reagents, for 1.5 h, washed, incubated with secondary Alexafluor595 antibody (ThermoFisher), and visualized using the Odyssey Scanner (Li-Cor).

Genome editing and transfections

A CRSPR/Cas9 approach was used to mutate the SELENOK gene (NCBI geneID 58515), in SK-MEL28 cells, in order to generate a cell line expressing a truncated, nonfunctional SELENOK protein. First, SK-MEL28 cells were transfected with a pSpCase9(BB)-2A-GFP (Addgene) using Lipofectamine 2000 (ThermoFisher). After 24 h, FP-positive cells were sorted using a FACSaria (BD Bioscience) into RPMI 1640 medium with 20% FBS without antibiotics. These cells were then transfected with Integrated DNA Technologies (IDT) guide RNA/transactivating RNA complexes in IDT complex buffer for 30 min using Lipofectamine 2000. Cells were recovered in RPMI 1640 medium with 20% FBS without antibiotics for 24 h, then 7-AAD Viability Stain Solution (Biolegend, Inc.) was added and a final round of cell sorting carried out using the FACSaria instrument. The $GFP^{+}AAD^{-}$ cells were sorted into 96-well plates with one cell per well in 200 µL of RPMI 1640 media with 20% FBS and no antibiotics. After ~3 weeks, live clones were transferred to 24 well plates and further grown expanded. Colonies were screened by Sanger sequencing and western blot for truncated SELENOK.

Intracellular Ca^{2+} measurement

For time-lapse video microscopy, cells on coverslips were loaded with FuraRed (Enzo Life Sciences) with either 1.00 µg/mL, 0.500 µg/mL, 0.250 µg/mL, or 0.00 µg/mL caged IP3 (D-23-O-Isopropylidene-6-O-(2-nitro-4.5-dimethoxy)benzylmyo-inositol 1,4,5-trisphosphate-Hexakis(propionoxymethyl) ester) (Enzo Life Sciences) for 30 min at 37°C followed by a 1 h recovery. The coverslips were then mounted onto RC-25F chambers (Warner) and placed into the mount of a Zeiss Pascal inverted confocal microscope with LSM5 dual lasers and camera. The fluorescence intensity of the FuraRed was measured at 2 sec intervals for 1 min and then cells exposed to *uv* light for 2 sec to uncage the IP3 molecule and fluorescence measurements continued for 3 min. Thapsigargin was used as a control as previously described [37]. The ratio of red fluorescence was inverted to represent increased Ca2+ since FuraRed signal decreases with increased cytosolic Ca2+ and results expressed as F1/F0.

Calcineurin activity assays and NFAT localization

Phosphatase activity was measured from lysates prepared from SK-MEL28 unedited and clone 7 cells using the calcineurin cellular activity assay kit (Enzo). Cells were treated with either 2 µM cyclosporin A (Sigma) in DMSO or DMSO as vehicle control for 2 h. Cells were lysed as per the vendors instructions and lysates were normalized to equal total protein concentration as determined by Bradford assay. Phosphatase activity was measured from cellular protein extracts as the dephosphorylation rate of calcineurin specific phosphopeptide substrate (R-II phosphopeptide) in the presence of 0.5 mM CaCl2/0.25 µM calmodulin. The malachite green based colorimetric assay was measured on a SpectraMax 384 microplate reader (Molecular Devices Inc.). NFAT localization was assessed by transfecting cells with a plasmid encoding GFP-c1NFAT3 (Addgene) using Lipofectamine 2000 (Invitrogen) with or without 2 µM cyclosporin A (Sigma) for 18 h. Immunofluorescence microscopy was carried out with a Leica Microsystems LAS AF TCS SP5 confocal microscope to assess cytoplasmic and nuclear localization morphologically.

Microarrays

SK-MEL-28 unedited and Clone 7 cells were harvested at 80% confluency were plated in 6-well plates (6×10^5 cells per well) and grown for 48 h followed by RNA isolation using the EZNA Total RNA kit (Omega Biotek, Inc). RNA integrity was validated on Agilent 2100 Bioanalyzer using RNA Nano chip. For gene expression profiling, 100 ng of total RNA was used for downstream processing using GeneChip Whole Transcript Expression protocol followed by hybridization to Clariom S, Human Arrays (Affymetrix, Santa Clara, CA, USA). Subsequently, arrays were washed, stained and scanned using GeneChip Fluidics Station 450 and GeneChip Scanner (Affymetrix). Generated CEL files were normalized using the SSTRMA-GENE-FULL algorithm in the Affymetrix GeneChip Expression console software. Raw CEL files generated from Clarion S human microarray were preprocessed in Array Studio (version 9; OmicSoft, Cary, NC) using data normalization by the Robust Multi-array Average (RMA) approach. Genes with Exp2 (default) transformed fold change greater or less than 2 and Benjamine & Hochberg FDR-adjusted p-value < 0.05 were considered as differentially expressed in clone 7 cells with respect to unedited cells.

Histological and immunofluorescent analyses of tissues

Tails and ears from 4-month of age mice were excised in an equivalent manner from each mouse and weighed. To ensure the same areas of tails were analyzed for presence of tumors for each mouse, a cross-section was excised 20 mm from the base that was further cross-sectioned into 4 pieces 1mm in length. The cross-sectioned tails were mounted in the same orientation in tissue paper and incubated 10% buffered formalin for 1 wk fix samples. Ears were immediacy incubated with 10% buffered formalin for 1 wk for fixation. Both fixed tails and ears were then incubated in 10% EDTA (w/v) for 1 wk to remove cartilage. The tail and ear samples were dehydrated in a series of ethanol solutions and embedded in paraffin, sectioned, and stained using a Leica CM1900 UV cryosectioner, Leica EG1160 and Microm HM340E microtomes, and a Leica automated tissue processor followed by standard Hemotoxylin and Eosin (H&E) staining of tissues. The inguinal and axillary lymph nodes were processed for both immunohistological

and immunofluorescent staining. Processing for H&E staining followed the protocol described above except the lymph nodes were fixed with 10% buffered formalin for 1 d and were not incubated with EDTA. For immunofluorescent staining, sectioned samples on glass slides were dried overnight in 45-50 ºC overnight, deparaffinized, and rehydrated under high temperature and pressure in Trilogy™ (Millipore Sigma) to unmask antigens. ImmEdge pen was used to create a hydrophobic border around the tissue and 5% goat serum (Vectastain) was added for 1 h to block non-specific binding. Primary antibody (rabbit anti-Trp2; Abcam, Inc.) was added at a final concentration of 1:500 in 5% goat serum in PBS for 2 h at RT. After three washes with PBS, secondary antibody (rabbit Alexafluor594; ThermoFisher) was added at a final concentration of 1:1000 in 5% goat serum in PBS for 1h at RT. After three washes with PBS, tissues were mounted in vectashield H-1200 with DAPI (Vector Labs, Inc.).

The H&E stained sections were imaged using a Zeiss Axioskop 2 Plus upright light microscope with camera and AxioVs40 V 4.7.2.0 acquisition software, equipped with a 5X Plan neofluor objective, 5X/.15, α/.17 numerical aperture of 0.9. Light microscope images were analyzed using ImageJ software. The amount of tumor tissue present in ears and tails were determined by setting the signal intensity representing dark melanin at threshold and then measuring the total surface area of tissue along with the surface area above the threshold. The percentage of melanin tissue above color threshold per total surface area was calculated. The lymph nodes were analyzed by immunofluorescence using a Leica Microsytems LAS AF TCS SP5 confocal microscope with a 40x oil objective with 5x zoom, HCX PL APO CS with numerical aperture of 1.3. The Laser lines used were 405 nm (for DAPI) and 594 nm (for Alexafluor594). Images were captured using LAS AF version 2.7.3.9723 acquisition software, 1997–2012 LeicaMicrosystems CMS GmbH. A minimum of 4 fields per sample was captured and ImageJ was used to analyze tissue for Trp2 signal with data presented as mean fluorescence intensity.

Statistical analyses

Comparison of two means was carried out using an unpaired Student's t test using GraphPad Prism version 4.0. In assays involving three or more groups a one-way ANOVA was used to

analyze groups with Tukey post-test used to compare means of each group. All comparisons were considered significant at $p < 0.05$. GraphPad Prism was also used to generate standard curves with regression analyses from which values were calculated for sample measurements.

Figures

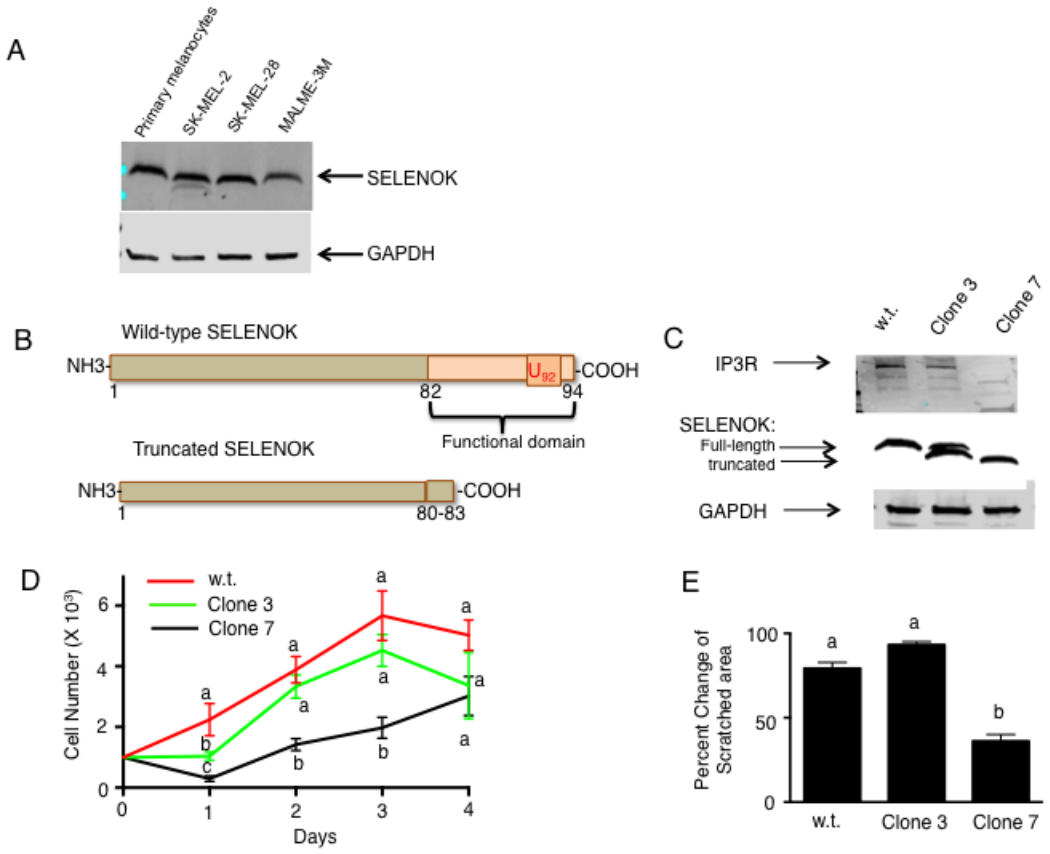

Figure 2.1: Loss of Functional SELENOK in melanoma cells leads to decreased proliferation. (**A**) Western blot analysis demonstrating similar SELENOK levels in primary human melanocytes and three human melanoma cell lines. GAPDH was used as a loading control. (**B**) Diagram illustrating how CRISPR/Cas9 was used to edit the genome of SK-MEL28 cells, generating a truncated version of SELENOK that has the functional domain deleted. (**C**) Western blot analysis confirmed the presence of full-length SELENOK in unedited cells, both full-length and truncated in clone 3 cells, and only truncated SELENOK in clone 7 cells. Only clone 7 exhibited reduced IP3R levels. GAPDH was used as a loading control. (**D**) Equal numbers of cells were plated in replicate well (N = 6 per cell line) and proliferation was measured over a 4-day period. Clone 7 demonstrated reduced growth on days 1-3. Results are

expressed as mean ± SEM and a one-way ANOVA with Tukey post-test was used to analyze the groups. Means at each time point without a common letter differ, $p < 0.05$. (**E**) Wound healing assays were performed in triplicate comparing unedited SK-MEL28 cells to clone 3 and clone 7 cells. Results showed less cellular closure of the scratched region for clone 7 cells. Results are expressed as mean ± SEM and a one-way ANOVA with Tukey post-test was used to analyze the groups. Means at each time point without a common letter differ, $p < 0.05$. For D-E, results were independently repeated in duplicate.

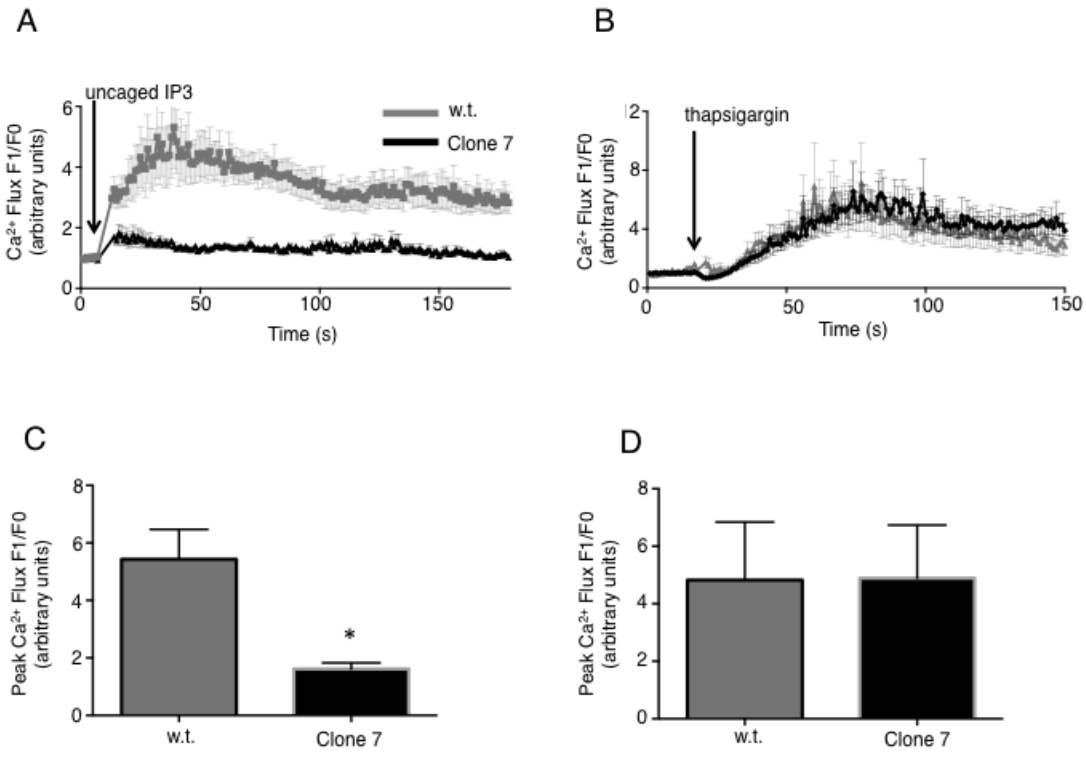

Figure 2.2: IP3R-dependent cytosolic Ca^{2+} concentration is reduced in SELENOK-truncated melanoma cells. (**A**) SK-MEL28 unedited and clone 7 cells were loaded with both caged IP3 (0.50 µg/mL) and the Ca^{2+} sensitive fluorochrome, FuraRed. Confocal microscopy was used to measure baseline fluorescence for 30 sec, followed by exposure to a 2 sec *uv* light pulse to uncage the IP3 and measurement of fluorescence in response to IP3 binding to the IP3R

within the cells. Because FuraRed fluorescence decreases upon Ca^{2+} in the system used, the fluorescence intensity was inverted and plotted as signal after uncaging of IP3 (F1) divided by the average baseline signal (F0). Results showed reduced Ca^{2+} flux in clone 7 cells. (**B**) Thapsigargin, which bypasses the IP3 receptor to induce Ca^{2+} flux, was used to compare unedited SK-MEL28 and clone 7 non-IP3 induced Ca^{2+} flux. No differences in Ca^{2+} flux was found. Results for A-B Ca^{2+} flux experiments represent three independent repeats that each included ≥ 30 cells per condition. (**C-D**) IP3 mediated and thapsigargin based experiments were independently repeated in triplicate, means of the replicates were compared using a student's t-test and expressed as mean ±SEM with $^{*}p < 0.05$.

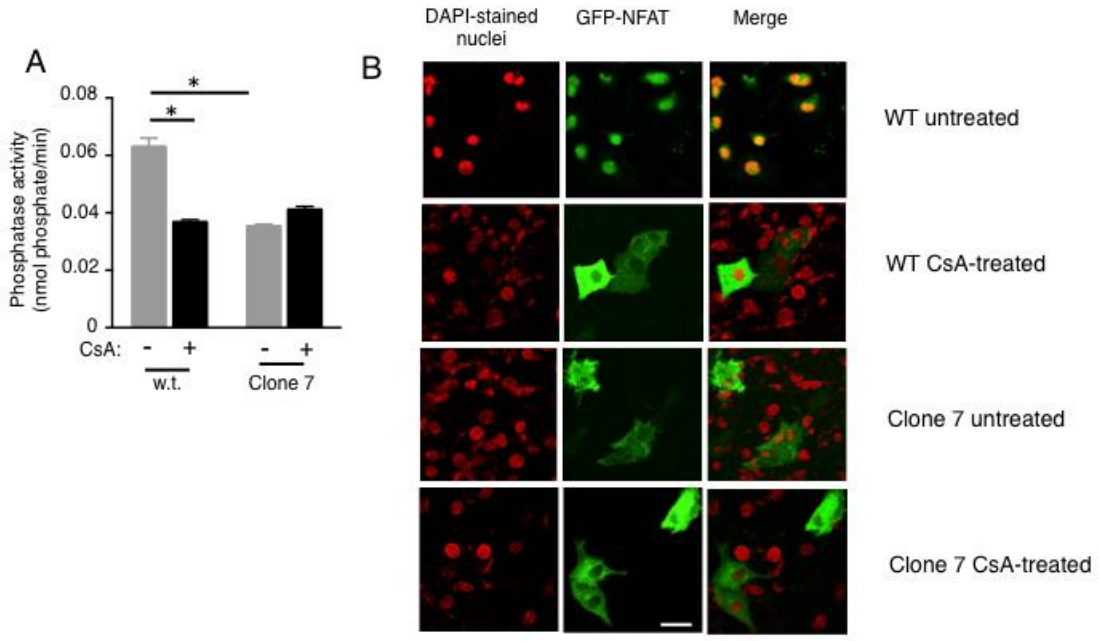

Figure 2.3: Calcineurin activity and NFAT nuclear localization are reduced in SELENOK-truncated melanoma cells. (**A**) SK-MEL28 w.t and clone 7 cells were incubated for 2 h with DMSO vehicle control or the calcineurin inhibitor, cyclosporin A (CsA) (2 µM), and then cell lysates prepared, normalized to total protein. The calcineurin substrate, RII phosphopeptide, was

added to lysates and colorimetry was used to detect production of phosphate. Means of replicates (N = 3) were compared using a student's t-test and expressed as mean ± SEM with $^{*}p < 0.05$. All experiments are representative of a minimum of two independent experiments. (**B**) GFP-NFAT was transfected into SK-MEL28 unedited and clone 7 cells and using the same CsA conditions as in A, GFP-NFAT localization was evaluated using confocal microscopy. Results showed that SELENOK-truncated clone 7 cells had accumulation of NFAT in the cytosol (identified morphologically) in a manner similar to cells treated with CsA. DAPI staining of the nuclei was recolored from blue to red to allow merged (yellow) to be more apparent. Scalebar represents 5 µm.

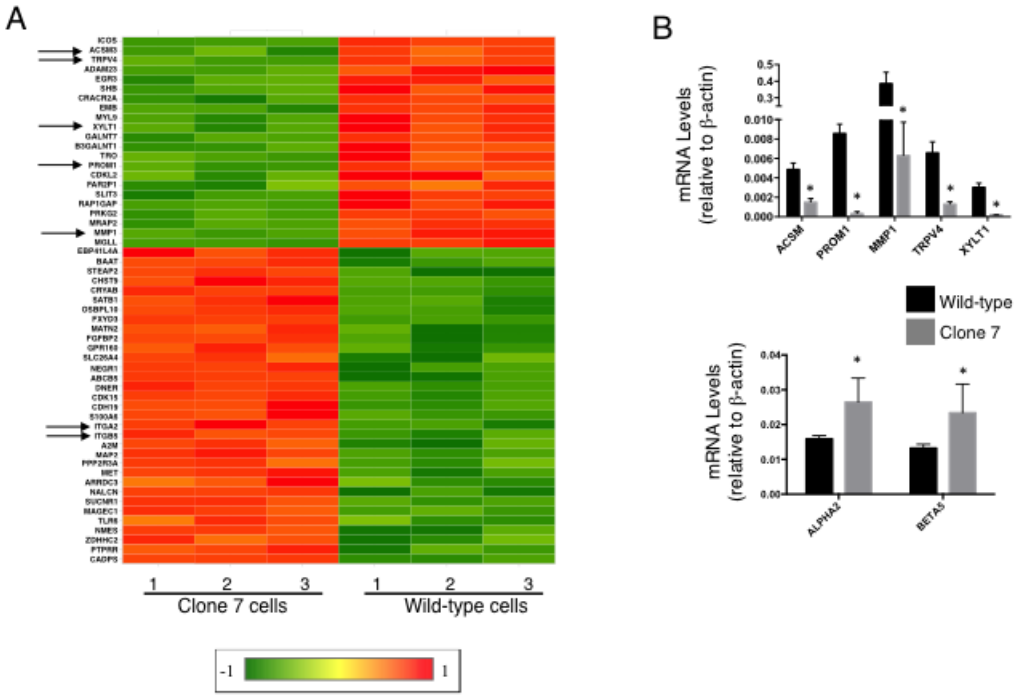

Figure 2.4: SELENOK deficiency alters transcriptional control of growth, migration and stemness. (**A**) Gene arrays were used to compare SELENOK-truncated clone 7 cells to unedited cells for transcript expression (N = 3 per group). Differentially expressed genes most related to

cancer progression and growth were selected based on Exp2 (Array Studio default) transformed > 2-fold higher or lower than unedited control cells with Benjamini & Hochberg FDR-adjusted *p*-value < 0.05. A heat map was generated using the linear gene expression values, which were normalized by dividing the unedited average and robust center scaling with a linear range of 1 to -1. Down-regulated (green) and up-regulated (red) genes are shown for clone 7 compared to unedited cells or vice versa. Arrows indicate genes that were further examined. (**B**) Real-time PCR was used to measure relative mRNA levels for selected genes. Results confirmed that clone 7 cells demonstrate down regulation of the five transcripts involved in promoting growth, stemness, and migration (upper graph) and up-regulation of 2 transcripts involved in adhesion (lower graph). Means of replicates (N = 4) were compared using a student's t-test and expressed as mean ± SEM with * p < 0.05.

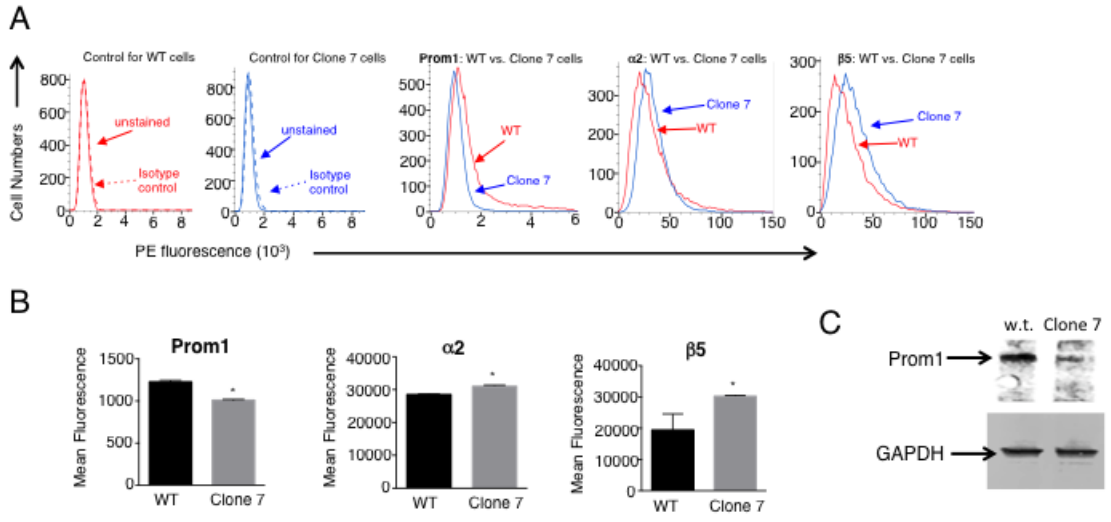

Figure 2.5: Protein levels for Prom1 as well as ITGA2 and ITGB5 integrin chains are altered in a manner similar to transcript levels with SELENOK deficiency. (**A**) Flow cytometry was used to evaluate surface expression of Prom1, ITGA2 (α2), and ITGB5 (β5). PE-labeled isotype control antibodies did not bind either wild-type (WT) cells or clone 7 cells (two left panels). For clone 7 cells, fluorescence intensity decreased from Prom1 and increased

intensity for ITGA2 (α2) and ITGB5 (β5) integrin chains. (**B**) The fluorescence intensity was measured for replicates (N = 3) and means were compared using a student's t-test and expressed as mean ± SEM * $p < 0.05$. (**C**) Prom1 protein levels were also measured using western blot with GAPDH used as a loading control.

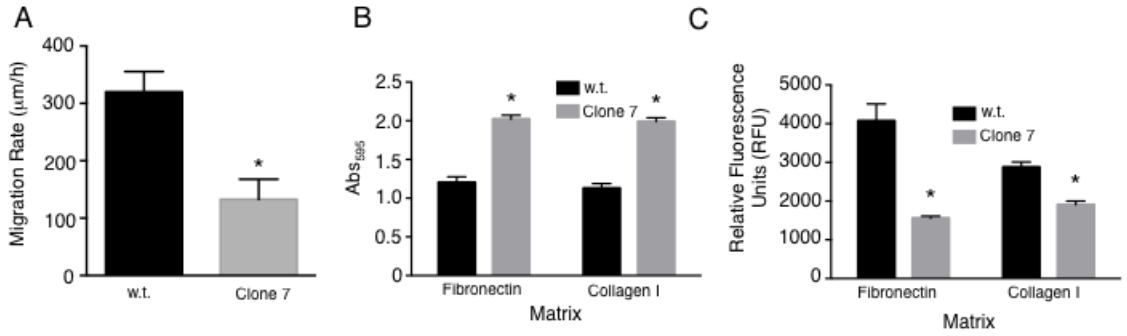

Figure 2.6: SELENOK deficiency alters adhesion and migration of melanoma cells. (**A**) Migration rates were measured for unedited SK-MEL28 cells and SELENOK-truncated clone 7 cells using electrode-created wounds and resistance to measure movement of cells into electrode cleared area. (**B**) Adherence to fibronectin and collagen I was measured for unedited SK-MEL28 cells and SELENOK-truncated clone 7. Clone 7 cells were found to exhibit increased adherence to both types of fibers compared to unedited cells. Crystal violet stained cells were measured using absorbance read on an ELISA plate reader at 595 nm. (**C**) Transwell assays were performed to test unedited and clone 7 cells for migration through fibronectin or collagen I. Migration through both matrices was lower for clone 7 compared to unedited cells as measured by fluorescent stating of the cells. Results represent three independent experiments. Means of replicates, N = 3 for A and N = 6 for C-D, were compared using a student's t-test and expressed as mean ± SEM * $p < 0.05$.

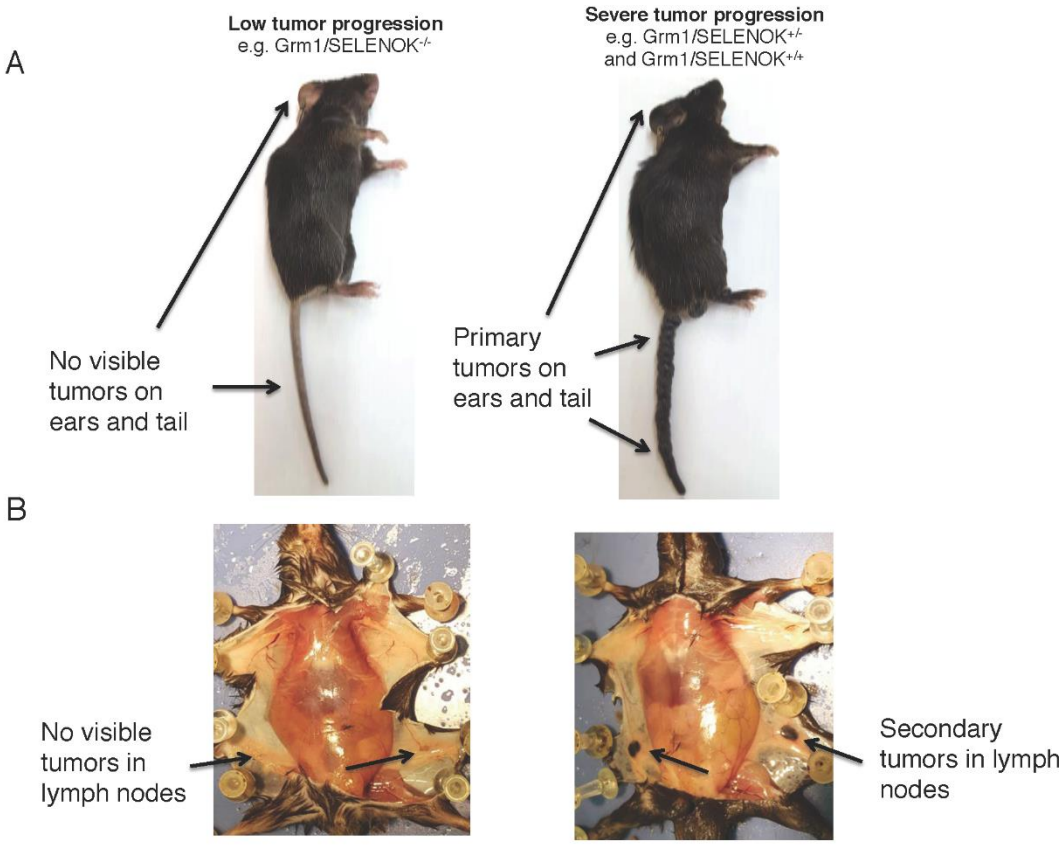

Figure 2.7: Deletion of SELENOK *in vivo* results in reduced primary and secondary tumors in Grm1-Tg mice as analyzed by gross anatomy. The Grm1-Tg mouse line spontaneously develops tumor on the tails, ears, and perianal region that metastasize to the draining lymph nodes by 4 months of age. Mice shown above were bred with SELENOK knockout mice to generate littermates: Grm1/SELENOK$^{+/+}$, Grm1/SELENOK$^{+/-}$, and Grm1/SELENOK$^{-/-}$ mice. (**A**) Examination of the primary tumors on the ear and tails revealed lower primary tumor formation for Grm1/SELENOK$^{-/-}$ mice compared to Grm1/SELENOK$^{+/+}$ and Grm1/SELENOK$^{+/-}$ which both exhibited tumor formation ranging from intermediate to high. (**B**) Evaluation of secondary tumors in the draining lymph nodes showed less secondary tumor formation in and Grm1/SELENOK$^{-/-}$ mice compared to Grm1/SELENOK$^{+/+}$, Grm1/SELENOK$^{+/-}$ mice.

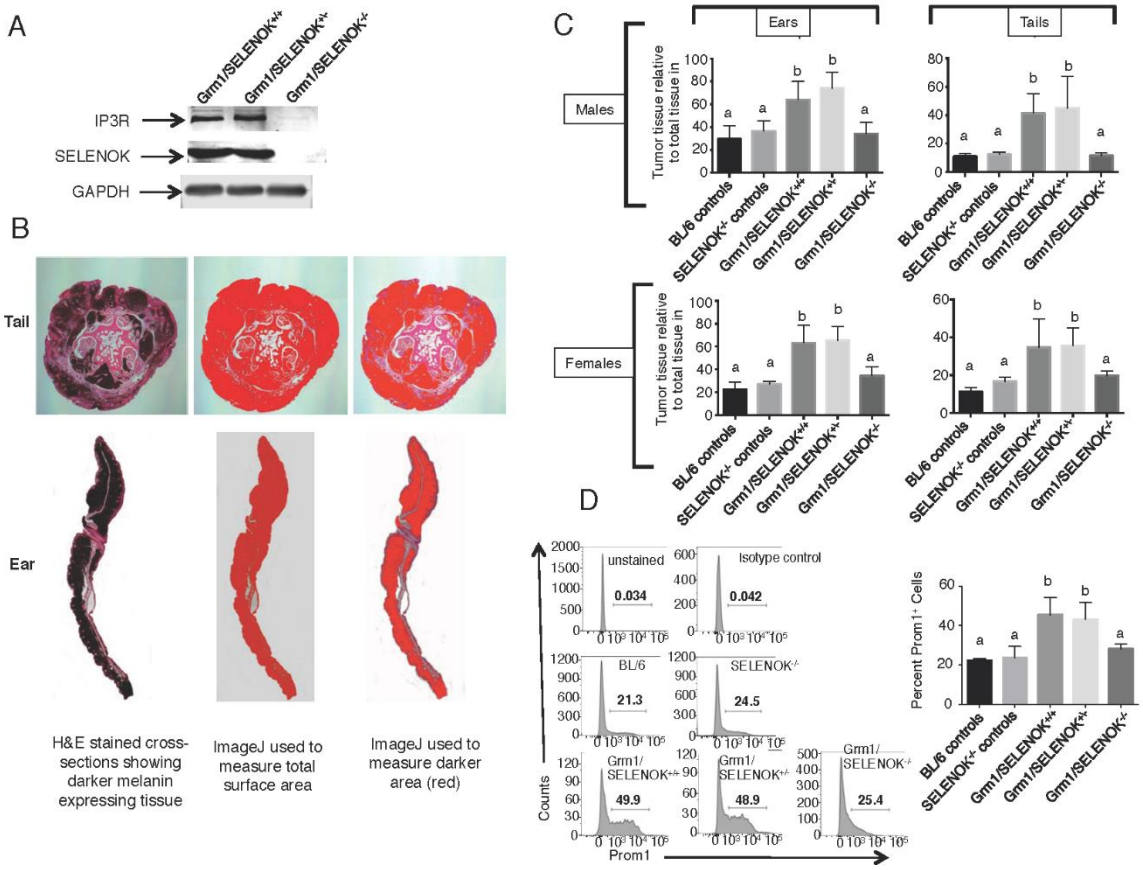

Figure 2.8: SELENOK deficiency reduces melanoma tumor burden on tails and ears. (**A**) Western blot analysis of splenocytes, which express relatively high levels of SELENOK and IP3R, confirm that complete knockout of SELENOK leads to reduced IP3R in Grm1/SELENOK$^{-/-}$ mice. (**B**) Male and female littermates at 4 months of age with genotypes of Grm1/SELENOK$^{+/+}$, Grm1/SELENOK$^{+/-}$, and Grm1/SELENOK$^{-/-}$ were compared for levels of melanin positive tissue relative to total tissue in tails and ears. (**C**) Cross-sections of tails and ears were H&E stained and evaluated using an ImageJ color threshold approach as described in the Methods section. The dark melanin area relative to total area of tissue was compared for all three littermate genotypes. We also included two control groups expected to form no tumors (C57BL/6 and SELENOK$^{-/-}$) due to a lack of the Grm1 transgene in melanocytes, which allowed assessment of melanin content in the absence of melanoma. Results showed that

Grm1/SELENOK$^{-/-}$ mice had significantly reduced tumor growth in tails and ears, while Grm1/SELENOK$^{+/+}$ and Grm1/SELENOK$^{+/-}$ mice were similar in progression of melanoma. Similar results were found with males and females. (**D**) Cells dissociated from were analyzed by flow cytometry for Prom1+ cancer stem cells and lower levels were found in Grm1/SELENOK$^{-/-}$ mice compared to Grm1/SELENOK$^{+/+}$ and Grm1/SELENOK$^{+/-}$ littermates. Both sexes were included in each group, with representative images shown on the left and data graphed on the left (N = 3). A one-way ANOVA with Tukey post-test was used to analyze groups and means without a common letter differ, $p < 0.05$.

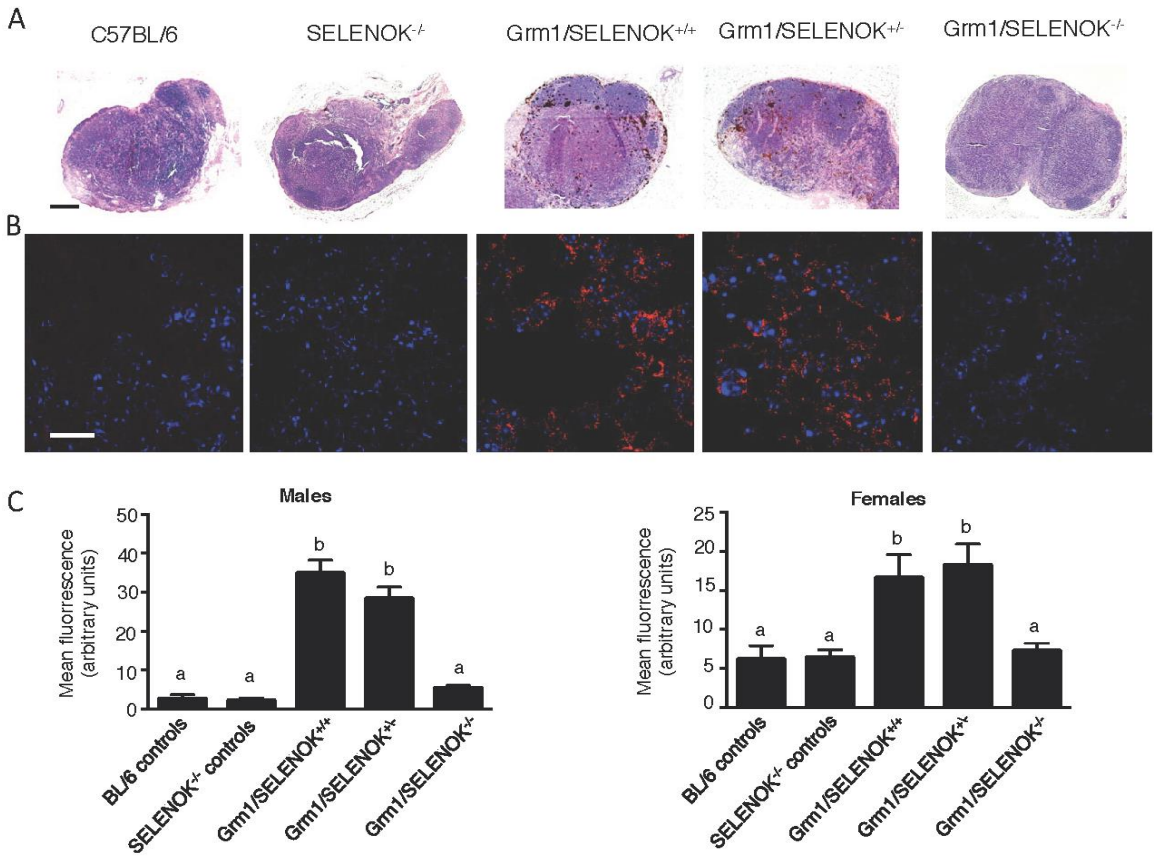

Figure 2.9: SELENOK deficiency reduces metastasis of melanoma to lymph nodes. Male and female littermates of 4 months of age with genotypes of Grm1/SELENOK$^{+/+}$, Grm1/SELENOK$^{+/-}$, Grm1/SELENOK$^{-/-}$ and non-tumor control groups consisting of C57BL/6 and SELENOK$^{-/-}$ were analyzed for the presence of infiltrating melanoma cells in the inguinal

and axillary lymph nodes (N = 7 per group). (**A**) H&E stained lymph node sections were examined low magnification (5x) for melanocytes, which appear as dark brown cells. Scalebar = 20 mm. (**B**) Immunofluorescence performed at 40x was used to detect the melanocyte specific antigen, Trp2 (red), in lymph node sections. DAPI (blue) was used to stain nuclei. Scalebar = 2 mm. (**C**) Trp2 fluorescence was quantified using ImageJ with a minimum of 7 mice per group and 3 sections analyzed per mouse A one-way ANOVA with Tukey post-test was used to analyze groups. Means without a common letter differ, $p < 0.05$.

Selenoprotein K immunohistology results

Patients with localized malignant melanoma	Patient 1	Patient 2	Patient 3	Patient 4	Patient 5
Normal tissue	1	1	1	0	0
Tumor tissue	1	1	0	0	0

Patients with distant or regional metastatic melanoma	Patient 1	Patient 2	Patient 3	Patient 4	Patient 5
Normal tissue	0	1	0	1	0
Tumor tissue	0	1	0	1	0

Glutathione peroxidase 1 immunohistology results

Patients with localized malignant melanoma	Patient 1	Patient 2	Patient 3	Patient 4	Patient 5
Normal tissue	2	2	2	1	2
Tumor tissue	2	2	2	2	2

Patients with distant or regional metastatic melanoma	Patient 1	Patient 2	Patient 3	Patient 4	Patient 5
Normal tissue	2	2	1	1	2
Tumor tissue	2	2	1	1	2

Glutathione peroxidase 4 immunohistology results

Patients with localized malignant melanoma	Patient 1	Patient 2	Patient 3	Patient 4	Patient 5
Normal tissue	1	2	1	1	1
Tumor tissue	2	2	1	1	1

Patients with distant or regional metastatic melanoma	Patient 1	Patient 2	Patient 3	Patient 4	Patient 5
Normal tissue	1	1	1	1	1
Tumor tissue	2	2	1	2	1

Scale

0	Negative
1	Positive - Weak in at least 25% of the cells
2	Positive - Medium in at least 25% of the cells
3	Positive - Strong in at least 25% of the cells

Figure S2.1: Results from immunohistochemical (IHC) evaluation of early and late stage melanoma tissues obtained from the University of Hawaii Cancer Center (UHCC). IHC was performed and scored by the UHCC Pathology core for SELENOK along with two other selenoproteins, glutathione peroxidase-1 and -4. Results suggest no changes in SELENOK levels in tumor tissues compared to normal tissue.

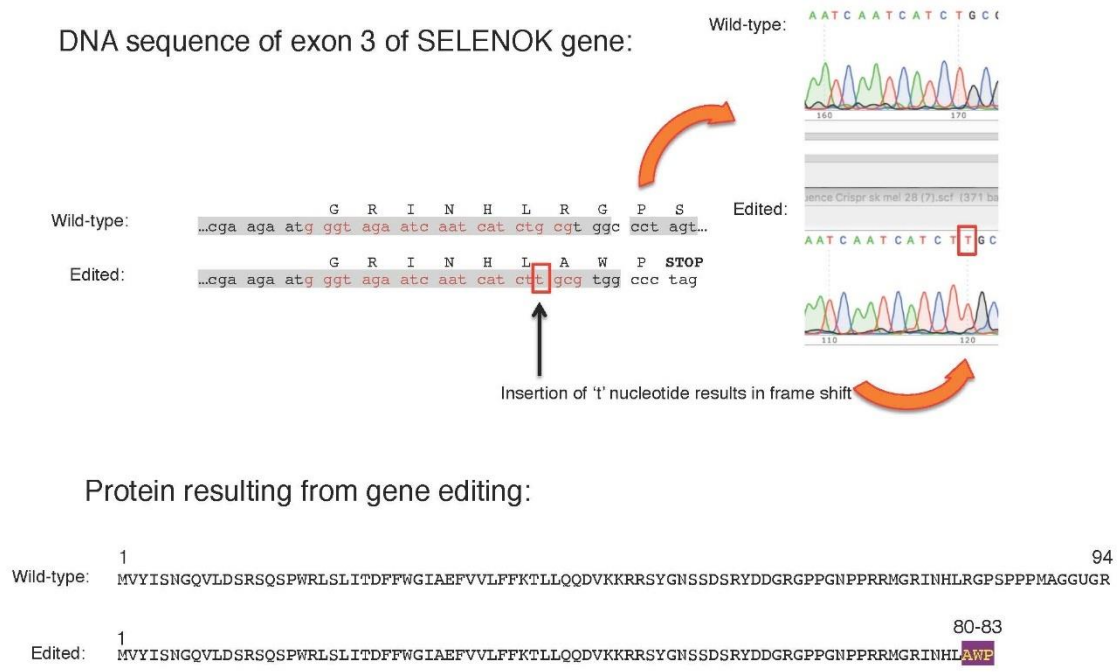

Figure S2.2: Sanger sequencing results for edited clones compared to unedited SK-MEL-28 melanoma cells. CRISPR/Cas9 editing led to introduction of a thymidine nucleotide causing a frame shift in DNA. This resulted in altered codons corresponding to amino acids 80–83 followed by a stop codon leading to a truncated SELENOK protein lacking the functional domain.

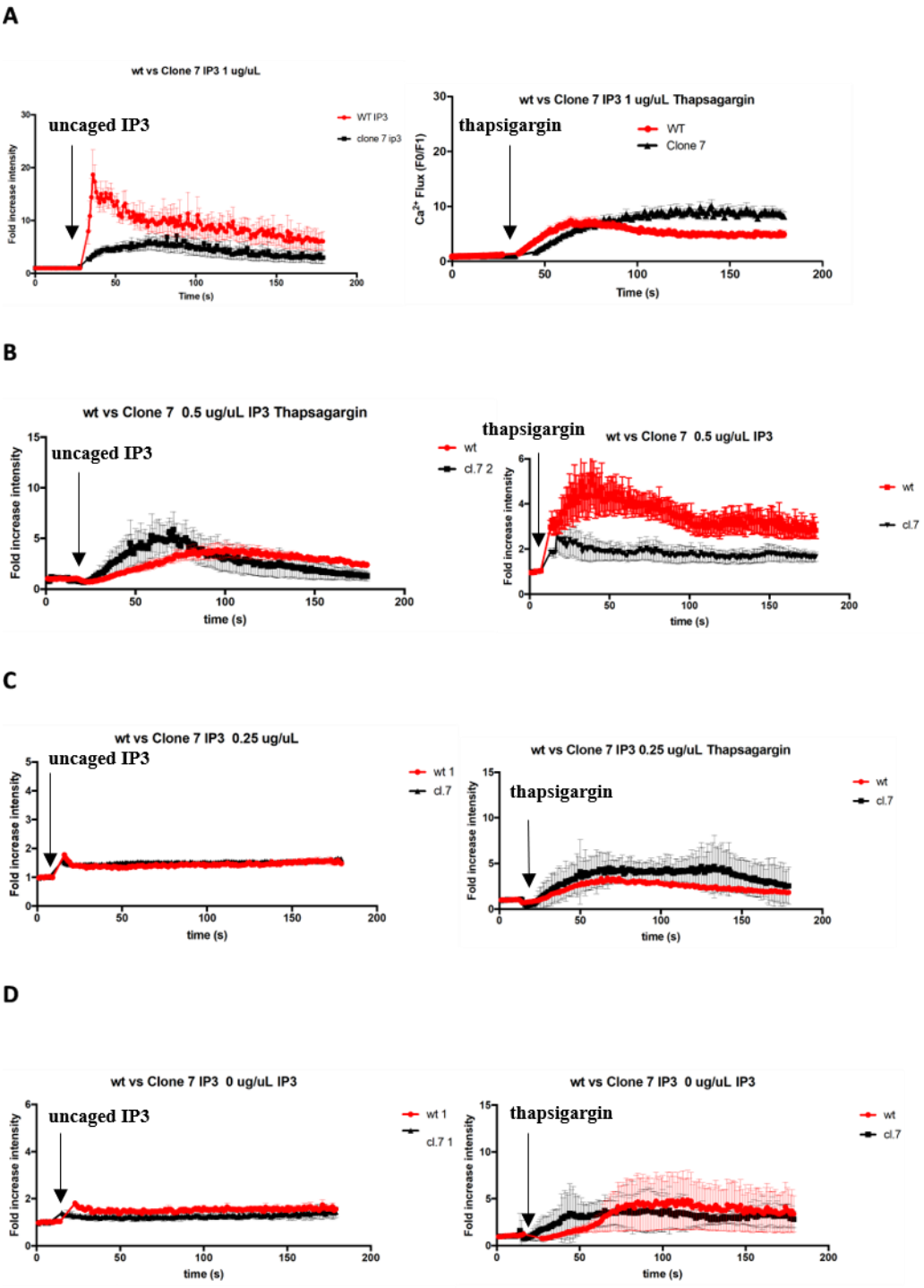

Figure S2.3: SELENOK-truncated cells (clone 7) compared to wild-type SK-MEL-28 cells were loaded with FuraRed along with various levels of caged IP3. Experiments were

performed as in Figure 2.1A-B but with differing concentrations of IP3 whereby SK-MEL28 w.t and clone 7 cells were loaded with (**A**)1.00 µg/mL, (**B**) 0.500 µg/mL (**C**) 0.250 µg/mL, or (**D**) 0.00 µg/mL caged IP3. Results show consistent reduced Ca^{2+} flux for clone 7 compared to unedited controls in higher concentrations of IP3 used and no differences in unedited and clone 7 calcium flux when only *uv* pulse was used.

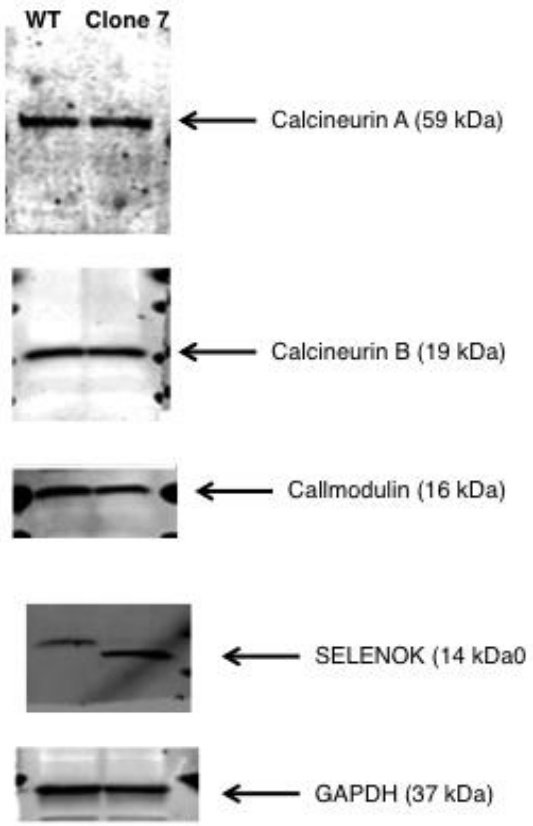

Figure S2.4: Western blotting was performed to determine levels of calcineurin subunits A and B, along with calmodulin in SELENOK-truncated cells (clone 7) compared to wild-type SK-MEL-28 cells. Results showed no differences. Western blot showing that protein levels of calcineurin subunits A and B and calmodulin were equivalent in unedited and clone 7

cells. SELENOK was detected in clone 7 cells as a smaller truncated form as expected and GAPDH was used as a loading control.

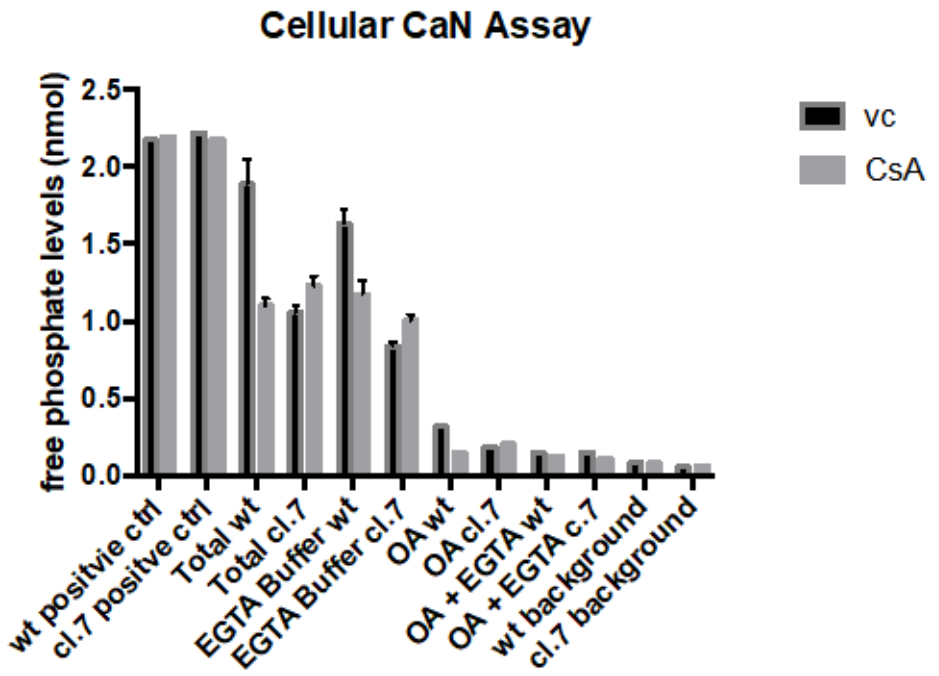

Figure S2.5: Additional controls to confirm equivalent levels of non-calcineurin phosphatase activity in unedited and SELENOK-truncated cells (clone 7). SK-MEL28 w.t and clone 7 cells were incubated for 2 h with DMSO vehicle control or the calcineurin inhibitor, cyclosporin A (CsA) (2 µM) with the following additional controls: Background reading to control for background phosphate/interfering substance. Total phosphate activity in extract. EGTA buffer, (Ca^{2+}/CaM free) for total activity in the absence of active calcineurin (PP2B). OA (okadaic acid), an inhibitor of other common phosphatases (PP1 and PP2A). OA + EGTA for total activity in the absence of active PP1, PP2A and calcineurin. Purified calcineurin enzyme was used as a positive control.

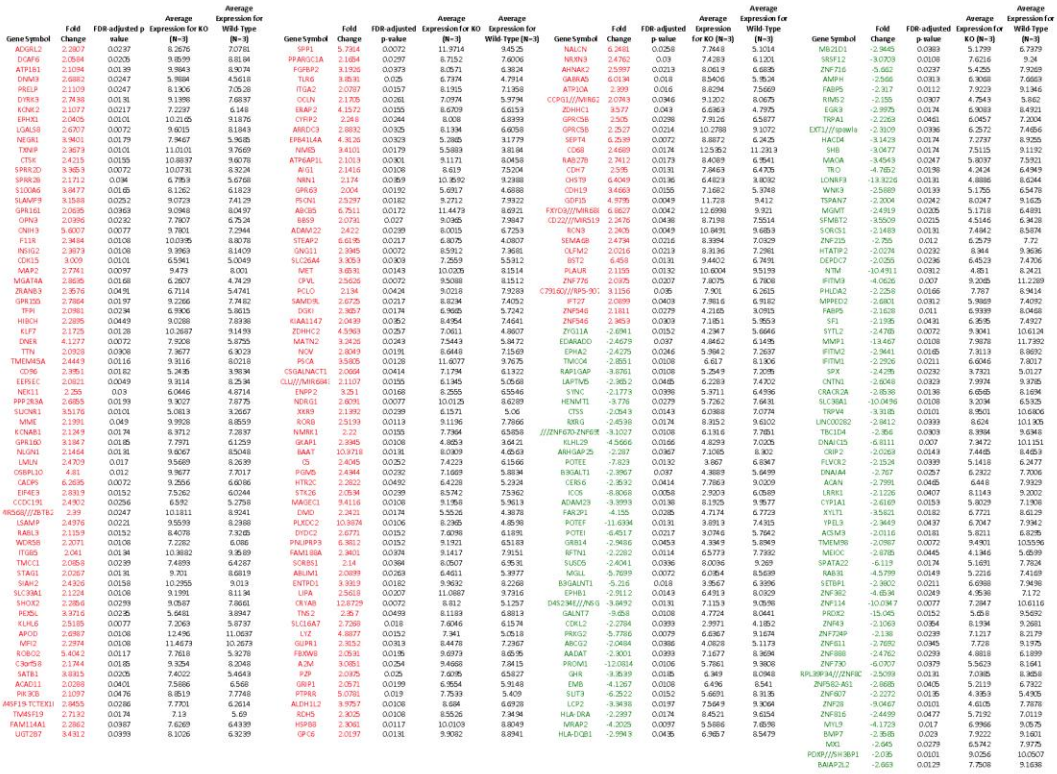

Gene Symbol	Fold Change	FDR-adjusted p-value	Average Expression for KO (N=3)	Average Expression for Wild-Type (N=3)
ADGRL2	2.2807	0.0297	8.2676	7.0781
DGAF6	2.0584	0.0205	9.8599	8.8194
ATP1B1	2.1094	0.0139	9.9843	8.9074
DNM3	2.6882	0.0247	5.7894	4.5618
PRELP	2.1109	0.0247	8.1906	7.0528
DYRK3	2.7438	0.0131	9.1398	7.6837
KCNK2	2.1027	0.0217	7.2297	6.148
EPHX1	2.0405	0.0101	10.2165	9.1876
LGALS8	2.6707	0.0072	9.6015	8.1843
NEGR1	3.9401	0.0179	7.9467	5.9685
TNNI3	2.3673	0.0101	11.0101	9.7669
CTSK	2.4215	0.0155	10.8837	9.6078
SPRR2D	3.3653	0.0072	10.0731	8.3224
SPRR2B	2.1712	0.034	6.7859	5.6768
S100A6	3.8477	0.0165	8.1262	6.1829
SLAMF9	3.1588	0.0252	9.0723	7.4129
GPR161	2.0635	0.0363	9.0368	8.0497
CPN1	2.0395	0.0232	7.7607	6.7524
CNIH3	5.6007	0.0077	9.7801	7.2944
F11R	2.3484	0.0108	10.0395	8.8078
INSIG2	2.3673	0.0108	9.1863	8.1409
CDK15	3.009	0.0101	6.5941	5.0049
MAP2	2.7761	0.0097	9.473	8.001
MGAT4A	2.8635	0.0168	6.2607	4.7429
ZBANK3	2.3576	0.0491	6.7114	5.4741
GPR155	2.7864	0.0197	9.2266	7.7482
TPPI	2.0981	0.0234	6.9306	5.8615
HIBCH	2.2895	0.0449	9.0288	7.8398
KLF7	2.1725	0.0128	10.2687	9.1499
DNER	4.1277	0.0072	7.9208	5.8755
TTN	2.0928	0.0308	7.9677	6.9029
TMEM45A	2.4419	0.0116	9.3116	8.0218
CD96	2.3851	0.0182	5.2435	3.9834
EEF1E1	2.0821	0.0049	9.3114	8.2534
NDE1	2.255	0.03	6.0446	4.8714
PPP2R3A	2.6855	0.0159	9.3027	7.8775
SUCNR1	3.5176	0.0101	5.0813	3.2667
MME	2.1991	0.049	9.3928	8.8559
KCNAB1	2.1349	0.0174	8.3712	7.2897
GPR160	3.1847	0.0185	7.7971	6.1259
NLGN1	2.1464	0.0181	9.6067	8.5048
LMLN	2.4709	0.017	9.5689	8.2699
OSBPL10	4.81	0.012	9.9877	7.7017
CADPS	6.2695	0.0072	9.2556	6.6086
EIF4E3	2.8319	0.0152	7.5262	6.0244
CCDC191	2.4702	0.0256	6.592	5.2758
RRS1///ZBTB2	2.39	0.0247	10.1811	8.9241
LSAMP	2.4976	0.0221	9.5593	8.2388
RABL3	2.1159	0.0152	8.4078	7.3265
WDR59	2.2071	0.0108	7.2282	6.086
ITGB5	2.041	0.0134	10.3882	9.3589
TMCC1	2.0858	0.0239	7.4893	6.4287
STAG1	2.0267	0.0131	9.701	8.6819
SIAH2	2.4326	0.0158	10.2955	9.0113
SLC39A1	2.1224	0.0108	9.1991	8.1134
SHOX2	2.2856	0.0293	9.0587	7.8661
RDBL	3.9716	0.0235	5.9481	3.8947
KLHL6	2.5185	0.0077	7.2063	5.8737
APOD	2.6867	0.0108	12.496	11.0637
MPI2	2.2974	0.0108	11.4673	10.2673
ROBO2	5.4042	0.0117	7.7818	5.3278
C9orf58	2.1744	0.0185	9.3254	8.2048
SATB1	3.8315	0.0205	7.4022	5.4643
AGAP11	2.0283	0.0401	7.5886	6.568
PIK3CB	2.1097	0.0476	8.8519	7.7748
ANKRD19B///TCTEX1D1	2.8455	0.0286	7.7701	6.2614
TMEM51	2.7132	0.0174	7.13	5.69
FAM114A1	2.2862	0.0367	7.6269	6.4399
UGT2B7	3.4312	0.0393	8.1026	6.9239
SPP1	5.7364	0.0072	11.9714	9.4525
PPARGC1A	2.1684	0.0297	8.7152	7.6006
FGFBP2	3.1926	0.0373	8.0571	6.3824
TLR6	3.8531	0.025	6.7374	4.7914
ITGA2	2.0787	0.0157	8.1915	7.1358
OCLN	2.1705	0.0261	7.0774	5.9794
ENAH2	4.1572	0.0155	8.6709	6.6153
CYFIP2	2.248	0.0244	8.008	6.8393
ARHGEF3	2.8832	0.0325	8.1334	6.6058
EPB41L4A	4.3126	0.0303	5.2985	3.1779
NAV3	3.4101	0.0179	5.5893	3.8194
ATP6AP1L	2.1013	0.0301	9.1171	8.0458
AIG1	2.1416	0.0108	8.619	7.5204
NRN1	2.174	0.0359	10.3592	9.2388
GPR69	2.004	0.0192	5.6917	4.6888
PSCN1	2.5297	0.0182	9.2712	7.9322
ABCB5	6.7511	0.0172	11.4473	8.6921
BIRC3	2.0731	0.027	9.0365	7.9847
ADAM22	2.422	0.0299	8.0015	6.7253
STEAP2	6.6135	0.0217	6.8075	4.0807
GNG11	2.3945	0.0072	8.5912	7.3681
SLC26A4	3.8353	0.0303	7.2559	5.5312
IVET	3.6531	0.0143	10.0205	8.1514
CPVL	2.5626	0.0072	9.5088	8.1512
PCLO	2.134	0.0424	9.0218	7.9283
SAMD9L	2.6725	0.0217	8.8234	7.4052
DGKI	2.3657	0.0174	6.9685	5.7242
KIAA1147	2.0439	0.0352	8.4054	7.4641
ZDHHC2	4.5363	0.0257	7.0611	4.8607
MATN2	3.2426	0.0243	7.5443	5.8472
NGV	2.8043	0.0191	8.6448	7.1569
PXDA	3.5925	0.0128	11.6077	9.7675
C5GALNACT1	2.0664	0.0414	7.1794	6.1322
CLU///MIR6861	2.1107	0.0155	6.1345	5.0568
ENPP2	3.251	0.0168	8.2555	6.5546
NDRG1	2.8091	0.0077	10.0125	8.6289
XKR9	2.1392	0.0299	6.1571	5.06
RORB	2.5193	0.0113	9.1196	7.7866
NAMPT	2.22	0.0195	7.7364	6.5858
GRAP1	2.3945	0.0108	4.8653	3.6421
BAAT	10.9718	0.0131	8.0309	4.6569
CS	2.4045	0.0252	7.4223	6.1566
PDMS	2.4364	0.0282	7.1669	5.8834
HTR2C	2.2822	0.0492	6.4228	5.2324
STK26	2.0534	0.0299	8.5742	7.5362
MAGEC1	9.4116	0.0108	9.1358	5.9613
DMD	2.2421	0.0174	5.5526	4.3878
PLXDC2	10.9874	0.0106	8.2365	4.8598
DYDC2	2.6771	0.0152	7.6098	6.1891
PNLIPRP3	6.3812	0.0152	9.1521	6.5183
FAM198A	2.3401	0.0374	9.1417	7.9151
SORBS1	2.14	0.0364	8.0507	6.9531
ARHJM1	2.0899	0.0263	6.4611	5.3977
ENTPD1	3.3303	0.0182	9.2268	8.0244
LIPA	2.5618	0.0207	11.0887	9.7316
OLFML3	12.8729	0.0072	8.812	5.1257
TNS2	2.857	0.0459	8.1183	6.8813
SLC16A7	2.7269	0.018	7.6046	6.1574
LYZ	4.8877	0.0152	7.341	5.0518
GUPR1	2.3152	0.0313	8.4478	7.2367
FBXW9	2.0531	0.0135	9.6973	8.6595
A2M	3.0851	0.0254	9.4668	7.8415
PZP	2.0925	0.025	7.6095	6.5827
GREP1	2.0571	0.0199	6.9554	5.9148
PTPRR	5.0781	0.019	7.7539	5.409
ALDH1L2	3.9757	0.0108	8.684	6.6928
RDH5	2.3025	0.0108	8.5526	7.3494
HSPB8	2.3061	0.0117	10.0109	8.8049
GPC6	2.0197	0.0131	9.9082	8.8941
NALCN	6.2481	0.0258	7.7448	5.1014
NRXN3	2.4762	0.03	7.4283	6.1201
AHNAK2	2.5997	0.0213	8.0619	6.6835
GABBR1	6.0134	0.018	8.5406	5.8524
ATP10A	2.999	0.016	8.8294	7.5669
CCPG1///MIR62	2.0743	0.0346	9.1202	8.0675
ZDHHC1	3.577	0.043	6.6863	4.7935
GPR158	2.505	0.0298	7.9126	6.5877
GPR158	2.2527	0.0214	10.2788	9.1072
SEPT4	6.2539	0.0072	8.8872	6.2435
CD68	2.4689	0.0174	12.5352	11.2913
RAB27B	2.7412	0.0173	8.4089	6.6541
CDH7	2.595	0.0131	7.8463	6.4705
GHSTP	6.4049	0.0136	6.4823	3.8032
CDH19	3.4663	0.0155	7.1682	5.3748
GDF15	4.8795	0.0049	11.728	9.412
FXYD3///MIR68	6.8627	0.0042	12.6998	9.921
CD22//DMRS19	2.2476	0.0436	8.7198	7.5514
RCN3	2.2605	0.0049	10.8491	9.6853
SEMA6B	2.4794	0.0216	8.3994	7.0329
OLFM2	2.0216	0.0219	8.3196	7.2981
EST2	6.459	0.0131	9.4402	6.7491
PLAUR	2.1155	0.0132	10.6004	9.5139
ZNF776	2.0305	0.0307	7.8075	6.7808
C7orf26//ERP5-90	3.1156	0.035	7.301	6.2615
IFT27	2.0899	0.0403	7.9816	6.9182
ZNF946	2.1811	0.0279	4.2165	3.0915
ZNF946	2.9859	0.0309	7.1851	5.3553
ZFG11A	-2.6941	0.0352	4.2367	5.6666
EDARADD	-2.4679	0.037	4.8462	6.1435
EPHA2	-2.4275	0.0246	5.3942	7.2637
TMCO4	-2.8551	0.0108	6.617	8.1306
RAP1GAP	-3.8761	0.0108	5.2543	7.2095
LAPTM5	-2.9832	0.0485	6.2283	7.4702
SYNC	-2.1773	0.0398	5.3711	6.4396
HEMK1	-9.776	0.0279	5.7262	7.6431
CTSS	-2.0543	0.0143	6.0368	7.0774
RBIG	-2.4598	0.0174	8.3152	9.6102
///ZNF670-ZNF695	-3.1027	0.0108	6.1316	7.7851
KLHL29	-4.5666	0.0166	4.8293	7.0205
ARHGAP25	-2.287	0.0367	7.1085	8.302
POTE6	-7.823	0.0132	3.867	6.8347
B3GALT1	-2.8967	0.0387	4.3889	5.6499
CERS6	-2.3592	0.0414	7.7869	9.0209
ICOS	-8.8068	0.0058	2.9203	6.0589
ADAM23	-3.9993	0.0136	8.1925	9.9577
FAR2P1	-4.155	0.0285	4.7174	6.7723
POTEF	-11.6304	0.0131	3.8913	7.4315
POTE1	-6.4517	0.0217	3.0746	5.7642
GRB14	-2.9466	0.0453	4.3845	5.8949
RFTN1	-2.2282	0.0114	6.5773	7.7392
SUSD5	-2.4041	0.0396	8.0096	9.269
MGLL	-5.7699	0.0072	6.0854	8.5699
B3GALNT1	-5.216	0.018	3.3567	6.8396
EPHB1	-2.9112	0.0443	6.4313	8.0929
GRB14	-2.9466	0.0453	4.3845	5.8949
RFTN1	-2.2282	0.0114	6.5773	7.7392
SUSD5	-2.4041	0.0396	8.0096	9.269
MGLL	-5.7699	0.0072	6.0854	8.5699
B3GALNT1	-5.216	0.018	3.3567	6.8396
EPHB1	-2.9112	0.0443	6.4313	8.0929
GRB14	-2.9466	0.0453	4.3845	5.8949
RFTN1	-2.2282	0.0114	6.5773	7.7392
SUSD5	-2.4041	0.0396	8.0096	9.269
MGLL	-5.7699	0.0072	6.0854	8.5699
B3GALNT1	-5.216	0.018	3.3567	6.8396
EPHB1	-2.9112	0.0443	6.4313	8.0929
MB21D1	-2.9645	0.0393	5.1799	6.7979
SRSF12	-3.0709	0.0108	7.6216	9.24
ZNF716	-5.662	0.0237	5.4255	7.9269
AMPH	-2.566	0.0183	6.3068	7.6869
FABP5	-2.317	0.0112	7.9229	9.1346
RIMS2	-2.155	0.0307	4.7543	5.862
EGR3	-2.9975	0.0174	6.9083	8.4921
TRPA1	-2.2269	0.0461	6.0457	7.2004
EXT1///ibaMis	-2.3109	0.0396	6.2572	7.4656
HACD4	-3.1429	0.0174	7.2737	8.9255
SHB	-3.0477	0.0174	7.5115	9.1192
MAOA	-3.4543	0.0247	5.8037	7.5921
TRO	-4.7652	0.0198	4.2424	6.4949
LONRF3	-13.8226	0.0131	4.8886	8.6244
WNK3	-2.5889	0.0139	5.1755	6.5478
TSPAN7	-2.2004	0.0242	8.0247	9.1625
MGMT	-2.4919	0.0235	5.1718	6.4891
SFMBT2	-3.5509	0.0235	4.5146	6.3428
SORCS1	-2.1489	0.0131	7.4842	8.5874
ZNF215	-2.755	0.012	6.2579	7.72
HTATIP2	-2.0274	0.0282	8.944	9.9636
DERC7	-2.0255	0.0236	6.4523	7.4706
NTM	-10.4911	0.0312	4.851	8.2421
PITM3	-4.0626	0.007	9.2065	11.2289
PHLDA2	-2.2258	0.0166	7.797	8.9414
MPPED2	-2.6801	0.0312	5.9869	7.4092
FABP5	-2.1628	0.011	6.9339	8.0468
SFI1	-2.1935	0.0431	6.3585	7.4927
SYTL2	-2.4783	0.0072	9.3041	10.6124
MMP1	-13.467	0.0108	7.9878	11.7392
PITM2	-2.3441	0.0165	7.3113	8.8692
PITM1	-2.2506	0.0211	6.6045	7.8017
SPX	-2.4285	0.0232	8.7321	9.0127
CNTN1	-2.6048	0.0323	7.9974	9.3785
CRACR2A	-2.6538	0.0136	6.6565	8.1694
SLC39A1	-10.0496	0.0108	9.2094	6.5325
TRPV4	-3.3185	0.0101	8.9501	10.6806
LINC00282	-2.9412	0.0393	8.624	10.1305
TBC1D4	-2.856	0.0303	8.9994	9.6943
DNAJC15	-6.8111	0.007	7.3472	10.1151
CKIP-2	-2.0269	0.0143	7.4485	8.4853
FLVCR2	-2.1524	0.0393	5.1418	6.2477
DNAJB4	-2.767	0.0257	6.2322	7.7006
AGAP1	-2.7991	0.0485	6.448	7.9329
LRRK1	-2.1226	0.0407	8.1143	9.2002
CYP1A1	-2.6169	0.0153	5.8029	7.1908
XYLT1	-3.5821	0.0182	6.7721	8.6129
YPEL3	-2.3649	0.0437	6.7047	7.7942
AGSM3	-2.0116	0.0181	5.8211	6.8285
TMEM59	-2.0987	0.0072	9.4701	10.5576
MEIOC	-2.8785	0.0445	4.1346	5.0599
SPATA22	-6.113	0.0174	5.1691	7.7824
KIAA1211	-4.5799	0.0149	5.2216	7.4169
SETBP1	-2.3802	0.0221	6.6988	7.9498
ZNF382	-4.6536	0.0249	4.3536	7.172
ZNF114	-10.0947	0.0077	7.2847	10.6116
PRDX2	-15.045	0.0152	5.4564	9.5692
ZNF43	-2.1069	0.0354	8.1194	9.2681
ZNF724P	-2.138	0.0239	7.1217	8.2179
ZNF611	-2.7692	0.0345	7.728	9.1375
ZNF888	-2.4762	0.0293	4.8818	6.1899
ZNF730	-6.0707	0.0379	5.5629	8.1641
RPL39P34//ZNF8C	-2.5099	0.0131	7.0385	8.3658
ZNF582-AS1	-2.6685	0.0405	5.2119	6.7322
ZNF607	-2.2272	0.0135	4.3059	5.4305
ZNF28	-9.0467	0.0101	4.6105	7.7878
ZNF816	-2.4499	0.0477	5.7192	7.0119
MYL9	-4.1729	0.017	6.7966	9.0575
BMP7	-2.3585	0.023	7.9222	9.1601
MX1	-2.645	0.0279	6.5742	7.9775
PDXP//SH3BP1	-2.035	0.0101	9.0256	10.0507
BAIAP2L2	-2.683	0.0129	7.7508	9.1638

Figure S2.6: Differentially expressed genes in Clone 7 with respect to unedited cells. SK-MEL-28 melanoma cells along with fold-change (red = up-regulated; green = down-regulated), Benjamine & Hochberg FDR-adjusted *p*-value and average gene expressions.

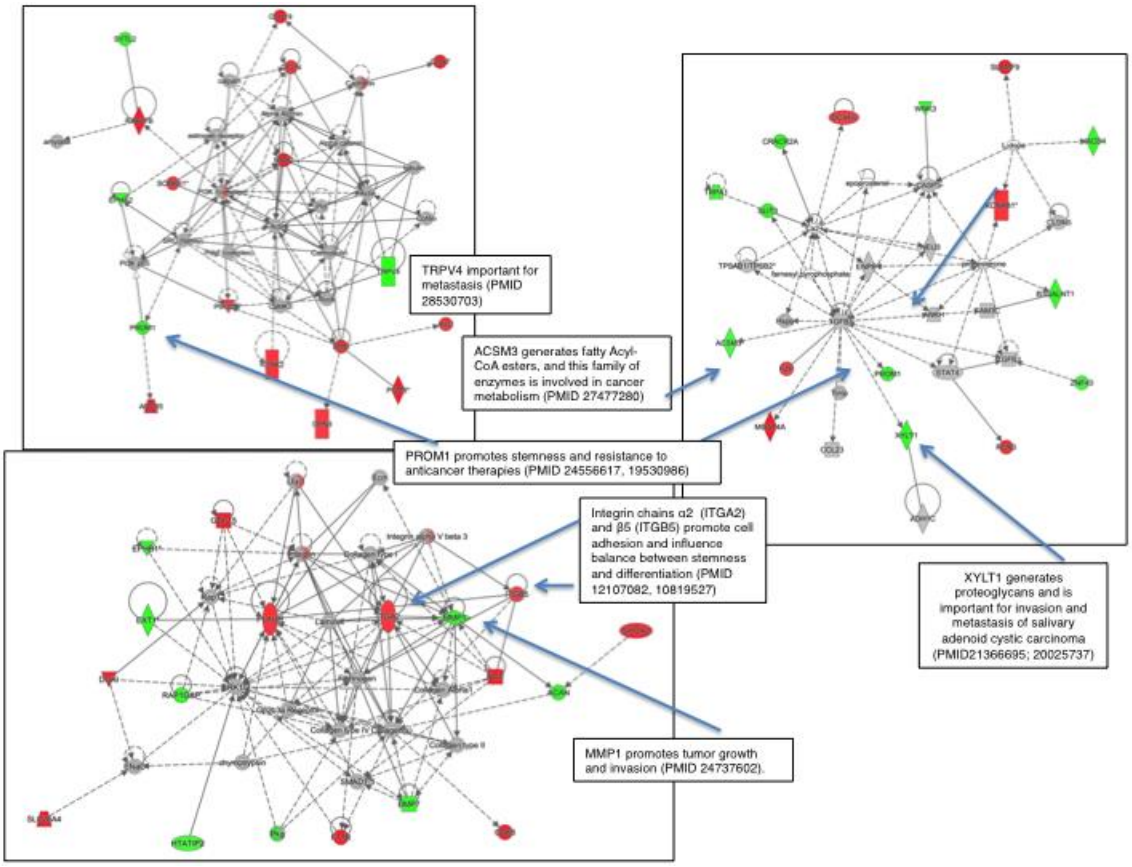

Figure S2.7: Signaling pathway analyses conducted with QIAGEN's Ingenuity pathway analysis (Ingenuity Systems). Green indicates down-regulated transcripts and red indicates up-regulated transcripts in SELENOK-truncated cells compared to wild-type SK-MEL-28 cells.

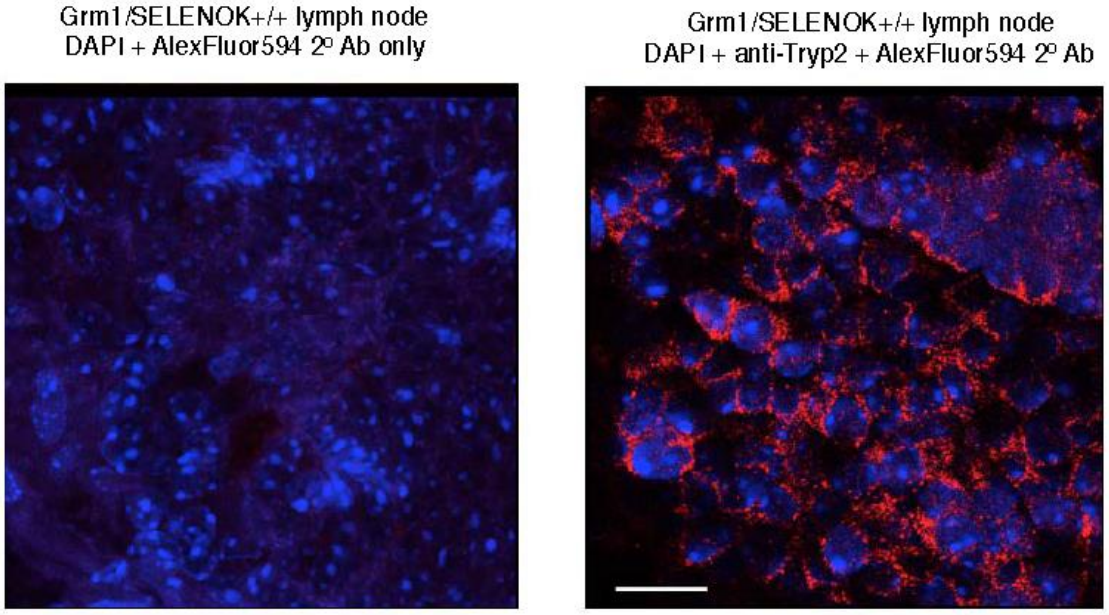

Figure S2.8: Specific immunofluorescence staining using anti-Trp2, scalebar = 20 µm. Blue staining are DAPI-positive nuclei and red cytosolic staining is Trp2 antigen.

Supplemental video 1: SELENOK deficient mice maintain low tumor burden up to 8 months. Video shows mice at 6 months of age that exhibit a lack of melanoma (Grm1-Tg/SELENOK$^{-/-}$) or high levels of melanoma (Grm1-Tg/SELENOK$^{-/+}$). As shown in the video, the mice with high tumor burden are not severely affected in terms of movement or healthy behavior. Several cohorts of both sexes were followed out to the age of 8 months and no increased tumor formation were found in the Grm1-Tg/SELENOK$^{-/-}$ mice

Chapter 3. Development of inhibitors against SELENOK for treatment of melanoma

Introduction

Although published data suggests that targeting SELENOK with inhibitors may be an effective approach for the treatment of cancers that rely on SOCE for disease progression, this approach presents several challenges. Preliminary studies have established that anti-SELENOK antibodies targeting the C-terminal portion of SELENOK can interfere with the palmitoylation reaction catalyzed by the SELENOK/DHHC6 complex. Thus, antibody-based inhibitors (immunotherapeutics) may be an effective therapy to treat melanoma and/or other cancers. However, SELENOK is an intracellular protein which renders standard immunotherapies unrealistic since targets for these drugs are conventionally extra-cellular proteins. Nevertheless, intracellular proteins constitute nearly half of the human proteome and represent a large reservoir of potential therapeutic targets [188]. Therefore, in order to effectively target intracellular proteins such as SELENOK, alternative approaches or new technologies that permit the entry of large, hydrophilic therapeutics across biological membranes must be considered.

Synthesis of small molecules that bind to critical regions of target proteins is a more conventional approach for developing inhibitors against intracellular proteins like SELENOK. However, this approach also presents challenges, such as a need for precise structural information of the target protein. This approach is particular limited by the fact that the exposed, cytosolic domain of SELENOK is intrinsically disordered [70], which limits the range and efficacy of small molecule inhibitors. Another approach for targeting intracellular proteins involves the combination of two emerging technologies: single domain antibodies (sdAbs, a.k.a. nanobodies) from camelids [189, 190] and cell penetrating peptides (CPPs) [191-193]. In theory, these small versions of Abs (~15 kDa) exhibit the high specificity of conventional Abs while demonstrating a greater ability to translocate across the cell membranes. Indeed, studies have demonstrated the use of humanized sdAb fused to CPPs to effectively inhibit their intracellular targets. For example, CPP-sdAb directed against different hepatitis C virus (HCV) proteins

inhibited viral replication within cells [194-196]. Small molecule inhibitors often have off target effects due to promiscuous protein binding, whereas sdAbs exhibit the septicity of conventional Abs and therefore may cause less side effects when applied to human health. However, further studies utilizing CPP-sdAbs in human trials need to be performed.

A third possible approach for targeting SELENOK for functional inhibition involves taking advantage of the SH3 binding domain (SH3BD) in its cytosolic region. Previous studies have demonstrated that the SH3BD in SELENOK binds to the SH3 domain of DHHC6 [10], and this interaction is required for the palmitoylating function of the SELENOK/DHHC6 complex. Numerous studies have demonstrated the possibility of disrupting protein-protein interactions as a potential therapy for cancer [197-199]. Furthermore, specificity and inhibitor binding strength can be increased via directed mutagenesis of the sequences flanking the PxxP motif within the SH3BD [200]. This chapter will focus on our efforts to design an SH3 based inhibitor of SELENOK and its successful inhibition of SELENOK/DHHC6 palmitoylation ability in a cell free environment.

Background

Cell penetrating peptides

Polypeptides, oligonucleotides, and antibodies are intriguing options for new pharmaceuticals that can provide specificity and a inhibit a wider range of drug targets. However, because of their low biomembrane permeability, delivering them inside of cells is a challenge that must be overcome. Fortunately, investigations into this problem have found that certain peptides can penetrate the cell membrane and gain entry into the cell. These so called cell penetrating peptides (CPPs) are defined as amphiphilic peptides that contain up to 30 amino acids, which can be internalized by cells in an energy independent manner or via receptor mediated endocytosis [201]. Thus, attaching CPPs to large or hydrophilic drugs can permit their entry into the cell where they can bind their intracellular targets. There exist several classes of CPPs that can be broadly categorized as either cationic (e.g. HIV TAT), amphipathic (e.g. Pep-1), and hydrophobic (e.g. HN-1). Several studies have shown the efficacy of CPPs in the delivery of cargo to tumor cells [202-204] but more investigation into their efficacy in treating human disease is necessary.

Penetratrin is a sequence of 16 amino acids (RQIKIWFQNRRM KWKK), derived from the third helix of the *Drosophila* Antennapedia homeodomain protein and was the first CPP derived from non-viral protein [205]. Translocation of penetratin through the cell membrane occurs even when bound to relatively large, hydrophilic molecules, including oligonucleotides, peptides, nucleic acids etc. For example, penetratin has been shown to be effective in the delivery of siRNA to primary mammalian neurons [206] and delivery of peptides containing cytotoxic T lymphocyte (CTL) epitopes to target cells [207]. In our efforts to generate an inhibitor against SELENOK, we have included the penetratin sequence proximal to the N-terminus of the peptide inhibitor, which may permit its entry into target cells.

Intrinsically disordered proteins

The protein structure-function paradigm, which states that a well-defined structure is necessary for protein function, dominated the scientific communities' understanding of protein function in the 20th century. Only recently, an appreciation for the number and importance of disordered proteins has developed. Indeed, it was only at the end of the 20th century when it was formally proposed that naturally flexible proteins are not just rare exceptions, but instead represent a unique and broad class of proteins [208-210]. The generally accepted definition of intrinsically disordered protein (IDP) is a protein, (or protein domain) that is biologically active, but exists as collapsed or dynamically mobile at either the level of secondary or tertiary structure [211]. IDPs are associated with a large variety of biological functions, including cell signaling, scaffolding, and recognition of misfolded proteins [212].

Many IDPs are characterized as promiscuous, meaning they interact with multiple protein partners in numerous interactions. Thus, IDPs frequently serve as hubs/nodes in protein interaction networks [213, 214]. IDPs can serve in protein hubs by three distinct mechanisms: 1) multiple intrinsic disordered regions (IDRs) can serve as docking sites for multiple binding partners; 2) multiple IDPs can bind to same structured proteins in the protein hub; and 3) IDRs can serve as flexible linkers between separate functional domains and enhance binding promiscuity [213, 215]. Protein hubs are essential for the normal functioning of organisms and their disruption can be extremely deleterious [216]. Therefore, it is not surprising that many IDPs are implicated in human diseases that demonstrate aberrant cell signaling such as cancer, cardiovascular disease, and some neurodegenerative diseases [217-219]. For these reasons, IDPs would theoretically make attractive drug targets to treat these diseases. However, because these disordered proteins do not directly perform catalysis via substrate interaction within enzymatic active sites, small molecule inhibitor against IDPs are difficult to generate.

SELENOK is predicted an IDP based on modeling and, as mentioned previously, may be a good target for the treatment of metastatic melanoma (see Chapter2). Therefore, design of inhibitors against SELENOK requires an understanding of the limitations involved in targeting IDPs.

Originally, to circumvent this challenge, our laboratory pursued a single domain antibody (sdAb) approach to target SELENOK, but due to technical limitations, this approach was abandoned. Therefore, we designed a peptide inhibitor based on disrupting the interaction of SELENOK with DHHC6, which will be described in detail later.

DHHC family of Protein Acyl-Transferases

Protein palmitoylation is a ubiquitous post translational modification that not only promotes the anchorage of proteins in the membrane, but also modulates protein trafficking, vesical fusion, organelle inheritance and hydrophobic protein-protein interactions [55]. S-palmitoylation is the addition of a saturated 16-carbon fatty acid moiety (or longer chain fatty acids) to sulfhydryl groups of cysteine residues via a thioester bond and is reversible [220]. The reversible nature of S-palmitoylation permits it to act in a regulatory fashion akin to other reversible post translational modifications such as protein phosphorylation and ubiquitination [221, 222] . Although the formation of the palmitoyl thioester bond can occur spontaneously in the presence of palmitoyl-CoA [223], a genetic screen in *Saccharomyces cerevisiae*, demonstrated the requirement for the first protein acyl-transferase (PAT), Erf2, along with a second protein Erf4, for the proper localization of a palmitoylation-dependent RAS protein in the plasma membrane [224]. Erf2 (mammalian ortholog DHHC9) contains a conserved domain referred to as the DHHC domain, which is shared by numerous genes in eukaryotes only and is integral to the palmitoyl transfer reaction. DHHC proteins are found in all eukaryotes (not yet been observed in prokaryotes or archaea) and range from 1 to 8 in fungi to greater than 20 in metazoans [222]. All DHHC proteins, except for yeast Yn1155W, are predicted to be polytopic integral membrane proteins with at least four transmembrane domains [222]. DHHC proteins are expressed in a variety of tissues and occupy different subcellular locations, including the Golgi apparatus, the ER, and the plasma membrane [225, 226].

The DHHC domain is embedded in a larger motif referred to as the DHHC-Cysteine Rich Domain (CRD) [227] with the following consensus sequence: $Cx_2Cx_9HCx_2Cx_4DHHCx_5Cx_4Nx_3F$ where x represents any amino acid. The DHHC-CRD is located between TM2 and TM3 [222]

and has been mapped to a cytosolic loop segment [228]. Although it is evident from the data that DHHC proteins catalyze the palmitoylation of cytosolic protein substrates, the mechanism by which this occurs is not fully understood. Current evidence suggests that the conserved DHHC domain is necessary for DHHC protein palmitoylation. For example, all DHHC proteins are palmitoylated on a cysteine residue when incubated with palmitoyl-CoA [225, 229] and this autopalmitoylation is abolished when one or more cysteine residues in the DHHC motif are mutated [229]. Furthermore, the acyl-enzyme intermediate of Erf2 is sensitive to hydroxylamine treatment, suggesting a putative labile thioester linkage to cysteine [230]. Taken together, the evidence suggests that autopalmitoylation, of which DHHC motif is necessary, represents an acyl-enzyme intermediate and is followed by transfer of the palmitoyl group to a target protein.

SELENOK deficiency leads to decreased IP3R palmitoylation and expression in immune and melanoma cells, leading to impaired SOCE in these cell types. Because SELENOK is not an enzyme, it was clear that SELENOK required one or more partners to enhance the palmitoylation of the IP3R. A clue as to which enzyme this could be came from the fact that the DHHC6 is the only acyl-transferase containing an SH3 domain, which may interact with SH3BD on SELENOK. Indeed, it was demonstrated that SELENOK and DHHC6 interact at the ER membrane and this interaction is required for the efficient palmitoylation of the IP3R. DHHC6 is one of two DHHC enzymes primary localized in the ER (the other being DHHC4) [231] and is a four-pass integral transmembrane protein with the DHHC domain located in the cytosol. In addition to its role in palmitoylating the IP3R, DHHC6 also mediates the palmitoylation of the E3 ubiquitin-protein ligase AMFR [232] Na^{+}/Ca^{2+} exchange protein (Calx) [233], transferrin receptor protein 1 (TFRC) [234], and may be regulated by another acyl-transferase DHHC16 [235].

The Src homology 3 domain as potential drug target

Eukaryotic signal transduction utilizes the transient assembly of protein-protein complexes for the induction of cellular programs such as survival, proliferation, and migration. The formation of many of these complexes requires protein-protein interaction domains such as SRC Homology

2 Domain (SH2) and SRC Homology 3 domain (SH3) [236, 237]. While SH2 domains interact with phosphotyrosine residues, SH3 domains recognize proline-rich motifs of their partner proteins [238, 239]. SH3 domains are approximately 60 amino acids in length and consist of five antiparallel β-sheets β-barrel-like structure that form a beta-barrel-like structure [240]. SH3 domains bind proline-rich peptides with relatively low affinity ($K_d = 10^{-6} – 10^{-4}$ M) and requires the minimal consensus sequence PXXP [241, 242]. Specificity is encoded into SH3/SH3BD protein interaction by residues adjacent to the protein binding motif itself [200] and manipulation of the adjacent residues or the proline residues themselves, can enhance the binding capacity of a variety of inhibitors.

Incorporation of non-natural N-substituted peptoids into the SH3 domain, in place of the naturally N-substituted proline residues, can increase SH3/SH3BD binding affinity to nanomolar levels [243]. Additionally, use of a proline-rich, dimeric peptide inhibitor against the SH3 containing protein, growth factor receptor-bound protein 2 (Grb2), was shown to be successful in disrupting the SH3/SH3BD GRB2/Sos interaction [244]. The dimeric peptide bound Grb2 with high affinity ($K_d = 40$ nM) and was shown to be effective in homogenates of human fibroblast cells at a concentration of 1 μM [244]. Most inhibitors in clinical trials are targeted against GPCRs and other enzymes. Targeting protein-protein interactions via SH3 domains provides new possibility in treating illnesses that are characterized by aberrant intracellular signaling. In this chapter, our progress in developing inhibitors that disrupt SELENOK/DHHC6 catalyzed palmitoylation is presented.

Results

Antibody based Inhibition of SELENOK reduces palmitoylation of a DHHC6 target in a cell free environment

Inhibition of SELENOK may disrupt SELENOK/DHHC6 mediated palmitoylation of important cellular targets and may represent a new therapy for cancers that utilize SOCE for their growth and development (see Chapter 2). In order to test the efficacy of various inhibitors to disrupt SELENOK/DHHC6 mediated palmitoylation, a protein acyl-transferase (PAT) assay was used. The PAT utilizes thin layer chromatography and fluorescence to visualize palmitoylation of a peptide derived from the known DHHC6 target protein, CD36 (MGCDRNCK), in the presence of SELENOK and various inhibitors (Figure 3.1). Because the assay is performed in an aqueous, cell free environment, a water-soluble version of DHHC6 (cDHHC6) was used for all PAT assays performed. To establish a premise for the inhibition of SELENOK as an effective drug target, an antibody (Ab) specific to the C-terminal portion of SELENOK was tested for its ability to inhibit SELENOK/DHHC6 mediated palmitoylation. SELENOK Ab treatment reduced the rate of SELENOK/DHHC6 mediated palmitoylation to levels equivalent to palmitoylation rates in the absence of SELENOK (Figure 3.2A-B). Furthermore, a non-specific isotype matched Ab had no effect on protein palmitoylation (Figure S3.1), suggesting that the reduction in palmitoylation observed was due to disruption of SELENOK specifically. Because protein thiols can be palmitoylated nonenzymatically in the presence of palmitoyl-CoA [245], we tested palmitoylation of CD36 in the absence of cDHHC6. However, without cDHHC6 protein palmitoylation was eliminated in this assay (Figure S3.2).

Next, because the functional domain of SELENOK for regulation of palmitoylation is located near the C-terminus (a.a. 81-93), including the biologically active Sec residue (a.a 92), inhibition of SELENOK may be epitope specific. Therefore, an N-terminal version of SELENOK Ab was compared to the C-terminal based Ab in terms of inhibitory capacity. Surprisingly, the N-terminal antibody reduced palmitoylation rates to the same extent as the C-terminal antibody (Figure 3.3A-B). This may be due to steric hinderance, resulting from binding of either Ab to

SELENOK, resulting in a disruption of the SELENOK/DHHC6 interaction. Taken together, the data suggests that inhibitors that can bind SELENOK may interfere with SELENOK/DHCC6 protein palmitoylation.

Recombinant SELENOK based inhibitor reduces palmitoylation

Because inhibition of SELENOK by antibody specific binding decreased the functional role of SELENOK in a cell free environment, we next asked if a peptide based inhibitory approach was feasible. SELENOK interacts with DHHC6 via an SH3/SH3BD interaction [52], therefore a short peptide (80 a.a) was designed with a similar primary amino acid sequence to SELENOK that included the proline rich SH3BD but lacked the biologically active functional domain (Figure 3.4).

Recombinant inhibitory peptide was purified from *E. coli* lysates and tested using the same palmitoylation assay as described above. Surprisingly, the purified inhibitory peptide increased SELENOK/DHHC6 mediated palmitoylation of CD36 above control levels and a mutated, putatively catalytically dead version of DHHC6 (DQHR) demonstrated palmitoylation rates equivalent to control (Figure 3.5A-C). These results indicate that either the inhibitory peptide interacts SELENOK/DHHC6 to enhance protein palmitoylation or impurities from the purification process of the inhibitor are interfering with the palmitoylation reaction. To examine the latter possibility, SDS page and Coomassie blue staining were performed for the inhibitor and DHHC6 (which is purified using a similar method). Results showed an abundance of proteins that did not correspond to the estimated size for DHHC6 (~ 26 kDa) or inhibitor (~10 kDa) (Figure 3.6). Efforts were made to increase the specificity of the purification process which resulted in substantially cleaner product for both DHHC6 and inhibitor (Figure 3.7A-B). The newly purified components were tested in the palmitoylation assay and the results demonstrated that incubation of purified inhibitor with SELENOK/DHHC6 reduced the rate of palmitoylation compared to control (Figure 3.8A-B). These results suggest that purified recombinant peptide could inhibit SELENOK/DHHC6 mediated palmitoylation but purification of the inhibitor or other components of palmitoylation may confound the results.

SELENOK inhibitor interacts physically with recombinant cDHHC6

Technical complications surrounding the purification of recombinant peptides led us to pursue a synthetic approach to generate inhibitory compounds. Because the cytosolic portion of SELENOK is predicted to be intrinsically disordered [70], misfolding issues in the absence of cellular folding machinery may not be an issue here. Therefore, an inhibitor of SELENOK was synthesized with the same primary amino acid sequence as recombinant SELENOK (Figure 3.4) but with the functional domain for the regulation of palmitoylation excluded. Also, the inhibitor peptide included the proline rich SH3BD that in concert with flanking amino acids, allows for SELENOK/DHHC6 interaction. This approach may disrupt SELENOK/DHHC6 mediated palmitoylation by acting as a competitive inhibitor and abrogating full-length SELENOK mediated palmitoylation of the IP3R. In addition, a control peptide was synthesized that contains the proline rich SH3BD mutated to 7 alanine residues that is putatively sufficient to disrupts peptide/DHHC6 binding (Figure 3.4).

As mentioned previously, SELENOK interacts with DHHC6 via an SH3/SH3BD motif. Therefore, to test if the synthetic inhibitory peptide can physically bind to cDHHC6 and if the SH3BD is necessary, co-Immunoprecipitation was performed. The results indicated that the synthetic inhibitor and the control peptide both interact with cDHHC6 (Figure 3.9). This suggests that the SELENOK inhibitor can bind cDHHC6 but the SH3BD is not necessary with the concentrations used. The overall specificity is likely a composite of the SH3BD and flanking amino acids, therefore, mutating the amino acids flanking the SH3BD and adjusting the concentration of control peptide/DHHC6 may elucidate what regions are sufficient for peptide/DHHC6 binding. Finally, the synthetic inhibitor peptide was tested for its ability to reduce SELENOK/DHHC6 mediated palmitoylation in a cell free system. Consistent with the co-Immunoprecipitation results, inhibitor peptide reduced palmitoylation of a DHHC6 target and the control peptide also reduced palmitoylation rates (Figure 3.10). This results suggest that the synthetic inhibitor and control peptide can bind DHHC6 and disrupt DHHC6/SELENOK mediated palmitoylation in a cell free environment.

CPP containing SELENOK inhibitor can translocate through the plasma membrane.

Because SELENOK is an intracellular target, any potential drug that targets SELENOK must be able to enter the cell to interfere with the biological function of SELENOK. To this end, we attached the CPP, penetratin, to the SELENOK inhibitor peptide (Fig 3.4). To test if attachment of this CPP was sufficient to allow translocation of inhibitor through the plasma membrane, human melanoma cells were treated with inhibitor or a vehicle control (v.c.) and subsequently stained for the presence of intracellular SELENOK inhibitor. Originally, the 6×His tag present on the inhibitor was the domain used to detect the presence of intracellular inhibitor, but non-specific background staining could not be distinguished from 6×His tag signal (Figure S3.3). Therefore, an antibody specific for the TEV cleavage site of the SELENOK inhibitor was used and intracellular inhibitor was detected in the melanoma cells treated with the inhibitor and not for the v.c. treated cells (Figure 3.11).

Discussion and future directions

The targeting of intracellular proteins that support tumor growth and progression, including components of SOCE, has demonstrated some limited success in the treatment of certain cancers [246]. However, tumor cells can rapidly develop resistance [247] and therefore the discovery of new drug targets is needed. The data presented here shows for the first time that it is possible to target SELENOK with either immunotherapy or peptides that can interact with the SELENOK protein and limit its biological function. SELENOK may be an attractive protein target for the treatment of cancers that utilize SOCE for their growth and proliferation as it is critical for the proper expression of an important SOCE component, the IP3R Ca^{2+} channel. Importantly, IP3R mediated Ca^{2+} flux is upstream of multiple Ca^{2+} dependent signaling pathways that can become constitutively activated by oncogenic mutations in a variety of their individual components such as BRAF [141]. Thus, inhibiting SELENOK may have multiple beneficial downstream effects by reversing calcium signaling remodeling in tumor cells.

The efficacy of antibody derived therapies that can act as inhibitors of intracellular protein targets was previously demonstrated by experiments including sequestration of an HCV viral protein that inhibited viral replication [194] or targeting of an F-actin capping protein, CapG, that reduced breast cancer metastasis [248]. Both treatments utilized sdAbs (described in the introduction) to bind and biologically inhibit their respective targets. The disruption of SELENOK/cDHHC6 mediated palmitoylation with an antibody specific to SELENOK suggest the possibility of targeting SELENOK with some form of immunotherapy, including sdAbs. Indeed, we originally planned to use sdAbs in combination with the CPP penetratin to target intracellular SELENOK in melanoma, but for technical reason we were unable to pursue this route. Interestingly, either an antibody raised against the C-terminus or the N-terminus displayed an ability to inhibit SELENOK/cDHHC6 mediated palmitoylation. This was surprising in that the functional domain of SELENOK (a.a. 82-94) which includes the biological relevant Sec residue (see Figure 1.1 and 1.3) is located proximal to the C-terminus and thus only the C-terminus raised antibody was expected to reduce rates of palmitoylation. Perhaps due to the relatively small size of SELENOK (~12 kDa) antibody engagement to any portion of SELENOK

resulted in steric interference that prevented SELENOK/cDHHC6 interaction and a resultant reduction in palmitoylation of the target peptide. Another possibly may be that the aqueous, cell-free environment that the reaction takes place in produces results that may not occur *in vivo* and thus, N-terminal SELENOK antibody interference may be an artifact of the experimental design. Further investigation utilizing additional antigenic epitopes of SELENOK may help to solve this problem.

Targeting SH3 domains on proteins involved in signal transduction, to specifically prevent protein-protein interaction has been considered for various disease states [249]. SH3 domains mediate signal transduction by providing platforms for disparate proteins to interact and therefore can be thought of as adaptor proteins. Because SELENOK and DHHC6 interact via an SH3/SH3BD arrangement the inhibitor designed to disrupt this interaction included the SH3BD of SELENOK and the surrounding residues. This may allow the inhibitor to act as a competitive inhibitor in regard to the SELENOK/DHHC6 complex. As shown by the co-Immunoprecipitation data, the SELENOK based inhibitor was able to physically interact with cDHHC6, but the control peptide, which does not contain the proline rich SH3BD, was also able to physically interact with cDHHC6. This may indicate several possibilities: 1) SELENOK and DHHC6 do not require an SH3/SH3BD motif for their interaction; 2) residues flanking the SH3BD contribute to SELENOK/DHHC6 interaction; or 3) the high concentrations and close proximity due to the artificial environment of the cell free reaction is responsible for non-specific binding that would not occur *in vivo*. The first possibility is unlikely in that experiments performed where the SH3BD of SELENOK was deleted, resulted in the abrogation of SELENOK/DHHC6 interaction as observed by co-Immunoprecipitation and *in vitro* fluorescent based colocalization [52]. The second possibility is interesting because the residues that flank SH3 domains provide some form of specificity for SH3/SH3BD interactions [250], which implies that these amino acids modulate the local energetics at the entire binding interface. Planned studies by our group will involve truncation of the inhibitor peptide to its smallest, effective version. This may help elucidate the importance of the residues flanking the SH3BD. The third possibility can be tested by investigating colocalization, of the inhibitor and DHHC6 *in vitr*o, which is an experiment that we also plan to perform.

The immunotherapies and SH3 based peptides described above are relatively large and hydrophilic, which makes their delivery inside cells challenging. Attachment of CPPs can enhance translocation of these drugs across biological membranes. For this reason, the design of the SELENOK inhibitor included the amino acid sequence for the CPP, penetratin, near the N-terminus. The confocal microscopy results seem to indicate that the inclusion of the penetratrin motif is sufficient to allow penetratin linked inhibitor to enter melanoma cells *in vitro*. However, other studies have demonstrated that the staining and fixation process of cells, for visualization of CPP-cargo entry into cells, can produce false positives [251]. Therefore, further investigation is requited to determine if penetratin or more/other CPPs is necessary to bring SELENOK based inhibitor cargo into cells.

In addition to the experiments planned for determining the smallest portion of SELENOK based inhibitor that can optimally inhibit SELENOK/DHHC6 based palmitoylation, we are planning on experiments that can test SELENOK/DHCC6 using thermophoresis and exploring new avenues for the design of SELENOK inhibitors. One of these new techniques for drug discovery is known as “tethering” ([252]). Tethering is a method of drug discovery that does not rely noncovalent interactions between target protein and small-molecule ligands alone, but instead uses a library of disulfide-containing fragments that form a disulfide bond with a cysteine residue of the target protein. This brings the fragments in proximity to the target protein and allows for the use of relatively little protein (10 – 50 mg) to screen more than 10,000 fragments.

Overall, the novel data demonstrating that SELENOK deficiency inhibits the progression of melanoma tumor cells *in vitro* and *in vivo* and the observation SELENOK can be targeted and rendered biologically inert by immunotherapy or peptide fragment application, supports further consideration for SELENOK as a potential therapeutic target for melanoma and SOCE dependent cancers.

Methods and Materials

Antibodies

Primary antibodies for immunofluorescence included rabbit monoclonal anti-TEV (Invitrogen, PA1-119) and mouse-monoclonal FITC labelled anti-His (Miltenyi biotec, 130-098-808). Goat-anti-rabbit immunofluorescence secondary Alexafluor595 antibody was purchased from ThermoFisher (A11011).

Co-Immunoprecipitation assays

In a microcentrifuge tube, 10 µL of recombinant cDHHC6 and 5 µL of the synthesized inhibitor/control peptide were combined with 5 uL of anti-TEV antibody and incubated overnight at 4 ºC. The next day, 100 uL of Protein A resin slurry (Thermo Scientific, 20365) was added to the antigen-antibody complex and incubated with gentle shaking for 2 h at room temperature. The reaction mixture was washed by adding 0.5 mL of 25mM Tris, 150mM NaCl; pH 7.2 and centrifuged for 2 min at 2500 × *g.* The wash step was repeated twice and a final wash with 0.5 mL dH_2O was performed, following by centrifugation for 3 min at 2500 × *g*. To elute the immune complex, 50 uL of Electrophoresis Loading Buffer (Bio-Rad) was added to the complex-bound resin and incubated for 5 min at 95 ºC. After incubation, the reaction mixture was centrifuged for 3 min at 2500 × *g* and the supernatant was collected and used immediately for SDS-PAGE.

In order to determine the size and band position for each protein component, recombinant cDHHC6, inhibitor, control peptide, and TEV were loaded into separate wells in addition to the immune complexes described above. After protein separation by SDS-PAGE the gel was stained by incubation with 50 mL GelCode Blue Safe Protein Stain (Thermo Fisher) for 1 h and de-stained overnight with ultrapure H_2O. Pictures of the gel were recorded using a Gel logic 200 imaging system in a Kodak *uv* illuminator.

Immunofluorescence

The validated human melanoma cell line, SK-MEL28, was obtained from the University of Hawaii Cancer Center. The cells were cultured in RPMI media with 10% fetal bovine serum and 1% Antibiotic-Antimycotic (all from GIBCO/ThermoFisher) and grown to 90 confluency. Cells were then trypsonized and seeded onto 18mm round microscope glass cover slides in a 12-well plate. Cell were washed with PBS and incubated with 2% PFA in PBS for 10 min on ice to fix the cells. After 3 washes with PBS, cells were then permeabilized by incubation with 0.1% Triton X in PBS for 3 min at room temperature. Cells were washed 3 more times with T-PBS and incubated with 5% goat serum in T-PBS for 1h. Next, cells were incubated with anti-TEV antibody in T-PBS with 5% goat serum for 1 h at room temperature. Cells were then washed three times with T-PBS and incubated with Alexafluor595 secondary antibody for 45 min at room temperature and protected from light. Finally, three more washes with T-PBS were performed and cells were mounted and the nuclei stained using VECTASHIELD mounting medium with DAPI (VECTOR laboratories). Images were obtained using a Leica Microsystems LAS AF TCS SP5 confocal microscope.

Recombinant inhibitor design and protein purification

The recombinant inhibitor of SELENOK and catalytically dead DQHR were both generated by VectorBuilder Inc. and encoded in the bacterial protein expression vector pBAD; provided in the bacterial cloning host Stbl3. The pBAD vector utilizes an arabinose-based operon and therefore pilot studies were performed that determined the optimal arabinose percentage for protein induction to be 0.002% arabinose in LB broth. Bacterial cultures were grown overnight at 37 °C in LB broth and 0.002% arabinose was added when bacterial cultures reached an OD_{600} = 0.5 and grown for an additional 4 h. To pellet the bacteria, cultures were centrifuged at 10,000 × *g* for 10 min and pellets were lysed by incubation with 50 nM NaH_2PO_4, 300 mM NaCl, 20 mM imidazole buffer with 1 mg/mL lysozyme, 10 µg/mL RNase, and 5 µg/mL DNase for 30 in at 4 °C. Additionally, cells were further lysed using a FB50 Fisher Scientific probe sonicator using six 10 s bursts at 200-300 W with a 10 s cooling period between each burst. Next, lysates were

incubated with 4 mL of Ni-NTA 50% slurry in methanol for 1h at 4 °C on a rotary shaker set at 200 rpm. The lysate-Ni-NTA mixture was loaded into a Pierce Centrifuge Column (Thermo Fisher) and supernatant was allowed to flow through. The column was washed twice with 50 nM NaH_2PO_4, 300 mM NaCl, 20 mM imidazole buffer and eluted in twenty 100 µL fractions using 50 nM NaH_2PO_4, 300 mM NaCl, 250 mM imidazole. Elution fractions were analyzed using SDS-PAGE and GelCode blue safe protein stain was used to determine the elution fractions that contained the recombinant protein of interest. These fractions were recombined and dialyzed overnight in 2 L of PBS at 4 °C to removed excess imizadole and stored at -20 °C.

Protein acyl-transferase assays

For all protein acyl-transferase assays a cytosolic version of DHHC6 termed cDHHC6 was used. cDHHC6 was generated by cloning the two functional cytosolic domains of DHHC6 connected by a flexible linker domain (GGGSGGGSGGGS) into a pET-14b His-tagged expression vector (GenScript, Piscataway, NJ). cDHHC6 was purified using a Ni-NTA (G Biosciences) agarose column and stored in aliquots at -20 ˚C. Recombinant SELENOK was obtained from the laboratory of Sharon Rozovsky (University of Delaware). FITC-labeled fluorescent peptide corresponding to the N-terminal dicysteine palmitoylation consensus sequence of CD36 (MCDRNCK) was purchased from Peptide 2.0 (Chantilly, VA). NBD labeled Palmitoyl-CoA was purchased from Peptide 2.0 (Chantilly, VA). Recombinant SELENOK inhibitor was purchased from (VectorBuilder) and purified as described in recombinant inhibitor design and protein purification section. Synthetic inhibitor and control peptide was purchases from AbClonal (Woburn, MA).Prior to protein acyl-transferase assay the FITC-labeled peptide (1 mM) was treated with 10 mM DTT at room temp. for 1 hr. to reduce disulfide linked dimers. Additionally, SELENOK was incubated with cDHHC6 for 1 hr. with the following treatments Ab, inhibitor, PBS. Next, the reaction mixtures and reduced peptides were added to 50 mM MES, pH 7.4 containing 0.05% DDM and 10 µM NBD-labelled Palmitoyl-CoA to yield a final concentration of 10 µM FITC-labeled peptide and incubated at 30 ˚C for 2 to 60 min. After reaction completion at desired time point, 10 uL of reaction mixture were collected and stored on ice and 5 uL aliquots were spotted on reverse-phase C-18 TLC plates (Millipore/Sigma) and

resolved using a 40% acetonitrile mobile phase. Fluorescent images were obtained using a Kodak *uv* illuminator with a Gel Logic 200 Imaging System. ImageJ was used to measure the fluorescent intensity of the FITC-labelled peptide and the palmitoylated FITV-labelled peptide to estimate rates of palmitoylation.

Figures

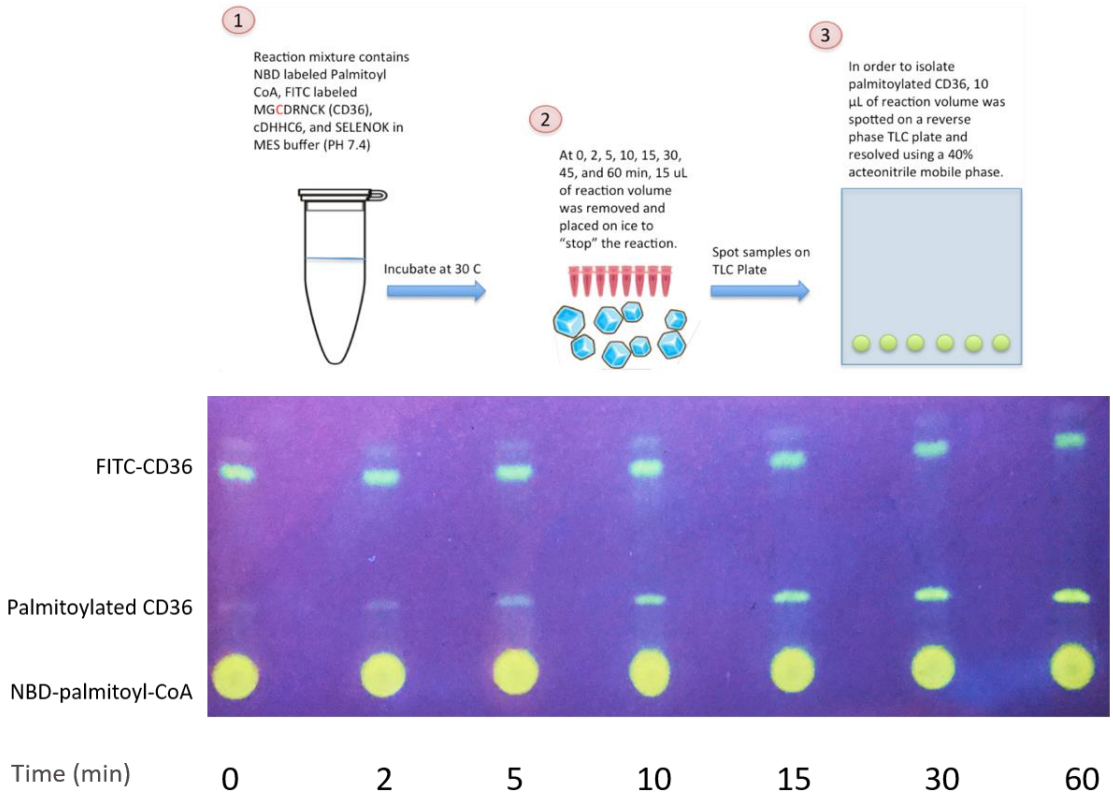

Figure 3.1 Design of Thin layer chromatography-based protein acyl-transferase assay. Schematic of protein acyl-transferase assay (i.e., palmitoylation assay). Assay utilizes fluorescence as a read out for rate of palmitoylation where the palmitate donor, palmitoyl-CoA, is fused with the fluorochrome nitrobenzoxadiazole (NBD)
on the palmitate moiety and the target of palmitoylation CD36, is labelled with the fluorochrome fluorescein isothiocyanate (FITC). Palmitoylated FITC-CD36 migrates to a lesser extent than palmitoylated CD36 on the TLC plate. Numbering describes the steps for the assay.

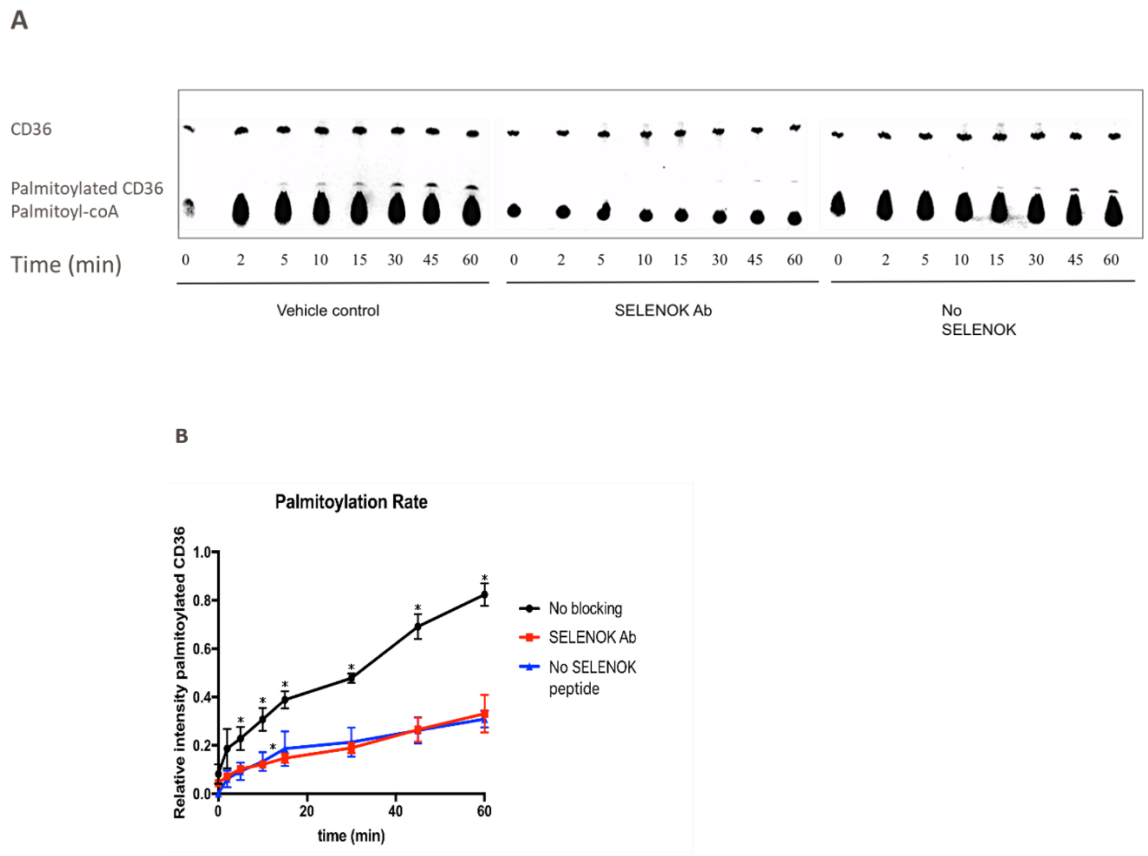

Figure 3.2 A SELENOK specific antibody can inhibit the rate of SELENOK/DHHC6 palmitoylation in a cell free system. Results of protein acyl-transferase assay with or without SELENOK protein present. (**A**) Image of *uv* illuminated TLC plate demonstrates reduced palmitoylation when reaction mixture does not include SELENOK or includes an antibody specific to SELENOK. (**B**) Graph represents relative rate of palmitoylation from three independent experiments. No blocking refers to no antibody present. Results are expressed as mean ± SEM and a one-way ANOVA with Tukey post-test was used to analyze the groups, $^{*}p < 0.05$.

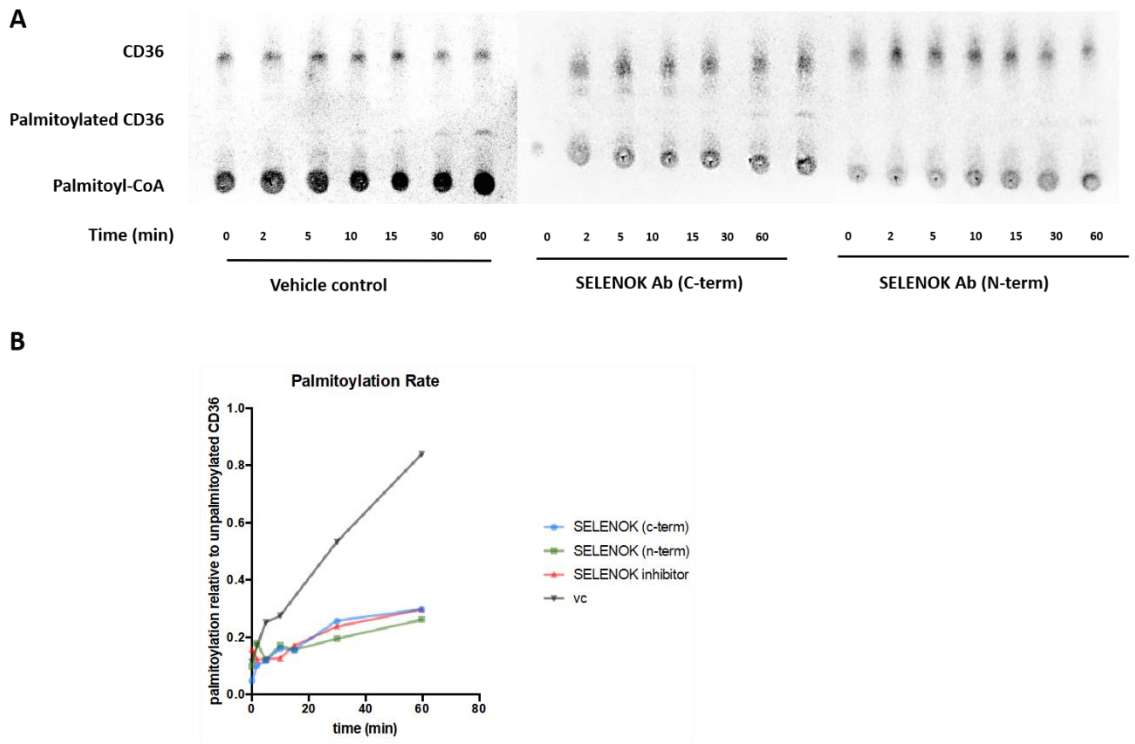

Figure 3.3 Both C-terminal and N-terminal SELENOK antibodies inhibit SELENOK/DHHC6 mediated palmitoylation. Results of protein acyl-transferase assay with antibodies specific to separate epitopes on SELENOK. (**A)** Image of *uv* illuminated TLC plate comparing palmitoylation at various time points for the two epitope specific antibodies that bind SELENOK. (**B**) Graph displaying palmitoylation rate of C-terminal antibodies (SELENOK (c-term)) and N-terminal antibodies (SELENOK (n-term)). Both SELENOK specific antibodies reduce palmitoylation compared to vehicle control (vc).

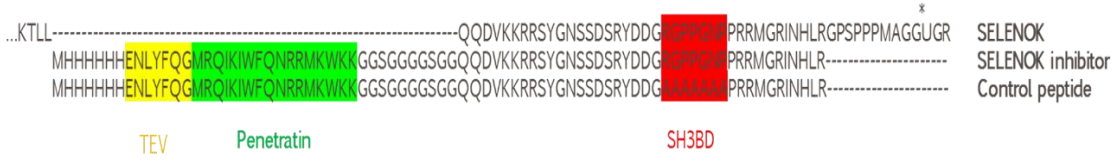

Figure 3.4 SELENOK inhibitor and control peptide are based on the SH3 binding domain of SELENOK. Top: relevant primary amino acid sequence of SELENOK. Middle: primary amino acid sequence of the SELENOK inhibitor. Bottom: primary amino acid sequence of the control peptide. Yellow highlighted area shows the TEV (Tobacco etch virus) cleavage site, green highlighted area shows the penetratin amino acid sequence, and the red highlighted area shows the SH3 binding domain (SH3BD).

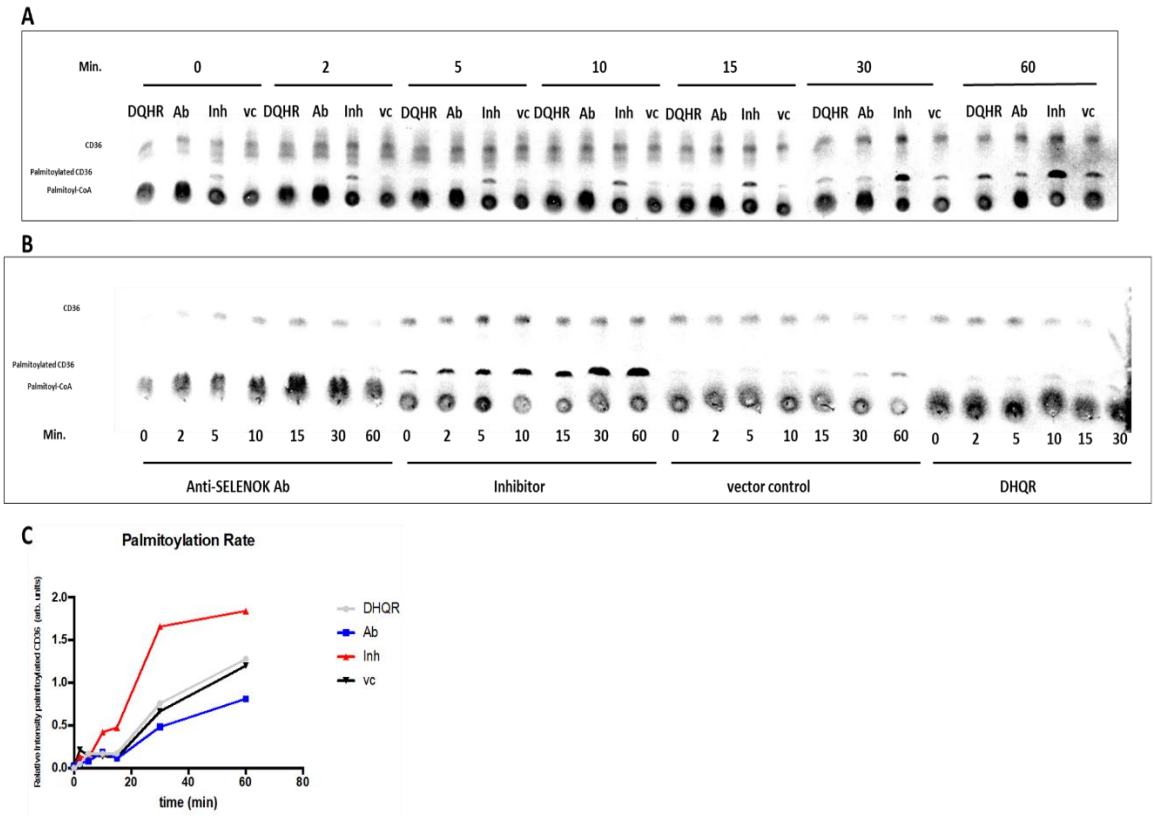

Figure 3.5 Purified inhibitor enhances SELENOK/DHHC6 mediated palmitoylation in a cell free system. Results of protein acyl-transferase assay comparing a recombinant inhibitor of SELENOK with a SELENOK specific antibody. (**A**) Image of *uv* illuminated TLC plate with the groups organized according to separate time points. DQHR refers to the putative catalytically dead version of DHHC6, Ab = anti-SELENOK antibody, inh = inhibitor, and vc = vehicle control. (**B**) Image of *uv* illuminated TLC plate with the groups organized according to group. (**C**) Graph demonstrating rate of palmitoylation derived from images above. Inhibitor increased palmitoylation rate compared to control and DQHR demonstrated an equal rate of palmitoylation compared to vc.

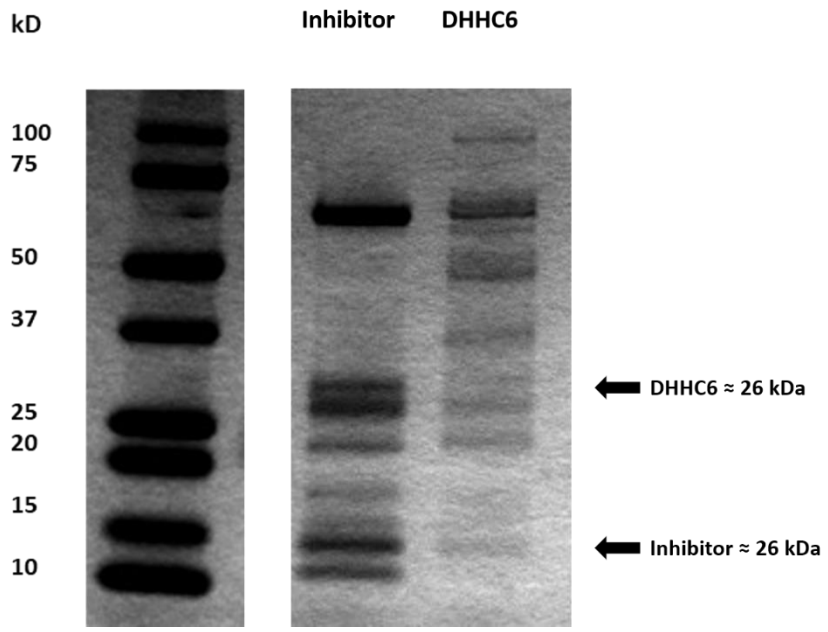

Figure 3.6 Purification of Recombinant proteins contains an abundance of non-specific bands. SDS-PAGE and Coomassie blue staining of recombinant inhibitor and cDHHC6. Protein ladder for determining protein size by position (left). Both inhibitor and cDHCC6 demonstrate non-specific bands that do not correlate with their predicted sizes (right).

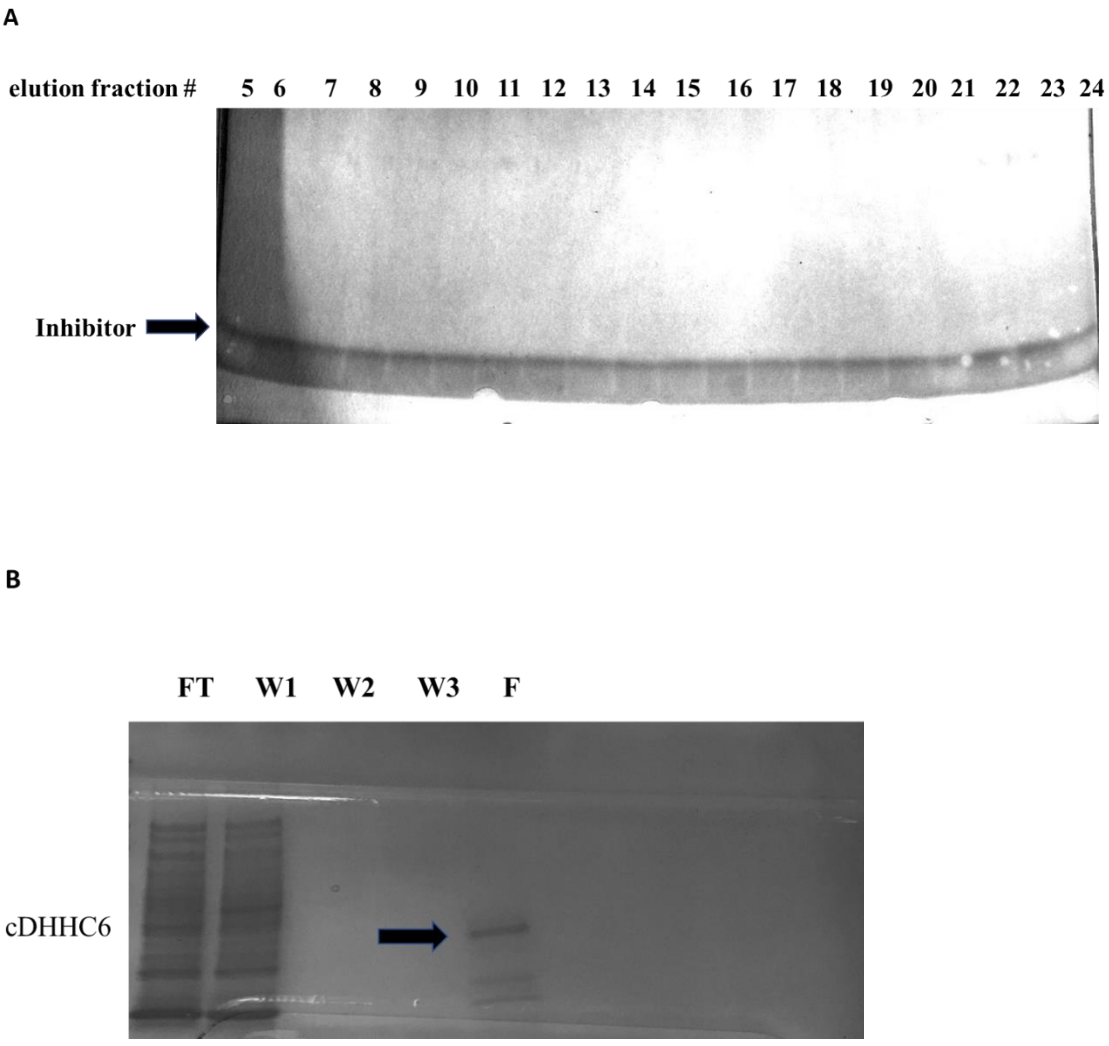

Figure 3.7 Increased specificity of recombinant proteins under new purification conditions. SDS-PAGE and Coomassie blue staining of recombinant inhibitor and DHHC6 after protein purification. (**A**) SDS-PAGE for purified inhibitor. Elution fraction number refers to 100 µL fractions obtained sequentially from nickel-column during protein purification. Arrow points out predicted size of inhibitor (~ 12 kDa). Note the lack of non-specific bands. (**B**) SDS-PAGE for purified cDHHC6. Flow-through (FT), W1 (wash 1), W2 (wash 2), W2 (wash 3), and F (cDHHC6 lane). Arrow points out predicted size of cDHHC6 (~ 26 kDa). Some non-specific bands near the bottom.

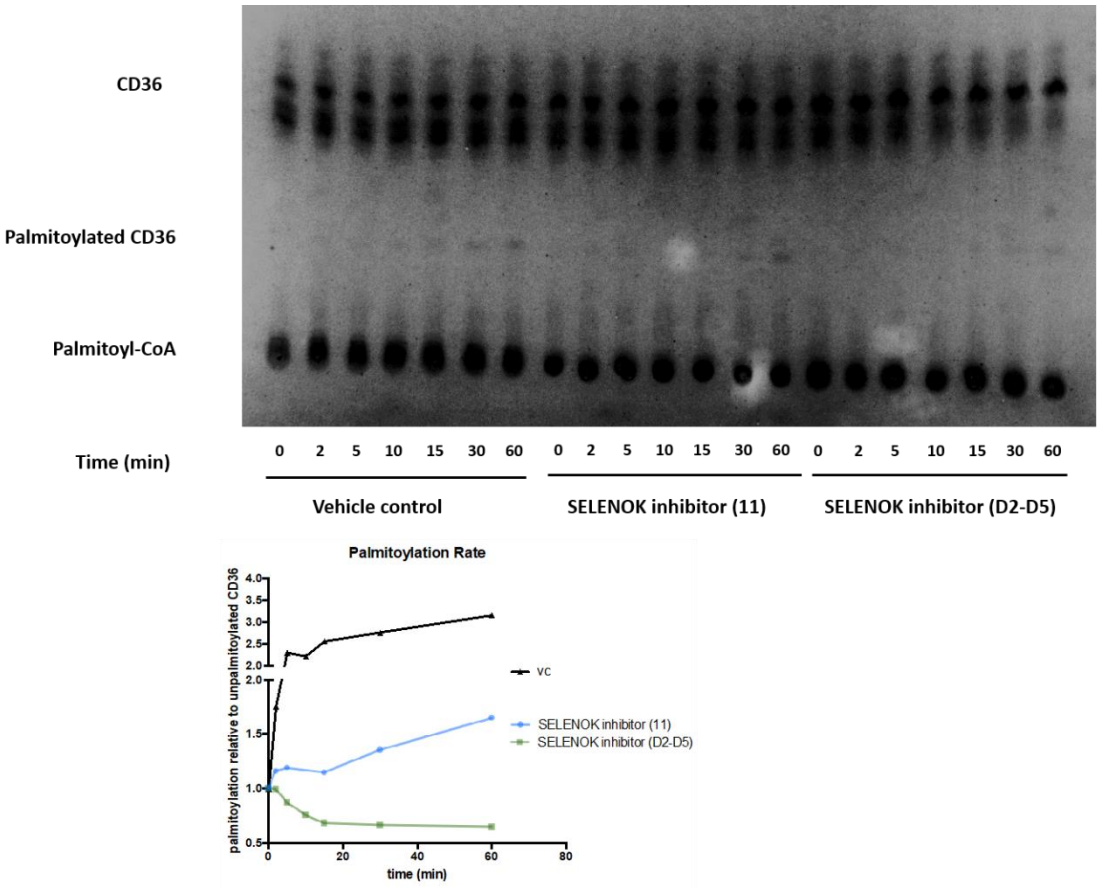

Figure 3.8 Highly specific purified recombinant SELENOK inhibitor reduces SELENOK/DHHC6 palmitoylation. Results of protein acyl-transferase assay with or two new elution batches of recombinant SELENOK inhibitor. (**A**) Image of *uv* illuminated TLC plate. Numbers after SELENOK inhibitor represent various elution fractions. (**B**) Graph showing slight reduction rate of palmitoylation for SELENOK (11) and stronger inhibition of palmitoylation when reaction mixture included SELENOK (D2-D5).

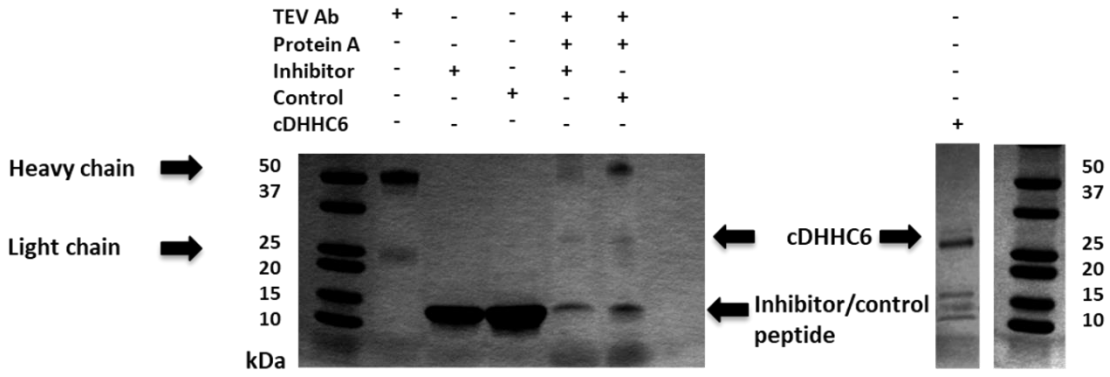

Figure 3.9 Inhibitor of SELENOK and control peptide physically interact with DHHC6. Image of results from co-Immunoprecipitation assay. cDHHC6 and synthetic SELENOK inhibitor or control peptide (control) lacking an SH3BD were incubated for 18 h with TEV antibody and subsequently incubated with protein A coated agarose beads for 2 h. Proteins were then separated using SDS-PAGE and stained with Coomassie blue to detect protein interaction. TEV antibody, Inhibitor, control, and cDHHC6 were run by themselves to determine band location. Lanes without cDHHC6 input but exhibiting a band for cDHHC6 show protein-protein interaction.

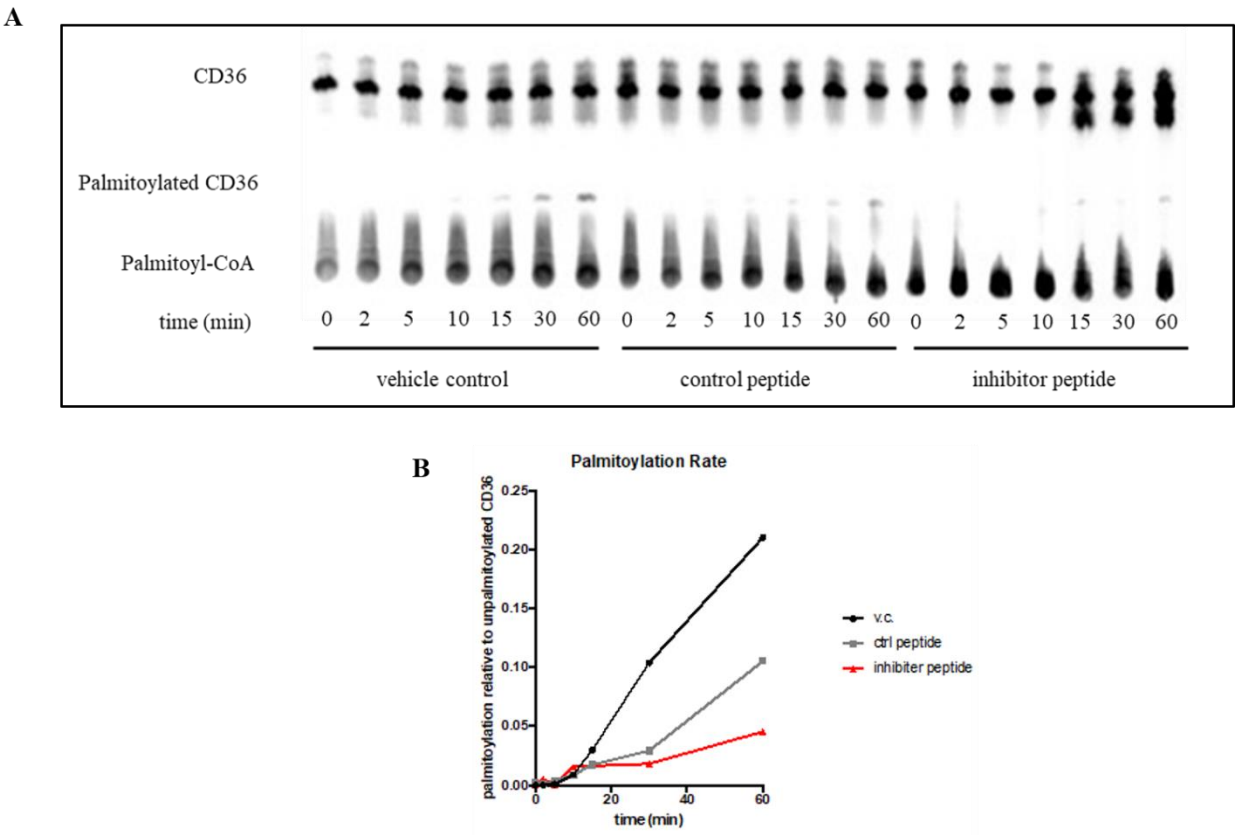

Figure 3.10 Synthetic SELENOK inhibitor reduces SELENOK/DHHC6 palmitoylation. Results of protein acyl-transferase assay with synthetic inhibitor of SELENOK/DHHC6 and control peptide. (**A**) Image of *uv* illuminated TLC plate showing palmitoylation at various time points. (**B**) Graph showing slight reduced palmitoylation rates for inhibitor peptide and control peptide compared to PBS vehicle control (v.c.)

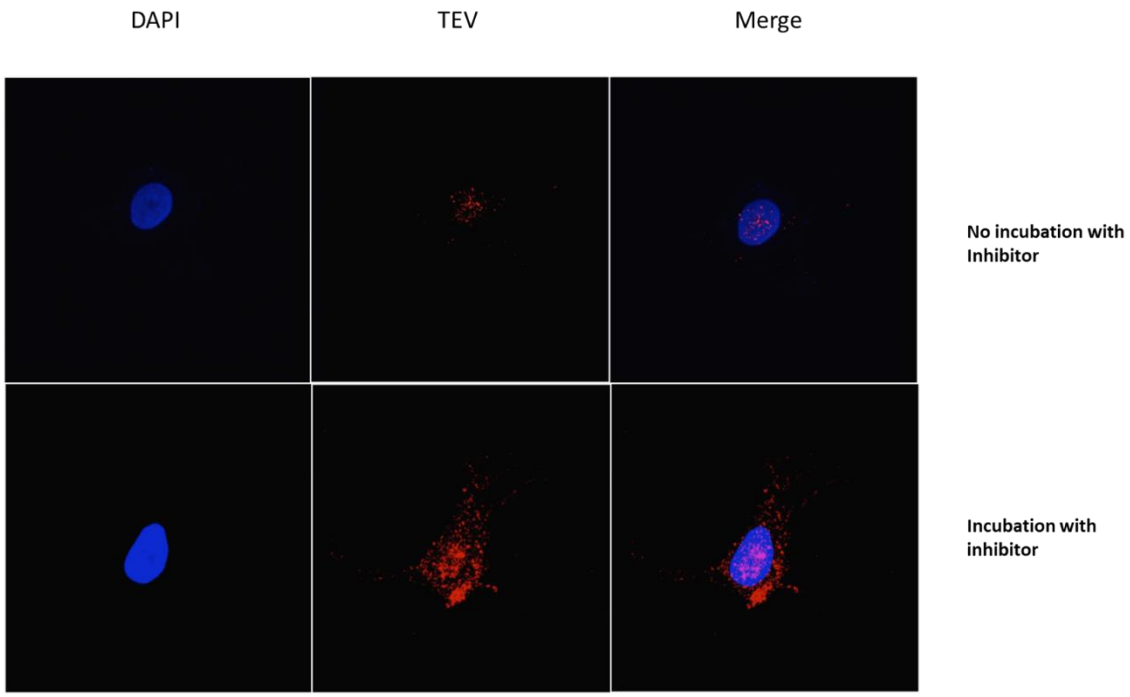

Figure 3.11 CPP containing SELENOK inhibitor can penetrate through cell membrane. Confocal microscopy image of a single SK-MEL28 cell. SK-MEL28 cells were incubated with either PBS vehicle control (top) or SELENOK inhibitor (bottom) for 1 h. Cells were stained with an Ab specific for the TEV cleavage motif which is linked to the SELENOK inhibitor. Results demonstrate presence of the inhibitor in the inhibitor treated cells but not in the non-treated cell.

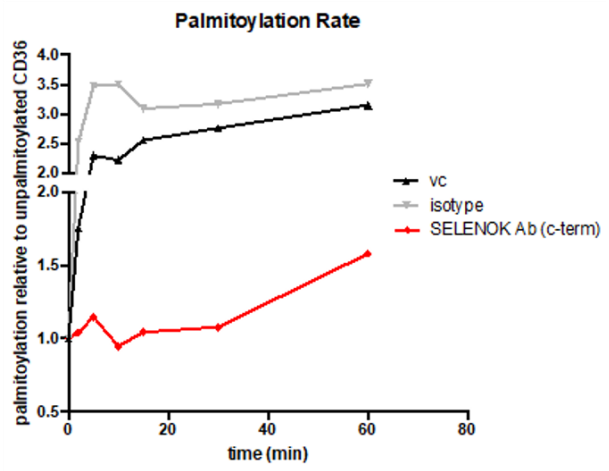

Figure S3.1 IgG isotype control has no effect on SELENOK/DHHC6 mediated palmitoylation. Graph showing palmitoylation rates with SELENOK antibody treatment (SELENO Ab (c-term)), or an isotype matched antibody control (isotype), or treatment with PBS vehicle control (vc). SELENOK antibdy reduced rates of palmitoylation compared to vehicle or isotype control.

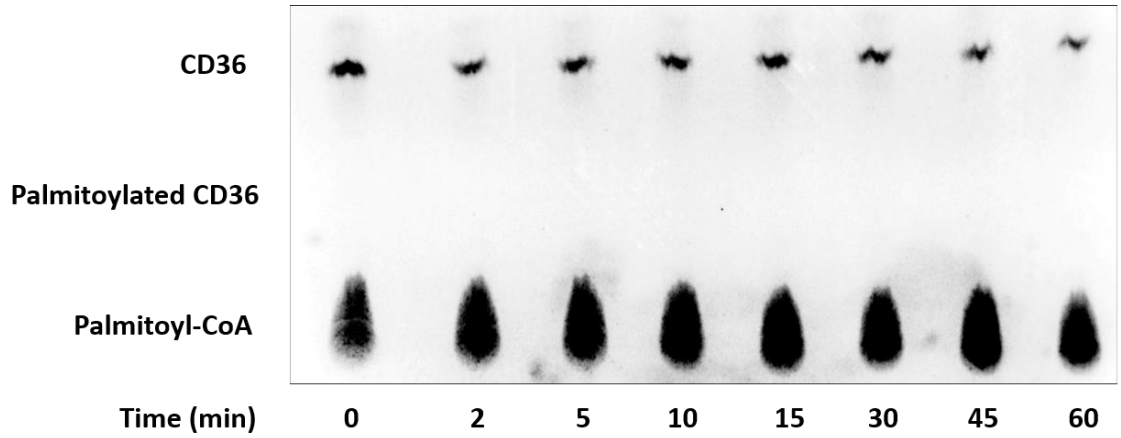

Figure S3.2 cDHHC6 is required for palmitoylation in the presence of palmitoyl-CoA. Picture of *uv* illuminanted TLC plate demonstrating lack of palmitoylation in the absence of cDHHC6

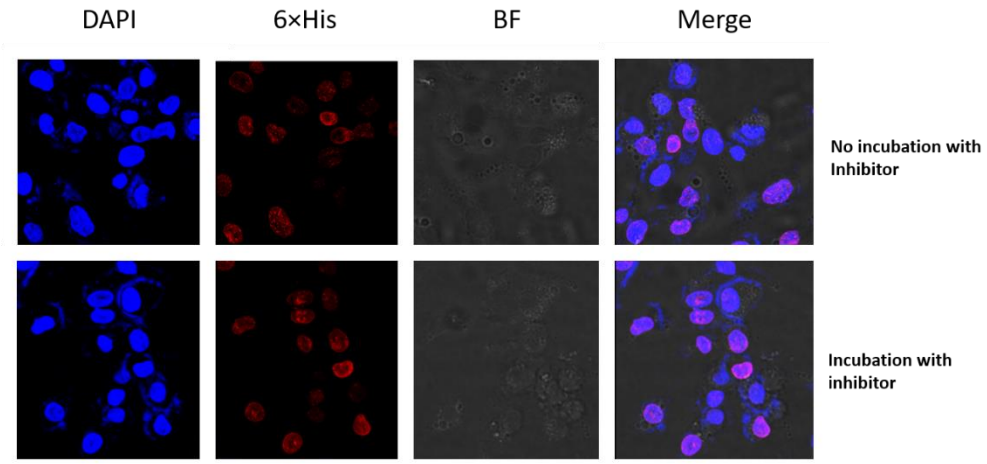

Figure S3.3 Staining for intracellular SELENOK inhibitor with 6×His antibody has non-specific nuclear targets. SK-MEL28 cells were incubated with either PBS vehicle control (top) or SELENOK inhibitor (bottom) for 1 h. Cells were stained with an antibody specific for 6×His tag which is linked to the SELENOK inhibitor. Results demonstrate nonspecific staining of nuclear protein (red) for treated and untreated groups.

References

1. Rayman, M.P., *Selenium and human health.* Lancet, 2012. **379**(9822): p. 1256-68.
2. Reeves, M.A. and P.R. Hoffmann, *The human selenoproteome: recent insights into functions and regulation.* Cell Mol Life Sci, 2009. **66**(15): p. 2457-78.
3. Schweizer, U. and N. Fradejas-Villar, *Why 21? The significance of selenoproteins for human health revealed by inborn errors of metabolism.* FASEB J, 2016. **30**(11): p. 3669-3681.
4. Qi, Y. and N.V. Grishin, *Structural classification of thioredoxin-like fold proteins.* Proteins, 2005. **58**(2): p. 376-88.
5. Du, S., et al., *SelK is a novel ER stress-regulated protein and protects HepG2 cells from ER stress agent-induced apoptosis.* Arch Biochem Biophys, 2010. **502**(2): p. 137-43.
6. Bellinger, F.P., et al., *Regulation and function of selenoproteins in human disease.* Biochem J, 2009. **422**(1): p. 11-22.
7. Polo, A., et al., *A study on the structural features of SELK, an over-expressed protein in hepatocellular carcinoma, by molecular dynamics simulations in a lipid-water system.* Mol Biosyst, 2016. **12**(10): p. 3209-22.
8. Simister, P.C. and S.M. Feller, *Order and disorder in large multi-site docking proteins of the Gab family--implications for signalling complex formation and inhibitor design strategies.* Mol Biosyst, 2012. **8**(1): p. 33-46.
9. Lee, J.H., et al., *Selenoprotein S-dependent Selenoprotein K Binding to p97(VCP) Protein Is Essential for Endoplasmic Reticulum-associated Degradation.* J Biol Chem, 2015. **290**(50): p. 29941-52.
10. Fredericks, G.J. and P.R. Hoffmann, *Selenoprotein K and protein palmitoylation.* Antioxid Redox Signal, 2015. **23**(10): p. 854-62.
11. Shchedrina, V.A., et al., *Selenoprotein K binds multiprotein complexes and is involved in the regulation of endoplasmic reticulum homeostasis.* J Biol Chem, 2011. **286**(50): p. 42937-48.
12. in *Selenium in Nutrition: Revised Edition*. 1983: Washington (DC).
13. Sun, G.X., et al., *Distribution of soil selenium in China is potentially controlled by deposition and volatilization?* Sci Rep, 2016. **6**: p. 20953.
14. C., R., *Selenium in Food and Health.* Blackie Academic and Professional,, 1996

15. Spallholz, J.E., L.M. Boylan, and H.S. Larsen, *Advances in understanding selenium's role in the immune system.* Ann N Y Acad Sci, 1990. **587**: p. 123-39.

16. Kiremidjian-Schumacher, L., et al., *Supplementation with selenium and human immune cell functions. II. Effect on cytotoxic lymphocytes and natural killer cells.* Biol Trace Elem Res, 1994. **41**(1-2): p. 115-27.

17. Roy, M., et al., *Selenium supplementation enhances the expression of interleukin 2 receptor subunits and internalization of interleukin 2.* Proc Soc Exp Biol Med, 1993. **202**(3): p. 295-301.

18. Beck, M.A., *Selenium and host defence towards viruses.* Proc Nutr Soc, 1999. **58**(3): p. 707-11.

19. Beck, M.A., et al., *Selenium deficiency increases the pathology of an influenza virus infection.* FASEB J, 2001. **15**(8): p. 1481-3.

20. Sappey, C., et al., *Stimulation of glutathione peroxidase activity decreases HIV type 1 activation after oxidative stress.* AIDS Res Hum Retroviruses, 1994. **10**(11): p. 1451-61.

21. Pace, G.W. and C.D. Leaf, *The role of oxidative stress in HIV disease.* Free Radic Biol Med, 1995. **19**(4): p. 523-8.

22. Dworkin, B.M., *Selenium deficiency in HIV infection and the acquired immunodeficiency syndrome (AIDS).* Chem Biol Interact, 1994. **91**(2-3): p. 181-6.

23. Beck, K.W., et al., *Serum trace element levels in HIV-infected subjects.* Biol Trace Elem Res, 1990. **25**(2): p. 89-96.

24. Look, M.P., et al., *Serum selenium versus lymphocyte subsets and markers of disease progression and inflammatory response in human immunodeficiency virus-1 infection.* Biol Trace Elem Res, 1997. **56**(1): p. 31-41.

25. Baum, M.K., et al., *High risk of HIV-related mortality is associated with selenium deficiency.* J Acquir Immune Defic Syndr Hum Retrovirol, 1997. **15**(5): p. 370-4.

26. Kupka, R., et al., *Selenium status is associated with accelerated HIV disease progression among HIV-1-infected pregnant women in Tanzania.* J Nutr, 2004. **134**(10): p. 2556-60.

27. Gupta, S., et al., *Plasma selenium level in cancer patients.* Indian J Cancer, 1994. **31**(3): p. 192-7.

28. Duffield-Lillico, A.J., I. Shureiqi, and S.M. Lippman, *Can selenium prevent colorectal cancer? A signpost from epidemiology.* J Natl Cancer Inst, 2004. **96**(22): p. 1645-7.

29. Overvad, K., et al., *Selenium in human mammary carcinogenesis: a case-cohort study.* Eur J Cancer, 1991. **27**(7): p. 900-2.

30. Clark, L.C., et al., *Effects of selenium supplementation for cancer prevention in patients with carcinoma of the skin. A randomized controlled trial. Nutritional Prevention of Cancer Study Group.* JAMA, 1996. **276**(24): p. 1957-63.

31. Thomson, C.D., et al., *Long-term supplementation with selenate and selenomethionine: selenium and glutathione peroxidase (EC 1.11.1.9) in blood components of New Zealand women.* Br J Nutr, 1993. **69**(2): p. 577-88.

32. Combs, G.F., Jr. and W.P. Gray, *Chemopreventive agents: selenium.* Pharmacol Ther, 1998. **79**(3): p. 179-92.

33. Mannisto, S., et al., *Toenail selenium and breast cancer-a case-control study in Finland.* Eur J Clin Nutr, 2000. **54**(2): p. 98-103.

34. Hunter, D.J., et al., *A prospective study of selenium status and breast cancer risk.* JAMA, 1990. **264**(9): p. 1128-31.

35. Rose, A.H., et al., *Increasing dietary selenium elevates reducing capacity and ERK activation associated with accelerated progression of select mesothelioma tumors.* Am J Pathol, 2014. **184**(4): p. 1041-1049.

36. Kelley, L.A., et al., *The Phyre2 web portal for protein modeling, prediction and analysis.* Nat Protoc, 2015. **10**(6): p. 845-58.

37. Verma, S., et al., *Selenoprotein K knockout mice exhibit deficient calcium flux in immune cells and impaired immune responses.* J Immunol, 2011. **186**(4): p. 2127-37.

38. Lu, C., et al., *Identification and characterization of selenoprotein K: an antioxidant in cardiomyocytes.* FEBS Lett, 2006. **580**(22): p. 5189-97.

39. Dolph L. Hatfield, U.S., Petra A. Tsuji, Vadim N. Gladyshev, *Selenium: its molecular biology and role in human health* 2016: p. 245-252

40. Seyedali, A. and M.J. Berry, *Nonsense-mediated decay factors are involved in the regulation of selenoprotein mRNA levels during selenium deficiency.* RNA, 2014. **20**(8): p. 1248-56.

41. Lin, H.C., et al., *C-Terminal End-Directed Protein Elimination by CRL2 Ubiquitin Ligases.* Mol Cell, 2018. **70**(4): p. 602-613 e3.

42. Burk, R.F. and K.E. Hill, *Regulation of Selenium Metabolism and Transport.* Annu Rev Nutr, 2015. **35**: p. 109-34.

43. Touat-Hamici, Z., et al., *Selenium-regulated hierarchy of human selenoproteome in cancerous and immortalized cells lines.* Biochim Biophys Acta Gen Subj, 2018.

44. Wright, S.E., et al., *Experience with second marrow transplants.* Exp Hematol, 1976. **4**(4): p. 221-6.

45. Cao, L., et al., *Analyses of Selenotranscriptomes and Selenium Concentrations in Response to Dietary Selenium Deficiency and Age Reveal Common and Distinct Patterns by Tissue and Sex in Telomere-Dysfunctional Mice.* J Nutr, 2017. **147**(10): p. 1858-1866.

46. Kaneko, M. and Y. Nomura, *ER signaling in unfolded protein response.* Life Sci, 2003. **74**(2-3): p. 199-205.

47. Addinsall, A.B., et al., *Emerging roles of endoplasmic reticulum-resident selenoproteins in the regulation of cellular stress responses and the implications for metabolic disease.* Biochem J, 2018. **475**(6): p. 1037-1057.

48. Huang, Z., et al., *Stimulation of unprimed macrophages with immune complexes triggers a low output of nitric oxide by calcium-dependent neuronal nitric-oxide synthase.* J Biol Chem, 2012. **287**(7): p. 4492-502.

49. Berridge, M.J., P. Lipp, and M.D. Bootman, *The versatility and universality of calcium signalling.* Nat Rev Mol Cell Biol, 2000. **1**(1): p. 11-21.

50. Venkatachalam, K., et al., *The cellular and molecular basis of store-operated calcium entry.* Nat Cell Biol, 2002. **4**(11): p. E263-72.

51. Prakriya, M., et al., *Orai1 is an essential pore subunit of the CRAC channel.* Nature, 2006. **443**(7108): p. 230-3.

52. Fredericks, G.J., et al., *Stable expression and function of the inositol 1,4,5-triphosphate receptor requires palmitoylation by a DHHC6/selenoprotein K complex.* Proc Natl Acad Sci U S A, 2014. **111**(46): p. 16478-83.

53. Meiler, S., et al., *Selenoprotein K is required for palmitoylation of CD36 in macrophages: implications in foam cell formation and atherogenesis.* J Leukoc Biol, 2013. **93**(5): p. 771-80.
54. Thorne, R.F., et al., *Palmitoylation of CD36/FAT regulates the rate of its post-transcriptional processing in the endoplasmic reticulum.* Biochim Biophys Acta, 2010. **1803**(11): p. 1298-307.
55. Smotrys, J.E. and M.E. Linder, *Palmitoylation of intracellular signaling proteins: regulation and function.* Annu Rev Biochem, 2004. **73**: p. 559-87.
56. Norton, R.L., et al., *Selenoprotein K regulation of palmitoylation and calpain cleavage of ASAP2 is required for efficient FcgammaR-mediated phagocytosis.* J Leukoc Biol, 2017. **101**(2): p. 439-448.
57. Bijlmakers, M.J. and M. Marsh, *The on-off story of protein palmitoylation.* Trends Cell Biol, 2003. **13**(1): p. 32-42.
58. Jennings, B.C. and M.E. Linder, *DHHC protein S-acyltransferases use similar ping-pong kinetic mechanisms but display different acyl-CoA specificities.* J Biol Chem, 2012. **287**(10): p. 7236-45.
59. Mitchell, D.A., et al., *Mutational analysis of Saccharomyces cerevisiae Erf2 reveals a two-step reaction mechanism for protein palmitoylation by DHHC enzymes.* J Biol Chem, 2010. **285**(49): p. 38104-14.
60. Fredericks, G.J., et al., *Selenoprotein K Increases Efficiency of DHHC6 Catalyzed Protein Palmitoylation by Stabilizing the Acyl-DHHC6 Intermediate.* Antioxidants (Basel), 2017. **7**(1).
61. Mitchell, D.A., et al., *The Erf4 subunit of the yeast Ras palmitoyl acyltransferase is required for stability of the Acyl-Erf2 intermediate and palmitoyl transfer to a Ras2 substrate.* J Biol Chem, 2012. **287**(41): p. 34337-48.
62. McGrath, N.A. and R.T. Raines, *Chemoselectivity in chemical biology: acyl transfer reactions with sulfur and selenium.* Acc Chem Res, 2011. **44**(9): p. 752-61.
63. Hondal, R.J. and E.L. Ruggles, *Differing views of the role of selenium in thioredoxin reductase.* Amino Acids, 2011. **41**(1): p. 73-89.

64. Biteau, B., J. Labarre, and M.B. Toledano, *ATP-dependent reduction of cysteine-sulphinic acid by S. cerevisiae sulphiredoxin.* Nature, 2003. **425**(6961): p. 980-4.

65. Bock, A., et al., *Selenoprotein synthesis: an expansion of the genetic code.* Trends Biochem Sci, 1991. **16**(12): p. 463-7.

66. Hatfield, D.L. and V.N. Gladyshev, *How selenium has altered our understanding of the genetic code.* Mol Cell Biol, 2002. **22**(11): p. 3565-76.

67. Jacob, C., et al., *Sulfur and selenium: the role of oxidation state in protein structure and function.* Angew Chem Int Ed Engl, 2003. **42**(39): p. 4742-58.

68. Stadtman, T.C., *Selenocysteine.* Annu Rev Biochem, 1996. **65**: p. 83-100.

69. Kryukov, G.V., et al., *Characterization of mammalian selenoproteomes.* Science, 2003. **300**(5624): p. 1439-43.

70. Liu, J., Z. Zhang, and S. Rozovsky, *Selenoprotein K form an intermolecular diselenide bond with unusually high redox potential.* FEBS Lett, 2014. **588**(18): p. 3311-21.

71. Huang, Z., et al., *Selenoprotein K is a novel target of m-calpain, and cleavage is regulated by Toll-like receptor-induced calpastatin in macrophages.* J Biol Chem, 2011. **286**(40): p. 34830-8.

72. Huang, Z., et al., *Calpastatin prevents NF-kappaB-mediated hyperactivation of macrophages and attenuates colitis.* J Immunol, 2013. **191**(7): p. 3778-88.

73. Reich, H.J. and R.J. Hondal, *Why Nature Chose Selenium.* ACS Chem Biol, 2016. **11**(4): p. 821-41.

74. Li, M., et al., *Selenoprotein K Mediates the Proliferation, Migration, and Invasion of Human Choriocarcinoma Cells by Negatively Regulating Human Chorionic Gonadotropin Expression via ERK, p38 MAPK, and Akt Signaling Pathway.* Biol Trace Elem Res, 2018. **184**(1): p. 47-59.

75. Ben, S.B., et al., *Overexpression of Selenoprotein SelK in BGC-823 Cells Inhibits Cell Adhesion and Migration.* Biochemistry (Mosc), 2015. **80**(10): p. 1344-53.

76. Potenza, N., et al., *Human MiR-544a Modulates SELK Expression in Hepatocarcinoma Cell Lines.* PLoS One, 2016. **11**(6): p. e0156908.

77. Meplan, C., et al., *Polymorphisms in thioredoxin reductase and selenoprotein K genes and selenium status modulate risk of prostate cancer.* PLoS One, 2012. **7**(11): p. e48709.

78. Hogan, P.G. and A. Rao, *Store-operated calcium entry: Mechanisms and modulation.* Biochem Biophys Res Commun, 2015. **460**(1): p. 40-9.

79. Zhou, Y., et al., *Initial activation of STIM1, the regulator of store-operated calcium entry.* Nat Struct Mol Biol, 2013. **20**(8): p. 973-81.

80. Stathopulos, P.B. and M. Ikura, *Store operated calcium entry: From concept to structural mechanisms.* Cell Calcium, 2017. **63**: p. 3-7.

81. Villalobos, C., et al., *Remodeling of Calcium Entry Pathways in Cancer.* Adv Exp Med Biol, 2016. **898**: p. 449-66.

82. Cui, C., et al., *Targeting calcium signaling in cancer therapy.* Acta Pharm Sin B, 2017. **7**(1): p. 3-17.

83. Stanisz, H., et al., *The role of Orai-STIM calcium channels in melanocytes and melanoma.* J Physiol, 2016. **594**(11): p. 2825-35.

84. Meplan, C., et al., *Transcriptomics and proteomics show that selenium affects inflammation, cytoskeleton, and cancer pathways in human rectal biopsies.* FASEB J, 2016. **30**(8): p. 2812-25.

85. Miller, A.J. and M.C. Mihm, Jr., *Melanoma.* N Engl J Med, 2006. **355**(1): p. 51-65.

86. Bennett, D.C., *Human melanocyte senescence and melanoma susceptibility genes.* Oncogene, 2003. **22**(20): p. 3063-9.

87. Hussussian, C.J., et al., *Germline p16 mutations in familial melanoma.* Nat Genet, 1994. **8**(1): p. 15-21.

88. Sviderskaya, E.V., et al., *p16/cyclin-dependent kinase inhibitor 2A deficiency in human melanocyte senescence, apoptosis, and immortalization: possible implications for melanoma progression.* J Natl Cancer Inst, 2003. **95**(10): p. 723-32.

89. Nogueira, C., et al., *Cooperative interactions of PTEN deficiency and RAS activation in melanoma metastasis.* Oncogene, 2010. **29**(47): p. 6222-32.

90. Geller, A.C. and G.D. Annas, *Epidemiology of melanoma and nonmelanoma skin cancer.* Semin Oncol Nurs, 2003. **19**(1): p. 2-11.

91. D'Orazio, J., et al., *UV radiation and the skin.* Int J Mol Sci, 2013. **14**(6): p. 12222-48.

92. Cadet, J. and J.R. Wagner, *DNA base damage by reactive oxygen species, oxidizing agents, and UV radiation.* Cold Spring Harb Perspect Biol, 2013. **5**(2).

93. Kadekaro, A.L., et al., *Significance of the melanocortin 1 receptor in regulating human melanocyte pigmentation, proliferation, and survival.* Ann N Y Acad Sci, 2003. **994**: p. 359-65.
94. Millington, G.W., *Proopiomelanocortin (POMC): the cutaneous roles of its melanocortin products and receptors.* Clin Exp Dermatol, 2006. **31**(3): p. 407-12.
95. Levy, C., M. Khaled, and D.E. Fisher, *MITF: master regulator of melanocyte development and melanoma oncogene.* Trends Mol Med, 2006. **12**(9): p. 406-14.
96. Kadekaro, A.L., et al., *alpha-Melanocortin and endothelin-1 activate antiapoptotic pathways and reduce DNA damage in human melanocytes.* Cancer Res, 2005. **65**(10): p. 4292-9.
97. Smith, A.G., et al., *Melanocortin-1 receptor signaling markedly induces the expression of the NR4A nuclear receptor subgroup in melanocytic cells.* J Biol Chem, 2008. **283**(18): p. 12564-70.
98. Berridge, M.J., M.D. Bootman, and H.L. Roderick, *Calcium signalling: dynamics, homeostasis and remodelling.* Nat Rev Mol Cell Biol, 2003. **4**(7): p. 517-29.
99. Samtleben, S., et al., *Direct imaging of ER calcium with targeted-esterase induced dye loading (TED).* J Vis Exp, 2013(75): p. e50317.
100. Motiani, R.K., et al., *STIM1 and Orai1 mediate CRAC channel activity and are essential for human glioblastoma invasion.* Pflugers Arch, 2013. **465**(9): p. 1249-60.
101. McAndrew, D., et al., *ORAI1-mediated calcium influx in lactation and in breast cancer.* Mol Cancer Ther, 2011. **10**(3): p. 448-60.
102. Bidaux, G., et al., *Prostate cell differentiation status determines transient receptor potential melastatin member 8 channel subcellular localization and function.* J Clin Invest, 2007. **117**(6): p. 1647-57.
103. Yang, S.L., et al., *Transient receptor potential channel C3 contributes to the progression of human ovarian cancer.* Oncogene, 2009. **28**(10): p. 1320-8.
104. Stewart, T.A., K.T. Yapa, and G.R. Monteith, *Altered calcium signaling in cancer cells.* Biochim Biophys Acta, 2015. **1848**(10 Pt B): p. 2502-11.
105. Sundivakkam, P.C., et al., *Store-operated Ca2+ entry (SOCE) induced by protease-activated receptor-1 mediates STIM1 protein phosphorylation to inhibit SOCE in endothelial cells through AMP-activated protein kinase and p38beta mitogen-activated protein kinase.* J Biol Chem, 2013. **288**(23): p. 17030-41.

106. Yang, S., J.J. Zhang, and X.Y. Huang, *Orai1 and STIM1 are critical for breast tumor cell migration and metastasis.* Cancer Cell, 2009. **15**(2): p. 124-34.

107. Umemura, M., et al., *Store-operated Ca2+ entry (SOCE) regulates melanoma proliferation and cell migration.* PLoS One, 2014. **9**(2): p. e89292.

108. Chen, Y.F., et al., *Calcium store sensor stromal-interaction molecule 1-dependent signaling plays an important role in cervical cancer growth, migration, and angiogenesis.* Proc Natl Acad Sci U S A, 2011. **108**(37): p. 15225-30.

109. Ferris, C.D., et al., *Purified inositol 1,4,5-trisphosphate receptor mediates calcium flux in reconstituted lipid vesicles.* Nature, 1989. **342**(6245): p. 87-9.

110. Foskett, J.K., et al., *Inositol trisphosphate receptor Ca2+ release channels.* Physiol Rev, 2007. **87**(2): p. 593-658.

111. Allbritton, N.L., T. Meyer, and L. Stryer, *Range of messenger action of calcium ion and inositol 1,4,5-trisphosphate.* Science, 1992. **258**(5089): p. 1812-5.

112. Blondel, O., et al., *Sequence and functional characterization of a third inositol trisphosphate receptor subtype, IP3R-3, expressed in pancreatic islets, kidney, gastrointestinal tract, and other tissues.* J Biol Chem, 1993. **268**(15): p. 11356-63.

113. Ross, C.A., et al., *Three additional inositol 1,4,5-trisphosphate receptors: molecular cloning and differential localization in brain and peripheral tissues.* Proc Natl Acad Sci U S A, 1992. **89**(10): p. 4265-9.

114. Patel, S., S.K. Joseph, and A.P. Thomas, *Molecular properties of inositol 1,4,5-trisphosphate receptors.* Cell Calcium, 1999. **25**(3): p. 247-64.

115. Adkins, C.E., et al., *Ca2+-calmodulin inhibits Ca2+ release mediated by type-1, -2 and -3 inositol trisphosphate receptors.* Biochem J, 2000. **345 Pt 2**: p. 357-63.

116. Fujino, I., et al., *Differential expression of type 2 and type 3 inositol 1,4,5-trisphosphate receptor mRNAs in various mouse tissues: in situ hybridization study.* Cell Tissue Res, 1995. **280**(2): p. 201-10.

117. Bush, K.T., et al., *Epithelial inositol 1,4,5-trisphosphate receptors. Multiplicity of localization, solubility, and isoforms.* J Biol Chem, 1994. **269**(38): p. 23694-9.

118. De Smedt, H., et al., *Isoform diversity of the inositol trisphosphate receptor in cell types of mouse origin.* Biochem J, 1997. **322 (Pt 2)**: p. 575-83.

119. De Smedt, H., et al., *Determination of relative amounts of inositol trisphosphate receptor mRNA isoforms by ratio polymerase chain reaction.* J Biol Chem, 1994. **269**(34): p. 21691-8.
120. Wojcikiewicz, R.J., *Type I, II, and III inositol 1,4,5-trisphosphate receptors are unequally susceptible to down-regulation and are expressed in markedly different proportions in different cell types.* J Biol Chem, 1995. **270**(19): p. 11678-83.
121. Miyakawa, T., et al., *Encoding of Ca2+ signals by differential expression of IP3 receptor subtypes.* EMBO J, 1999. **18**(5): p. 1303-8.
122. Nerou, E.P., et al., *Selective recognition of inositol phosphates by subtypes of the inositol trisphosphate receptor.* Biochem J, 2001. **355**(Pt 1): p. 59-69.
123. Newton, C.L., G.A. Mignery, and T.C. Sudhof, *Co-expression in vertebrate tissues and cell lines of multiple inositol 1,4,5-trisphosphate (InsP3) receptors with distinct affinities for InsP3.* J Biol Chem, 1994. **269**(46): p. 28613-9.
124. Wilson, B.S., et al., *Calcium-dependent clustering of inositol 1,4,5-trisphosphate receptors.* Mol Biol Cell, 1998. **9**(6): p. 1465-78.
125. Supattapone, S., et al., *Solubilization, purification, and characterization of an inositol trisphosphate receptor.* J Biol Chem, 1988. **263**(3): p. 1530-4.
126. Uchida, K., et al., *Critical regions for activation gating of the inositol 1,4,5-trisphosphate receptor.* J Biol Chem, 2003. **278**(19): p. 16551-60.
127. Finch, E.A., T.J. Turner, and S.M. Goldin, *Calcium as a coagonist of inositol 1,4,5-trisphosphate-induced calcium release.* Science, 1991. **252**(5004): p. 443-6.
128. Kaftan, E.J., B.E. Ehrlich, and J. Watras, *Inositol 1,4,5-trisphosphate (InsP3) and calcium interact to increase the dynamic range of InsP3 receptor-dependent calcium signaling.* J Gen Physiol, 1997. **110**(5): p. 529-38.
129. Iino, M., *Biphasic Ca2+ dependence of inositol 1,4,5-trisphosphate-induced Ca release in smooth muscle cells of the guinea pig taenia caeci.* J Gen Physiol, 1990. **95**(6): p. 1103-22.
130. Shinohara, T., et al., *Mechanistic basis of bell-shaped dependence of inositol 1,4,5-trisphosphate receptor gating on cytosolic calcium.* Proc Natl Acad Sci U S A, 2011. **108**(37): p. 15486-91.

131. Vanderheyden, V., et al., *Regulation of inositol 1,4,5-trisphosphate-induced Ca2+ release by reversible phosphorylation and dephosphorylation.* Biochim Biophys Acta, 2009. **1793**(6): p. 959-70.
132. Schillhorn van Veen, T.W., et al., *Fatal reactions in bison following systemic organophosphate treatment for the control of Hypoderma bovis.* J Vet Diagn Invest, 1991. **3**(4): p. 355-6.
133. Manning, B.D. and L.C. Cantley, *AKT/PKB signaling: navigating downstream.* Cell, 2007. **129**(7): p. 1261-74.
134. Szado, T., et al., *Phosphorylation of inositol 1,4,5-trisphosphate receptors by protein kinase B/Akt inhibits Ca2+ release and apoptosis.* Proc Natl Acad Sci U S A, 2008. **105**(7): p. 2427-32.
135. Oakes, S.A., et al., *Proapoptotic BAX and BAK regulate the type 1 inositol trisphosphate receptor and calcium leak from the endoplasmic reticulum.* Proc Natl Acad Sci U S A, 2005. **102**(1): p. 105-10.
136. Kolch, W., *Meaningful relationships: the regulation of the Ras/Raf/MEK/ERK pathway by protein interactions.* Biochem J, 2000. **351 Pt 2**: p. 289-305.
137. Anjum, R. and J. Blenis, *The RSK family of kinases: emerging roles in cellular signalling.* Nat Rev Mol Cell Biol, 2008. **9**(10): p. 747-58.
138. Blume-Jensen, P. and T. Hunter, *Oncogenic kinase signalling.* Nature, 2001. **411**(6835): p. 355-65.
139. Herlyn, M. and K. Satyamoorthy, *Activated ras. Yet another player in melanoma?* Am J Pathol, 1996. **149**(3): p. 739-44.
140. Carr, J. and R.M. Mackie, *Point mutations in the N-ras oncogene in malignant melanoma and congenital naevi.* Br J Dermatol, 1994. **131**(1): p. 72-7.
141. Davies, H., et al., *Mutations of the BRAF gene in human cancer.* Nature, 2002. **417**(6892): p. 949-54.
142. Pollock, P.M., et al., *Melanoma mouse model implicates metabotropic glutamate signaling in melanocytic neoplasia.* Nat Genet, 2003. **34**(1): p. 108-12.

143. McCaffrey, P.G., A.E. Goldfeld, and A. Rao, *The role of NFATp in cyclosporin A-sensitive tumor necrosis factor-alpha gene transcription.* J Biol Chem, 1994. **269**(48): p. 30445-50.

144. Rusnak, F. and P. Mertz, *Calcineurin: form and function.* Physiol Rev, 2000. **80**(4): p. 1483-521.

145. Rumi-Masante, J., et al., *Structural basis for activation of calcineurin by calmodulin.* J Mol Biol, 2012. **415**(2): p. 307-17.

146. Shibasaki, F., et al., *Role of kinases and the phosphatase calcineurin in the nuclear shuttling of transcription factor NF-AT4.* Nature, 1996. **382**(6589): p. 370-3.

147. Chen, L., et al., *Structure of the DNA-binding domains from NFAT, Fos and Jun bound specifically to DNA.* Nature, 1998. **392**(6671): p. 42-8.

148. Garcia-Cozar, F.J., et al., *Two-site interaction of nuclear factor of activated T cells with activated calcineurin.* J Biol Chem, 1998. **273**(37): p. 23877-83.

149. Crabtree, G.R. and E.N. Olson, *NFAT signaling: choreographing the social lives of cells.* Cell, 2002. **109 Suppl**: p. S67-79.

150. Buchholz, M. and V. Ellenrieder, *An emerging role for Ca2+/calcineurin/NFAT signaling in cancerogenesis.* Cell Cycle, 2007. **6**(1): p. 16-9.

151. Flockhart, R.J., et al., *NFAT signalling is a novel target of oncogenic BRAF in metastatic melanoma.* Br J Cancer, 2009. **101**(8): p. 1448-55.

152. Neal, J.W. and N.A. Clipstone, *A constitutively active NFATc1 mutant induces a transformed phenotype in 3T3-L1 fibroblasts.* J Biol Chem, 2003. **278**(19): p. 17246-54.

153. Buchholz, M., et al., *Overexpression of c-myc in pancreatic cancer caused by ectopic activation of NFATc1 and the Ca2+/calcineurin signaling pathway.* EMBO J, 2006. **25**(15): p. 3714-24.

154. Duque, J., M. Fresno, and M.A. Iniguez, *Expression and function of the nuclear factor of activated T cells in colon carcinoma cells: involvement in the regulation of cyclooxygenase-2.* J Biol Chem, 2005. **280**(10): p. 8686-93.

155. Reya, T., et al., *Stem cells, cancer, and cancer stem cells.* Nature, 2001. **414**(6859): p. 105-11.

156. Fialkow, P.J., *Clonal origin of human tumors.* Biochim Biophys Acta, 1976. **458**(3): p. 283-321.

157. Nowell, P.C., *The minute chromosome (Phl) in chronic granulocytic leukemia.* Blut, 1962. **8**: p. 65-6.

158. Park, C.H., D.E. Bergsagel, and E.A. McCulloch, *Mouse myeloma tumor stem cells: a primary cell culture assay.* J Natl Cancer Inst, 1971. **46**(2): p. 411-22.

159. Bergsagel, D.E. and F.A. Valeriote, *Growth characteristics of a mouse plasma cell tumor.* Cancer Res, 1968. **28**(11): p. 2187-96.

160. Bonnet, D. and J.E. Dick, *Human acute myeloid leukemia is organized as a hierarchy that originates from a primitive hematopoietic cell.* Nat Med, 1997. **3**(7): p. 730-7.

161. Collins, A.T., et al., *Prospective identification of tumorigenic prostate cancer stem cells.* Cancer Res, 2005. **65**(23): p. 10946-51.

162. O'Brien, C.A., et al., *A human colon cancer cell capable of initiating tumour growth in immunodeficient mice.* Nature, 2007. **445**(7123): p. 106-10.

163. Ricci-Vitiani, L., et al., *Identification and expansion of human colon-cancer-initiating cells.* Nature, 2007. **445**(7123): p. 111-5.

164. Singh, S.K., et al., *Identification of a cancer stem cell in human brain tumors.* Cancer Res, 2003. **63**(18): p. 5821-8.

165. Shmelkov, S.V., et al., *AC133/CD133/Prominin-1.* Int J Biochem Cell Biol, 2005. **37**(4): p. 715-9.

166. Yin, A.H., et al., *AC133, a novel marker for human hematopoietic stem and progenitor cells.* Blood, 1997. **90**(12): p. 5002-12.

167. Roper, K., D. Corbeil, and W.B. Huttner, *Retention of prominin in microvilli reveals distinct cholesterol-based lipid micro-domains in the apical plasma membrane.* Nat Cell Biol, 2000. **2**(9): p. 582-92.

168. Maw, M.A., et al., *A frameshift mutation in prominin (mouse)-like 1 causes human retinal degeneration.* Hum Mol Genet, 2000. **9**(1): p. 27-34.

169. Rappa, G., O. Fodstad, and A. Lorico, *The stem cell-associated antigen CD133 (Prominin-1) is a molecular therapeutic target for metastatic melanoma.* Stem Cells, 2008. **26**(12): p. 3008-17.

170. Hooper, R., M.R. Zaidi, and J. Soboloff, *The heterogeneity of store-operated calcium entry in melanoma.* Sci China Life Sci, 2016. **59**(8): p. 764-9.
171. Stetler-Stevenson, W.G., S. Aznavoorian, and L.A. Liotta, *Tumor cell interactions with the extracellular matrix during invasion and metastasis.* Annu Rev Cell Biol, 1993. **9**: p. 541-73.
172. Schiffner, S., et al., *Highly pigmented Tg(Grm1) mouse melanoma develops non-pigmented melanoma cells in distant metastases.* Exp Dermatol, 2012. **21**(10): p. 786-8.
173. Cherciu, I., et al., *Stem cells, colorectal cancer and cancer stem cell markers correlations.* Curr Health Sci J, 2014. **40**(3): p. 153-61.
174. Wang, C., et al., *Selenoprotein K modulate intracellular free Ca(2+) by regulating expression of calcium homoeostasis endoplasmic reticulum protein.* Biochem Biophys Res Commun, 2017. **484**(4): p. 734-739.
175. Pan, Z. and J. Ma, *Open Sesame: treasure in store-operated calcium entry pathway for cancer therapy.* Sci China Life Sci, 2015. **58**(1): p. 48-53.
176. Sun, J., et al., *STIM1- and Orai1-mediated Ca(2+) oscillation orchestrates invadopodium formation and melanoma invasion.* J Cell Biol, 2014. **207**(4): p. 535-48.
177. Feldman, B., et al., *Coupling of mitochondria to store-operated Ca(2+)-signaling sustains constitutive activation of protein kinase B/Akt and augments survival of malignant melanoma cells.* Cell Calcium, 2010. **47**(6): p. 525-37.
178. Fiorio Pla, A., K. Kondratska, and N. Prevarskaya, *STIM and ORAI proteins: crucial roles in hallmarks of cancer.* Am J Physiol Cell Physiol, 2016. **310**(7): p. C509-19.
179. Vervloessem, T., et al., *The type 2 inositol 1,4,5-trisphosphate receptor, emerging functions for an intriguing Ca(2)(+)-release channel.* Biochim Biophys Acta, 2015. **1853**(9): p. 1992-2005.
180. Monteith, G.R., N. Prevarskaya, and S.J. Roberts-Thomson, *The calcium-cancer signalling nexus.* Nat Rev Cancer, 2017. **17**(6): p. 367-380.
181. Grosse, J., et al., *An EF hand mutation in Stim1 causes premature platelet activation and bleeding in mice.* J Clin Invest, 2007. **117**(11): p. 3540-50.
182. Hogan, P.G., R.S. Lewis, and A. Rao, *Molecular basis of calcium signaling in lymphocytes: STIM and ORAI.* Annu Rev Immunol, 2010. **28**: p. 491-533.

183. Oh-Hora, M., et al., *Dual functions for the endoplasmic reticulum calcium sensors STIM1 and STIM2 in T cell activation and tolerance.* Nat Immunol, 2008. **9**(4): p. 432-43.

184. Varga-Szabo, D., et al., *The calcium sensor STIM1 is an essential mediator of arterial thrombosis and ischemic brain infarction.* J Exp Med, 2008. **205**(7): p. 1583-91.

185. Perotti, V., et al., *NFATc2 is a potential therapeutic target in human melanoma.* J Invest Dermatol, 2012. **132**(11): p. 2652-60.

186. Keese, C.R., et al., *Electrical wound-healing assay for cells in vitro.* Proc Natl Acad Sci U S A, 2004. **101**(6): p. 1554-9.

187. Gawecka, J.E., et al., *R-Ras regulates migration through an interaction with filamin A in melanoma cells.* PLoS One, 2010. **5**(6): p. e11269.

188. Trenevska, I., D. Li, and A.H. Banham, *Therapeutic Antibodies against Intracellular Tumor Antigens.* Front Immunol, 2017. **8**: p. 1001.

189. Gonzalez-Sapienza, G., M.A. Rossotti, and S. Tabares-da Rosa, *Single-Domain Antibodies As Versatile Affinity Reagents for Analytical and Diagnostic Applications.* Front Immunol, 2017. **8**: p. 977.

190. Harmsen, M.M. and H.J. De Haard, *Properties, production, and applications of camelid single-domain antibody fragments.* Appl Microbiol Biotechnol, 2007. **77**(1): p. 13-22.

191. Frankel, A.D. and C.O. Pabo, *Cellular uptake of the tat protein from human immunodeficiency virus.* Cell, 1988. **55**(6): p. 1189-93.

192. Green, M. and P.M. Loewenstein, *Autonomous functional domains of chemically synthesized human immunodeficiency virus tat trans-activator protein.* Cell, 1988. **55**(6): p. 1179-88.

193. Joliot, A., et al., *Antennapedia homeobox peptide regulates neural morphogenesis.* Proc Natl Acad Sci U S A, 1991. **88**(5): p. 1864-8.

194. Glab-Ampai, K., et al., *Inhibition of HCV replication by humanized-single domain transbodies to NS4B.* Biochem Biophys Res Commun, 2016. **476**(4): p. 654-664.

195. Phalaphol, A., et al., *Humanized-VH/VHH that inhibit HCV replication by interfering with the virus helicase activity.* J Virol Methods, 2013. **194**(1-2): p. 289-99.

196. Thueng-in, K., et al., *Cell penetrable humanized-VH/V(H)H that inhibit RNA dependent RNA polymerase (NS5B) of HCV.* PLoS One, 2012. **7**(11): p. e49254.

197. Migliaccio, A., et al., *Inhibition of the SH3 domain-mediated binding of Src to the androgen receptor and its effect on tumor growth.* Oncogene, 2007. **26**(46): p. 6619-29.
198. Scapin, G., *Structural biology in drug design: selective protein kinase inhibitors.* Drug Discov Today, 2002. **7**(11): p. 601-11.
199. Zhao, L., et al., *Promotion of colorectal cancer growth and metastasis by the LIM and SH3 domain protein 1.* Gut, 2010. **59**(9): p. 1226-35.
200. Nguyen, J.T., et al., *Improving SH3 domain ligand selectivity using a non-natural scaffold.* Chem Biol, 2000. **7**(7): p. 463-73.
201. Zorko, M. and U. Langel, *Cell-penetrating peptides: mechanism and kinetics of cargo delivery.* Adv Drug Deliv Rev, 2005. **57**(4): p. 529-45.
202. Jiang, T., et al., *Tumor imaging by means of proteolytic activation of cell-penetrating peptides.* Proc Natl Acad Sci U S A, 2004. **101**(51): p. 17867-72.
203. Jin, E., et al., *Acid-active cell-penetrating peptides for in vivo tumor-targeted drug delivery.* J Am Chem Soc, 2013. **135**(2): p. 933-40.
204. Myrberg, H., et al., *Design of a tumor-homing cell-penetrating peptide.* Bioconjug Chem, 2008. **19**(1): p. 70-5.
205. Derossi, D., et al., *The third helix of the Antennapedia homeodomain translocates through biological membranes.* J Biol Chem, 1994. **269**(14): p. 10444-50.
206. Davidson, T.J., et al., *Highly efficient small interfering RNA delivery to primary mammalian neurons induces MicroRNA-like effects before mRNA degradation.* J Neurosci, 2004. **24**(45): p. 10040-6.
207. Lu, J., et al., *TAP-independent presentation of CTL epitopes by Trojan antigens.* J Immunol, 2001. **166**(12): p. 7063-71.
208. Dunker, A.K., et al., *Protein disorder and the evolution of molecular recognition: theory, predictions and observations.* Pac Symp Biocomput, 1998: p. 473-84.
209. Uversky, V.N., J.R. Gillespie, and A.L. Fink, *Why are "natively unfolded" proteins unstructured under physiologic conditions?* Proteins, 2000. **41**(3): p. 415-27.
210. Wright, P.E. and H.J. Dyson, *Intrinsically unstructured proteins: re-assessing the protein structure-function paradigm.* J Mol Biol, 1999. **293**(2): p. 321-31.

211. Uversky, V.N., *Intrinsically disordered proteins from A to Z.* Int J Biochem Cell Biol, 2011. **43**(8): p. 1090-103.

212. Tompa, P., *Intrinsically disordered proteins: a 10-year recap.* Trends Biochem Sci, 2012. **37**(12): p. 509-16.

213. Dunker, A.K., et al., *Flexible nets. The roles of intrinsic disorder in protein interaction networks.* FEBS J, 2005. **272**(20): p. 5129-48.

214. Patil, A. and H. Nakamura, *Disordered domains and high surface charge confer hubs with the ability to interact with multiple proteins in interaction networks.* FEBS Lett, 2006. **580**(8): p. 2041-5.

215. Uversky, V.N., C.J. Oldfield, and A.K. Dunker, *Showing your ID: intrinsic disorder as an ID for recognition, regulation and cell signaling.* J Mol Recognit, 2005. **18**(5): p. 343-84.

216. Jeong, H., et al., *Lethality and centrality in protein networks.* Nature, 2001. **411**(6833): p. 41-2.

217. Cheng, Y., et al., *Abundance of intrinsic disorder in protein associated with cardiovascular disease.* Biochemistry, 2006. **45**(35): p. 10448-60.

218. Uversky, V.N., *Intrinsic disorder in proteins associated with neurodegenerative diseases.* Front Biosci (Landmark Ed), 2009. **14**: p. 5188-238.

219. Uversky, V.N., et al., *Protein intrinsic disorder and human papillomaviruses: increased amount of disorder in E6 and E7 oncoproteins from high risk HPVs.* J Proteome Res, 2006. **5**(8): p. 1829-42.

220. Fukata, Y. and M. Fukata, *Protein palmitoylation in neuronal development and synaptic plasticity.* Nat Rev Neurosci, 2010. **11**(3): p. 161-75.

221. Blaskovic, S., M. Blanc, and F.G. van der Goot, *What does S-palmitoylation do to membrane proteins?* FEBS J, 2013. **280**(12): p. 2766-74.

222. Mitchell, D.A., et al., *Protein palmitoylation by a family of DHHC protein S-acyltransferases.* J Lipid Res, 2006. **47**(6): p. 1118-27.

223. Quesnel, S. and J.R. Silvius, *Cysteine-containing peptide sequences exhibit facile uncatalyzed transacylation and acyl-CoA-dependent acylation at the lipid bilayer interface.* Biochemistry, 1994. **33**(45): p. 13340-8.

224. Bartels, D.J., et al., *Erf2, a novel gene product that affects the localization and palmitoylation of Ras2 in Saccharomyces cerevisiae.* Mol Cell Biol, 1999. **19**(10): p. 6775-87.
225. Swarthout, J.T., et al., *DHHC9 and GCP16 constitute a human protein fatty acyltransferase with specificity for H- and N-Ras.* J Biol Chem, 2005. **280**(35): p. 31141-8.
226. Uemura, T., H. Mori, and M. Mishina, *Isolation and characterization of Golgi apparatus-specific GODZ with the DHHC zinc finger domain.* Biochem Biophys Res Commun, 2002. **296**(2): p. 492-6.
227. Putilina, T., P. Wong, and S. Gentleman, *The DHHC domain: a new highly conserved cysteine-rich motif.* Mol Cell Biochem, 1999. **195**(1-2): p. 219-26.
228. Politis, E.G., A.F. Roth, and N.G. Davis, *Transmembrane topology of the protein palmitoyl transferase Akr1.* J Biol Chem, 2005. **280**(11): p. 10156-63.
229. Roth, A.F., et al., *The yeast DHHC cysteine-rich domain protein Akr1p is a palmitoyl transferase.* J Cell Biol, 2002. **159**(1): p. 23-8.
230. Lobo, S., et al., *Identification of a Ras palmitoyltransferase in Saccharomyces cerevisiae.* J Biol Chem, 2002. **277**(43): p. 41268-73.
231. Gorleku, O.A., et al., *Endoplasmic reticulum localization of DHHC palmitoyltransferases mediated by lysine-based sorting signals.* J Biol Chem, 2011. **286**(45): p. 39573-84.
232. Fairbank, M., et al., *RING finger palmitoylation of the endoplasmic reticulum Gp78 E3 ubiquitin ligase.* FEBS Lett, 2012. **586**(16): p. 2488-93.
233. Lakkaraju, A.K., et al., *Palmitoylated calnexin is a key component of the ribosome-translocon complex.* EMBO J, 2012. **31**(7): p. 1823-35.
234. Senyilmaz, D., et al., *Regulation of mitochondrial morphology and function by stearoylation of TFR1.* Nature, 2015. **525**(7567): p. 124-8.
235. Abrami, L., et al., *Identification and dynamics of the human ZDHHC16-ZDHHC6 palmitoylation cascade.* Elife, 2017. **6**.
236. Cohen, G.B., R. Ren, and D. Baltimore, *Modular binding domains in signal transduction proteins.* Cell, 1995. **80**(2): p. 237-48.
237. Pawson, T., *Protein modules and signalling networks.* Nature, 1995. **373**(6515): p. 573-80.

238. Morton, C.J. and I.D. Campbell, *SH3 domains. Molecular 'Velcro'.* Curr Biol, 1994. **4**(7): p. 615-7.

239. Musacchio, A., et al., *SH3--an abundant protein domain in search of a function.* FEBS Lett, 1992. **307**(1): p. 55-61.

240. Musacchio, A., et al., *Crystal structure of a Src-homology 3 (SH3) domain.* Nature, 1992. **359**(6398): p. 851-5.

241. Alexandropoulos, K., G. Cheng, and D. Baltimore, *Proline-rich sequences that bind to Src homology 3 domains with individual specificities.* Proc Natl Acad Sci U S A, 1995. **92**(8): p. 3110-4.

242. Feng, S., et al., *Two binding orientations for peptides to the Src SH3 domain: development of a general model for SH3-ligand interactions.* Science, 1994. **266**(5188): p. 1241-7.

243. Nguyen, J.T., et al., *Exploiting the basis of proline recognition by SH3 and WW domains: design of N-substituted inhibitors.* Science, 1998. **282**(5396): p. 2088-92.

244. Vidal, M., V. Gigoux, and C. Garbay, *SH2 and SH3 domains as targets for anti-proliferative agents.* Crit Rev Oncol Hematol, 2001. **40**(2): p. 175-86.

245. Duncan, J.A. and A.G. Gilman, *Autoacylation of G protein alpha subunits.* J Biol Chem, 1996. **271**(38): p. 23594-600.

246. Mo, P. and S. Yang, *The store-operated calcium channels in cancer metastasis: from cell migration, invasion to metastatic colonization.* Front Biosci (Landmark Ed), 2018. **23**: p. 1241-1256.

247. Maione, P., et al., *Overcoming resistance to targeted therapies in NSCLC: current approaches and clinical application.* Ther Adv Med Oncol, 2015. **7**(5): p. 263-73.

248. Van Impe, K., et al., *A nanobody targeting the F-actin capping protein CapG restrains breast cancer metastasis.* Breast Cancer Res, 2013. **15**(6): p. R116.

249. Corbi-Verge, C. and P.M. Kim, *Motif mediated protein-protein interactions as drug targets.* Cell Commun Signal, 2016. **14**: p. 8.

250. Gorelik, M. and A.R. Davidson, *Distinct peptide binding specificities of Src homology 3 (SH3) protein domains can be determined by modulation of local energetics across the binding interface.* J Biol Chem, 2012. **287**(12): p. 9168-77.

251. Richard, J.P., et al., *Cell-penetrating peptides. A reevaluation of the mechanism of cellular uptake.* J Biol Chem, 2003. **278**(1): p. 585-90.
252. Erlanson, D.A., J.A. Wells, and A.C. Braisted, *Tethering: fragment-based drug discovery.* Annu Rev Biophys Biomol Struct, 2004. **33**: p. 199-223.